KBS TEKNISK RAPPORT

47

Investigations of groundwater flow in rock around repositories for nuclear waste

John Stokes
Roger Thunvik

Inst för Kulturteknik KTH maj 1978

KÄRN - BRÄNSLE - SÄKERHET

POSTADRESS: Kärnbränslesäkerhet, Fack. 102 40 Stockholm. Telefon 08-67 95 40

Correction to the English version of
KBS Technical report 47:

J. Stokes, R. Thunvik: INVESTIGATIONS OF GROUNDWATER FLOW IN ROCK AROUND REPOSITORIES FOR NUCLEAR WASTE.

Page 92, figure 4b: The calculated ages of the groundwater are 100 times to high. All numbers given in the figure should be decreased by 2 units.

INVESTIGATIONS OF GROUNDWATER FLOW IN ROCK AROUND REPOSITORIES FOR NUCLEAR WASTE

John Stokes
Roger Thunvik
Inst för Kulturteknik KTH maj 1978

Denna rapport utgör redovisning av ett arbete som utförts på uppdrag av KBS. Slutsatser och värderingar i rapporten är författarens och behöver inte nödvändigtvis sammanfalla med uppdragsgivarens.

I slutet av rapporten har bifogats en förteckning över av KBS hittills publicerade tekniska rapporter i denna serie.

DOCUMENTS INCLUDED IN THE REPORT

- GROUNDWATER FLOW DUE TO TOPOGRAPHICAL AND GEOLOGICAL EFFECTS
- LOCAL GROUNDWATER DEPRESSION AROUND A REPOSITORY
- THREE DIMENSIONAL MODEL OF GROUNDWATER FLOW GOVERNED BY TOPOGRAPHY

Summary.

INVESTIGATIONS OF GROUNDWATERFLOW IN ROCK AROUND REPOSITORIES FOR NUCLEAR WASTE

I. Groundwater Flow due to Topographical and Geological Effects.

A first investigation of the principal aspects of groundwater flow when varying topography, hydraulic conductivity and geometri is presented. The groundwater table was assumed coincident with topography. The conductivity was assumed constant or exponentially decreasing with depth. The bottom was either fixed or infinite. Numerical examples containing equipotentials, streamlines, lines of equal flux and travel times are presented. Several profiles in the Forsmark area were analysed to show the effects of regional flow. This model is based on the analytical solution of the equations

$$\varphi_{xx} + \varphi_{zz} + \frac{K'(z)}{K(z)} \varphi_z = 0$$

and

$$\varphi_{rr} + \varphi_{zz} + \frac{1}{r}\varphi_r + \frac{K'(z)}{K(z)}\varphi_z = 0$$

where $K(z) = c \cdot e^{2\mu z}$ is the hydraulic conductivity. Here c and μ are empirical constants.

II. Local Groundwater Depression around a Repository.

A two-dimensional flow analysis was made to study the effect on the groundwater table due to drainage of the storage tunnels during the construction resp. operation period. The geometry was chosen the same as for the principal study in section I. The net accretion to the phreatic surface was assumed evenly distributed in space and time. Numerical examples with equipotentials and consecutive positions of the phreatic surface are presented. The model is based on the numerical solution of the following equation of flow:

$$\nabla^2\varphi(x,z,t) = 0$$

The phreatic surface is defined by the following boundary contion:

$$\frac{\phi}{K}\frac{\partial \eta(x,t)}{\partial t} - \frac{\partial \varphi}{\partial x}\frac{\partial \eta}{\partial x} + \frac{\partial \varphi}{\partial z} + \frac{\varepsilon}{K} = 0$$

where ϕ is porosity, η is the elevation of the phreatic surface and ε is the net accretion.

III. Three-Dimensional Model for Groundwater Flow due to Topographical and Geological Effects.

As a complement to the two-dimensional computations for the Forsmark area performed in section I, a three-dimensional flow model was developed. In this model, which is a finite-element model, the conductivity is defined separately for each element. In this way fracture zones have been included as well as a conductivity varying in space. In the equation of flow

$$\frac{\partial}{\partial x}\left(K_x \frac{\partial \varphi}{\partial x}\right) + \frac{\partial}{\partial y}\left(K_y \frac{\partial \varphi}{\partial y}\right) + \frac{\partial}{\partial z}\left(K_z \frac{\partial \varphi}{\partial z}\right) = 0$$

the K-value is subsequently a function of space.
Numerical examples for a K-value eponentially decreasing with depth, and with a given geometry of the fracturezones, are studied. The results are presented as equipotentials, travel times and maps describing conditions of in- and out flow.

1978.02.28

INVESTIGATIONS OF GROUNDWATER FLOW IN ROCK AROUND REPOSITORIES FOR NUCLEAR WASTE

I. Groundwater Flow due to Topographical and Geological Effects

John Stokes

Royal Institute of Technology

Stockholm, Sweden

Introduction

Groundwater flow is generally considered a highly complicated process which is generated by the force of gravity and which is determined, in detail, by precipitation, topography and by the nature of the ground. Physically, these properties are described in terms of pressure, hydraulic conductivity and porosity, all of which are variable in space. The mathematical dificulties encountered when the equations which determine flow are to be solved are insurmountable in the general case. Analytic solutions are known only for certain problems for which highly simplified conditions can be accepted, and in most cases one is limited to studying individual examples using numerical methods. However, it is possible to obtain essential information about flow in more realistic examples by studying the simpler cases. Starting with (among other things) the viewpoints set forth by Yngve Gustafsson in the general volume entitled Grundvatten (Groundwater)[1], different effects are discussed in this investigation by presenting a number of examples for which calculations have been carried out.

Even if the mathematical procedure when solving flow equations can be implemented fully in three dimensions, it is usually difficult to obtain an overall picture of the results. Since many questions associated with groundwater flow are 1-dimensional or 2-dimensional in nature, all of the examples selected for this investigation are 2-dimensional. The mathematical procedure when investigating 2-dimensional flow is presented in an appendix at the end of this report.

Flow within a specified area is uniquely defined when the pressure head or its gradient is known at the boundary of this area. Throughout this paper the upper part of the boundary is

---

1 Yngve Gustafsson, Topografins inverkan på Grundvattenbildningen, Grundvatten (Effect of Topography on Formation of Groundwater, Groundwater), pages 15 - 33, Stockholm 1970.

determined by assuming that the groundwater level coincides with topography. In Sweden precipitation is ordinarily plentiful and well-distributed with regard to time. Consequently the aforesaid assumption is a good approximation[1]. The bottom part of the boundary is assumed impervious and is, in certain examples, at infinite depth. Finally, the area covered by the calculations is bounded by impervious vertical sides. This latter boundary condition is not always realistic, but its effect on flow can be limited by locating the sides at long distances from the part of the area in which one is interested.

The first part of this investigation deals with questions involving principles. To answer these questions, a number of synthetic examples have been analyzed. The following questions governed, for the most part, the selection of these examples:

I) What are the differences in flow conditions between (on the one hand) long stretches of seashores and (on the other hand) islands (i.e. the plane-parallel case and the axisymmetric case)?

II) What are the differences in flow conditions between seashores and valley slopes (how is flow affected by a water surface)?

III) What changes when hydraulic conductivity changes?

IV) What flow rates are obtained for typical values of head differences, conductivity and porosity?

V) What are the flowtimes associated with these flow rates?

VI) What are the qualitative differences between isotropic and anisotropic flow?

---

1 Yngve Gustafsson, Topografins inverkan på Grundvattenbildningen, Grundvatten (Effect of Topography on Formation of Groundwater, Groundwater), pages 15 - 33, Stockholm 1970.

Synthetic examples

A set of examples, for which calculations have been carried out to illustrate and, as far as possible, answer the above questions, was defined as follows:

To study question I, two different kinds of flow were investigated:

Ia) 2-dimensional flow in the xz-plane. This flow is thus perpendicular to the y-axis throughout. (examples 1 - 12).

Ib) Axisymmetric flow around the z-axis in the rz-plane. This flow is thus such that its directional vector intersects the z-axis throughout. (examples 13 - 24).

To study question II, two different geometries are provided in the x-direction and r-direction respectively, as illustrated below:

IIa) Two cases were studied: (a = 50, b = 150) and (a = 100, b = 300). A lake with a flat shore is located with its water surface a/2 beneath the upper boundary. (examples 1 - 6, 13 - 18).

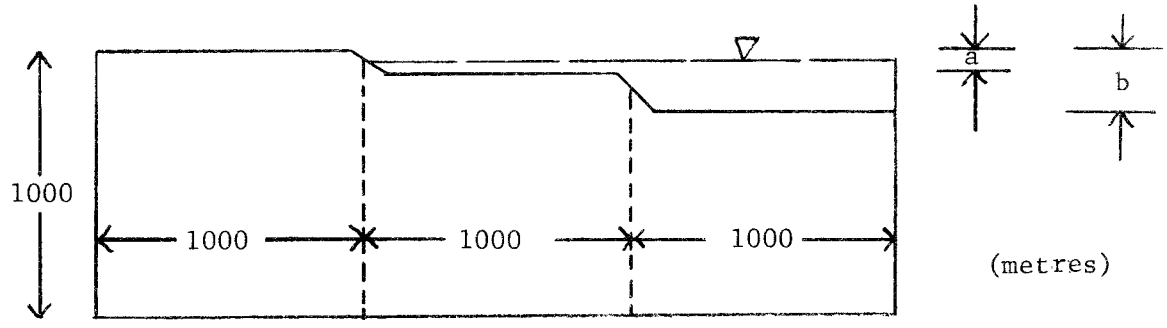

IIb) Two cases wre studied: (c = 75) and (c = 150). No lake was inserted in these examples. (examples 7 - 12, 19 - 24).

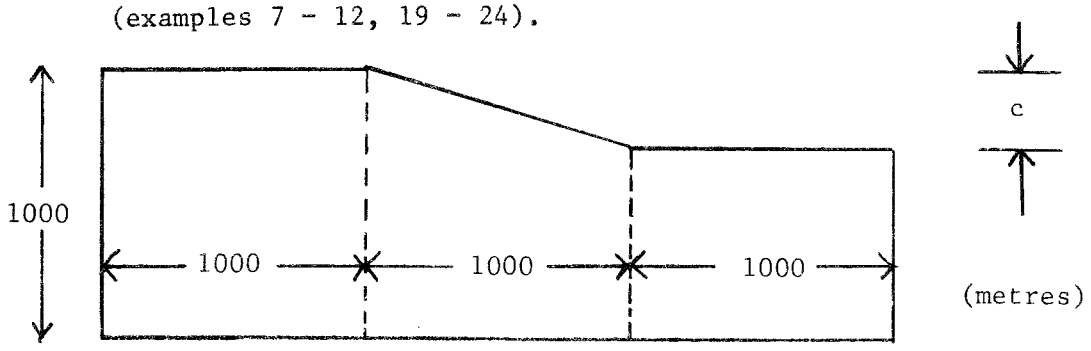

Two study question III, flows were investigated for different forms of depth-dependant conductivity:

IIIa) Impervious bottom at a depth of 1000 metres.
The hydraulic conductivity above this depth is constant:
$K = 0.000\ 001\ m^3/(m^2s)$.

IIIb) No bottom at finite depth.
The hydraulic conductivity is constant:
$K = 0.000\ 001\ m^3/(m^2s)$.

IIIc) Impervious bottom at depth of 1000 metres.
Above this level the hydraulic conductivity decreases exponentially with depth:

$K = K(z) = 0.000\ 001 \cdot 10^{0.0013z}\ m^3/(m^2s)$

This very moderate rate of decrease was selected to give flow patterns which are easy to read. In certain cases, calculations were carried out using the following empirically obtained function[2]:

$K = K(z) = 0.000\ 001 \cdot 10^{0.0030z}\ m^3/(m^2s)$

This is indicated by the letter b appended to the example number.

Conditions I, II and III have been combined into 24 different examples which are presented in a lower diagram (showing flow lines and equipotential lines) and an upper diagram (showing lines of equal flow in units $10^{-9}\ m^3/(m^2s)$). These diagrams appear in figs. 1 - 24. Details for the lower left and right corners are presented in figs. 25 - 31.

To study question V, flow times are given for several selected examples in figs. 32 - 38.

The source material for discussion of question VI is theoretical and is presented, together with the rest of the theory, in the Appendix.

---

2 Anders Carlsson, Tommy Olsson, Bestämning av Berggrundens Permeabilitet genom Vattenförlustmätning (Determination of Groundwater Permeability by measuring Water Loss), Vannet i Norden No. 3, 1976.

An overview of all examples appears in the table given below. This table also contains information about increments in flow function Ψ and potential function φ as well as flow $|q|$.

example	I	II	III	a	b	c	$\Delta\psi$	$\Delta\varphi$	$\Delta\|q\|$
1	a	a	a	50	150		2	2	8
2	a	a	b	50	150		2	2	8
3	a	a	c	50	150		2	2	8
4	a	a	a	100	300		4	4	16
5	a	a	b	100	300		4	4	16
6	a	a	c	100	300		4	4	16
7	a	b	a			75	8	5	8
8	a	b	b			75	8	5	8
9	a	b	c			75	8	5	8
10	a	b	a			150	16	10	16
11	a	b	b			150	16	10	16
12	a	b	c			150	16	10	16
13	b	a	a	50	150		0.5	2	8
14	b	a	b	50	150		0.5	2	8
15	b	a	c	50	150		0.5	2	8
16	b	a	a	100	300		1	4	16
17	b	a	b	100	300		1	4	16
18	b	a	c	100	300		1	4	16
19	b	b	a			75	2	5	8
20	b	b	b			75	2	5	8
21	b	b	c			75	2	5	8
22	b	b	a			150	4	10	16
23	b	b	b			150	4	10	16
24	b	b	c			150	4	10	16

The following numerical values apply for the hydraulic conductivities set forth in condition IIIc:

z (meter)	$0.000\ 001 \cdot 10^{0.0013z}$	$0.000\ 001 \cdot 10^{0.0030z}$
0	0.000 001 00	0.000 001 00
-100	74	50
-200	55	25
-300	41	12
-400	30	061
-500	22	030
-600	17	015
-700	12	007
-800	091	004
-900	068	002
-1000	050	001

Discussion

A number of aspects of questions I-V can be illustrated by making a comparative study of figs. 1 - 38. Note that all the illustrations are symmetrical around the left hand vertical axis. This axis will be called the centre axis. Figs. 1 - 12 are also symmetrical around the right hand vertical axis.

I. A comparison of the figure pairs (1,13), (2,14), ..., (12,24) indicates that in the axisymmetric case, the flow quantities are about four times lower than in the plane-parallel case. In addition, a flow is obtained that is stronger close to the center and weaker closer to the periphery for axisymmetric flow. In situations where the topographic gradient is constant within a large area (figs. 7 - 12, 19 - 24), the entire flow pattern is shifted towards the periphery as compared with the conditions that prevail in the plane-parallel case.

II. The introduction of a water surface at a given head means that the boundary beneath the water surface has a constant potential. In consequence, all flow through the bottom of a lake is orthogonal to the bottom. Since the flow is proportional to the potential gradient, and this is determined by the topography of the land, the flow diminshes as one moves away from the shore and out into the lake. This effect also occurs for flat areas on the land and can be described in such a way that the flow pattern caused by a change in head is approximately local. Moreover, the flow is proportional to the change in head. A study of all patterns indicates that the flow is strongest close to a change in head and weakest at the center of lakes and flat areas.

III. The hydraulic conductivity (which is the relationship between the flow and the pressure gradient) is a function of location in the general case. Studying the flow pattern for

an arbitrary conductivity $K = K(x,y,z)$ is very complicated. Here the K-value is assumed constant or diminishing exponentially with depth. In addition the K-value is assumed independent of flow direction (isotropy). One can then expect that a decreasing K-value will provide a more surface-oriented flow than a constant K-value. This effect is evident when comparing figs. (1,2), (3,2), (4,5), (6,5), etc. Moreover figs. 7 - 12 and 19 - 24 show that a constant K-value down to an unlimited depth provides concave equipotentials, while a K-value which decreases with depth provides convex equipotentials except in the vicinity of the surface. As a consequence, the flow tends to become more horizontal at deep depths for a decreasing K-value.

IV. The porosity must be known in order to calculate the true flow rates. As a rule, porosity is not known and is often assumed to be constant. Here it has been assumed to have the value $\phi = 0.001$. This value should only be seen as an illustration of the conditions in the Swedish bedrock. A rough estimate of flow rate v can be obtained using Darcy's law, i.e. $\phi v = K|\nabla\varphi|$. With a K-value of 10^{-6} m/s at the surface and a potential gradient equal to 10^{-3}, we obtain $v = 10^{-6}$ m/s which corresponds to 30 metres per year. If the K-value is assumed to decrease by half for each additional 100 metres of depth, we obtain $v = 0.03$ metres per year at a depth of 1000 metres.

A more detailed picture of the flow rates can be obtained from the upper diagrams in figs. 1 - 24 and from figs. 25 - 31 by dividing by ϕ. As stated in the comments on question II, the flow rates at a constant K-value are greatest in connection with extensive and abrupt changes in head and also at the surface. The lowest flow rates are obtained at great depths, beneath lakes and beneath flat areas. When the K-value decreases with depth, this effect is further accentuated.

V. A constant porosity of $\phi = 0.001$ has also been assumed for calculating flow times. Since these calculations require a great deal of time, only a few examples have been calculated. The results appear in figs. 32 - 38. It is evident that the flow times generally increase as depth increases. However, the longest times are found at surface points of maximum potential (at the centre of the inflow area). The flow times at depth are generally longer in the axisymmetric case due to the fact that this flow reaches the periphery where the potential gradients are lower than in the plane-parallel case. A general characteristic which appears in all of figs. 32 - 38 is the enormous variation in flow time that is encountered for small changes in location.

VI. The theoretical investigation presented in the Appendix indicates that the flow pattern for anisotropic flow can be obtained from the flow patterns for isotropic flow if the anisotropy is of the following form: $K_x/K_z = \xi = \text{constant}$. The depth scale will then be multiplied by a factor $1/\sqrt{\xi}$ while the exponent in the depth-dependance of conductivity is multiplied by $\sqrt{\xi}$. If, for example, ξ is assumed to be 2, the depth scale in figs. 1 - 24 will span an interval of $-707 < z < 0$ metres and the rate of decrease in conductivity is given by

$$K_x = 0.000002 \cdot 10^{0.0018z}$$
$$K_z = 0.000001 \cdot 10^{0.0018z}$$

The scale selected for the z-axis causes the flow lines to shift upwards. Increasing the K-value exponent has the same effect. This can be interpreted in such a way that any increase in conductivity in the x-direction without a corresponding increase in the z-direction provides a flatter flow pattern.

Problems associated with storage

When radioactive waste is to be stored in bedrock, one wishes to select a repository site in such a way that the flow time to the surface will be as long as possible. Long flow times are obtained primarily beneath the inflow area (descending flow lines). One should then not select an area immediately beneath the highest point in the terrain since the outflow from this point is superficial and will reach the ground in a short time. Primarily one should study local terrain minima in large inflow areas. If the terrain minimum itself is an outflow area is of no significance. The local nature of the minimum causes up-currents only near the surface, while down-currents are obtained at greater depths. If the selected repository site is in this down-current, local outflow from the site is avoided. Here the determining factor is how deep the local flow extends, and this is determined by the depth-dependancy of the hydraulic conductivity.

Application for a particular case

To obtain additional material that will illustrate the above question, flow lines have been calculated for several profiles at Finnsjön. The groundwater surface is assumed to follow topography as in the previous examples. The profiles (NW- and NE-) appear in the map shown in figs.39 - 40. The following calculations have been carried out:

fig. 41 NE-profile. $K = 0.000001 \cdot 10^{0.0030z}$
No bottom
Groundwater level lowered to a depth of 600 metres around a repository

fig. 42a) NE-profile. $K = 0.000001 \cdot 10^{0.0030z}$
No bottom
Groundwater level not lowered.

b) Special from a)

c) Special from b)

fig. 43) NW-profile. $K = 0.000001 \cdot 10^{0.0030z}$
No bottom
Groundwater level lowered to a depth of 600 metres around a repository

fig. 44) NW-profile. $K = 0.000001 \cdot 10^{0.0030z}$
No bottom
Groundwater level not lowered

fig. 45) NW-profile. $K = 0.000001$
Impervious bottom at depths of 1000, 3000 and 5000 metres
Groundwater level not lowered.

fig. 46) NE-profile. $K = 0.000001 \cdot 10^{0.0030z}$ $\phi = 0.001$
Lines of equal times of flow to surface
No bottom

fig. 47) NW-profile. $K = 0.000001 \cdot 10^{0.0030z}$ $\phi = 0.001$
Lines of equal times of flow to surface
No bottom

The flow lines in figs. 41, 42a, 43 and 44 are selected logarithmically with a factor of 10^{-4} (if l_1, l_2 and l_3 are three consecutive flowlines at increasing depths, 10^4 times as much water runs between l_1 and l_2 than between l_2 and l_3). The same thing applies to fig. 42b, but here 10^{-4} is replaced by 10^{-1}. The flow lines in figs. 42c and 45 are equidistant. All figures are drawn to scale. Figs. 41, 42a and 43 - 45 were calculated for each 500th metre, fig. 42b for each 100th metre and fig. 42c for each 20th metre. The curve in the upper part of each figure represents the terrain.

It is evident from fig. 44 that x = 12000 (just to the east of Finnsjön, fig. 40) is a local terrain minimum in a large inflow area. It is also evident that with the K-value selected for this example, the local flow is so deep that the area is unsuitable for use as a repository (closer analysis shows that the descending flow line at x = 13800 extends to a depth of at least 15000 metres).

Fig. 45 gives the flow pattern when the K-value is constant above an impervious bottom. In the top pattern, the bottom is at a depth of 1000 metres. All flow around x = 12000 is local, also in this

case. If, on the other hand, the bottom lies at a depth of 3000 or 5000 metres, the conditions are completely different. At x = 12500 and z = -1000 water from the surface at x = 11000 and x = 13500 should pass. After a long time (compared with the flow times for points in the surroundings) this water reaches the ground after first descending to a depth of at least 2500 metres. The flow in these cases is more regional. Note that all the water reaches the ground at x = 7600. In spite of the marked divergence in the first part of the flow, all water flows out through a very limited area. This effect appears in all patterns, regardless of how the conductivity varies with depth, i.e. the outflow areas that provide old water are small. There is one exception: the outflow from the sea bottom provides old water except close to the shore.

A general conclusion can be drawn from figs. 44 and 45: The tendency of a flow to be local or regional is determined by the variation of the K-value with depth. The exponentially decreasing conductivity in fig. 44 causes all flow to be local. The same flow pattern is obtained with constant K-value and an impervious bottom at a depth of 1000 metres (fig. 45 at top). If, instead, the bottom is deeper, the flow tends to be regional at greater depths (fig. 45, centre and bottom). If the K-value decreases exponentially down to a certain depth and thereafter remains constant, local flow is obtained at shallow and moderate depths, while the flow at deep depths is regional. The constant K-value at greater depths can of course be so low that the regional flow is negligible. Since the examples that are illustrated in figs. 41 -45 have been selected with as realistic parameters as possible, one must conclude that nothing can be said about the regional flow at Finnsjön until further knowledge has been acquired about the variation of hydraulic conductivity with depth.

The local flow that is obtained when the K-value decreases with depth is also evident from a comparison of figs. (41,42a) and (43,44). An imaginary repository is located northeast of Finnsjön at a depth of 400 to 800 metres (see figs. 39 - 40). Figs. 42a

and 44 depict the flow when the groundwater level follows topography. Figs. 41 and 43 depict the flow when the groundwater level has been lowered in connection with a storage operation. It is evident that this very severe disturbance in groundwater potential only affects flow within a radius of 5000 metres. If, instead, the K-value is constant down to an unlimited depth, the lowering of the groundwater level will determine the flow within the entire area.

Finally, the flow times needed for water to flow from the imaginary repository to the surface were calculated. These are presented in figs. 46 - 47. It is evident that, for these examples as well, the flow times for adjacent points can vary throughout several orders of magnitude.

fig 1
exempel 1
Ia IIa IIIa
a = 50
b = 150

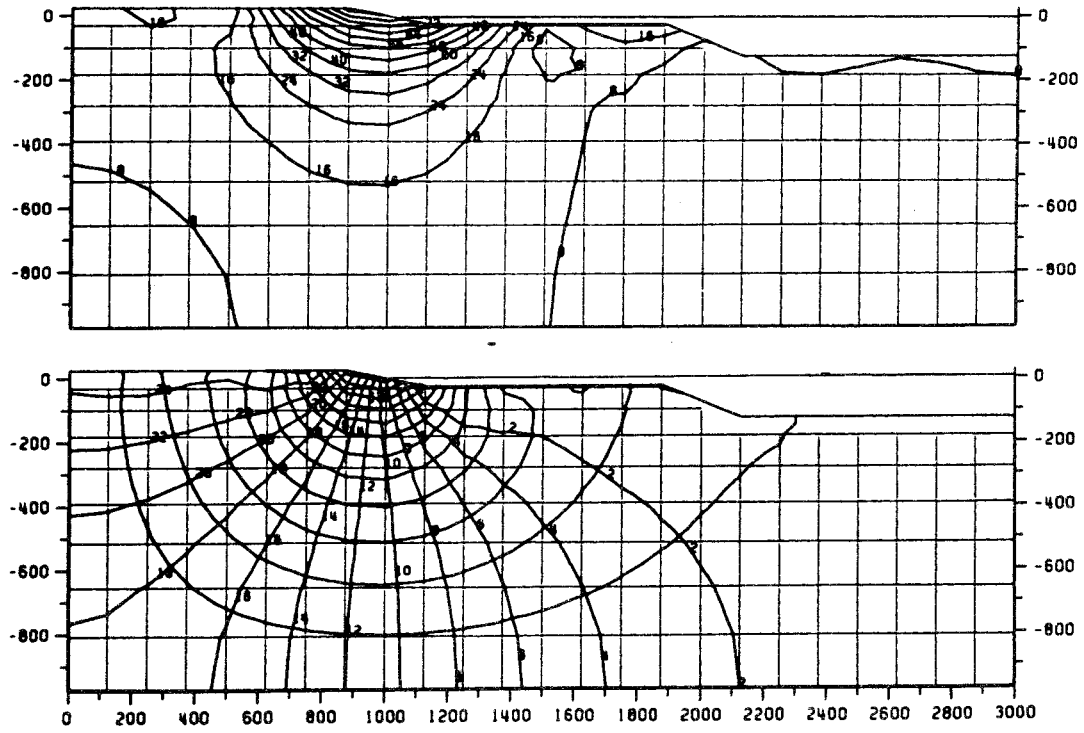

fig 2
exempel 2
Ia IIa IIIb
a = 50
b = 150

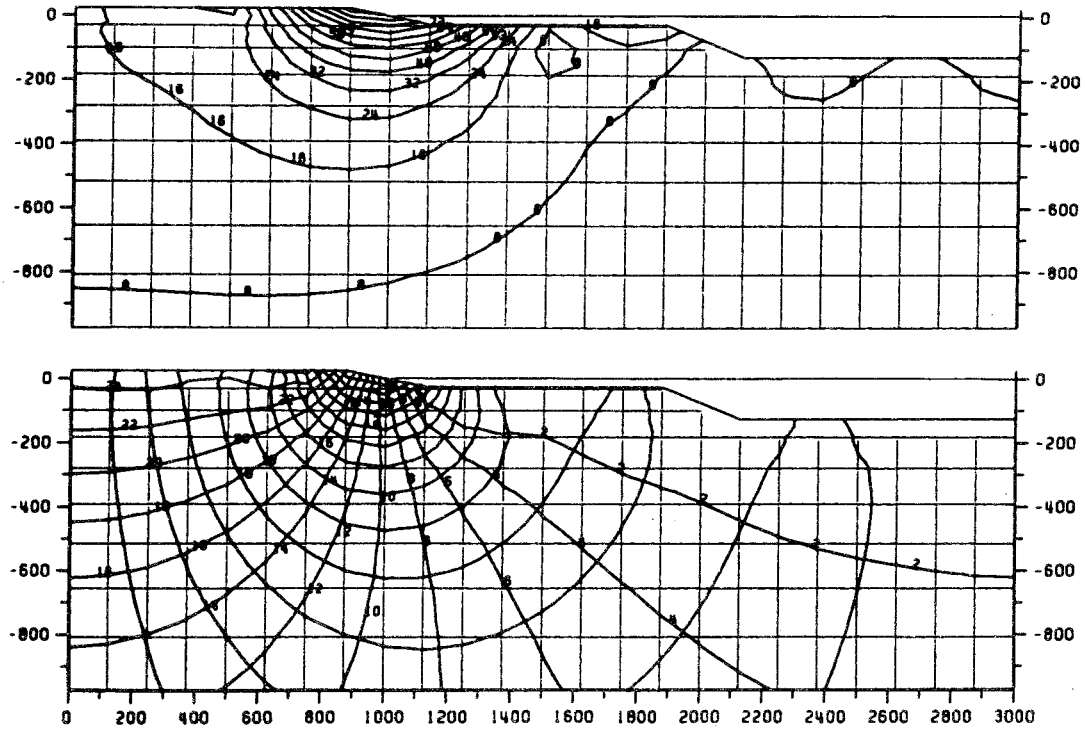

fig 3
exempel 3
Ia IIa IIIc
a = 50
b = 150

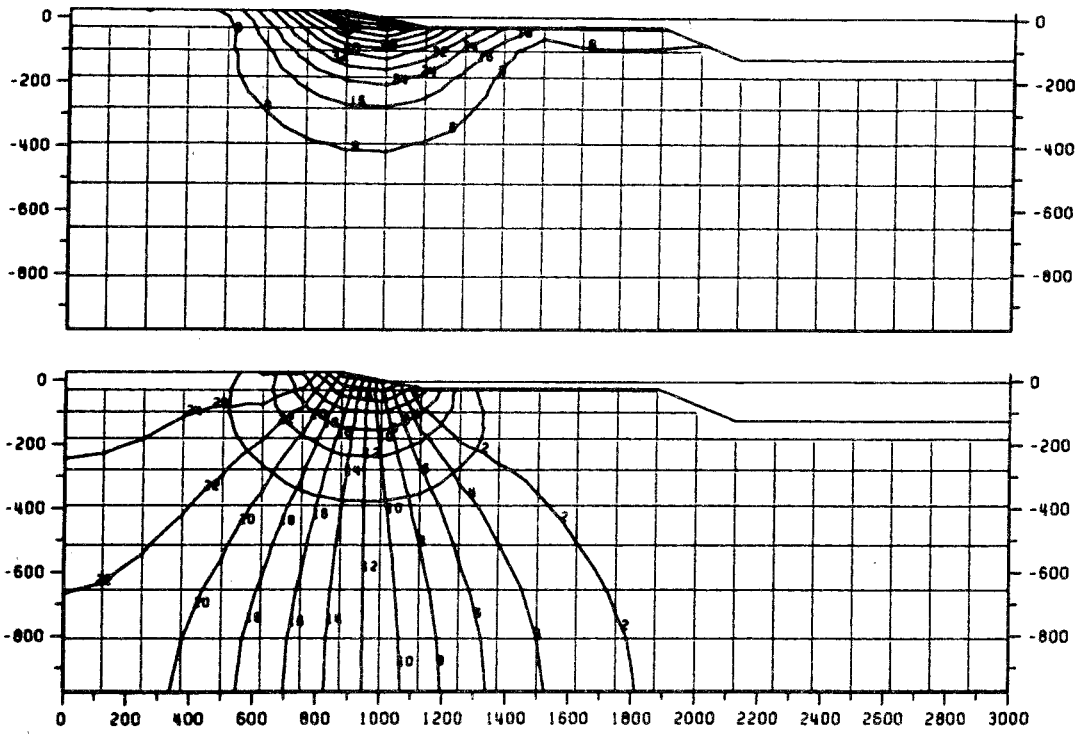

fig 4
exempel 4
Ia IIa IIIa
a = 100
b = 300

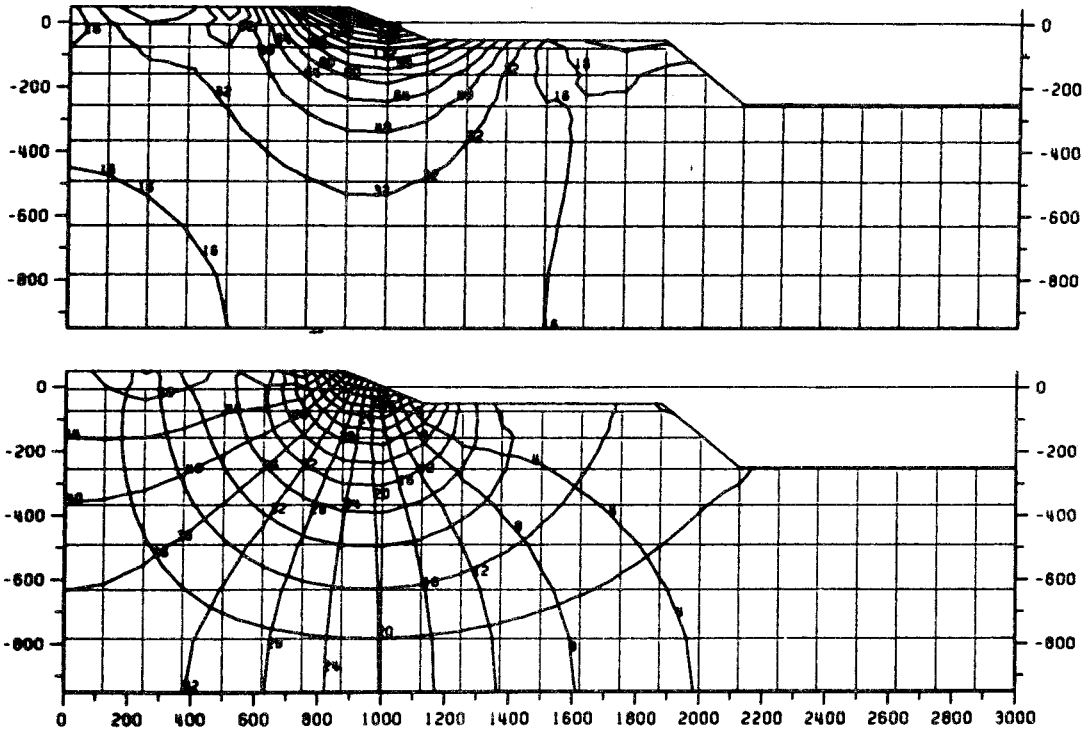

fig 5
exempel 5
Ia IIa IIIb
a = 100
b = 300

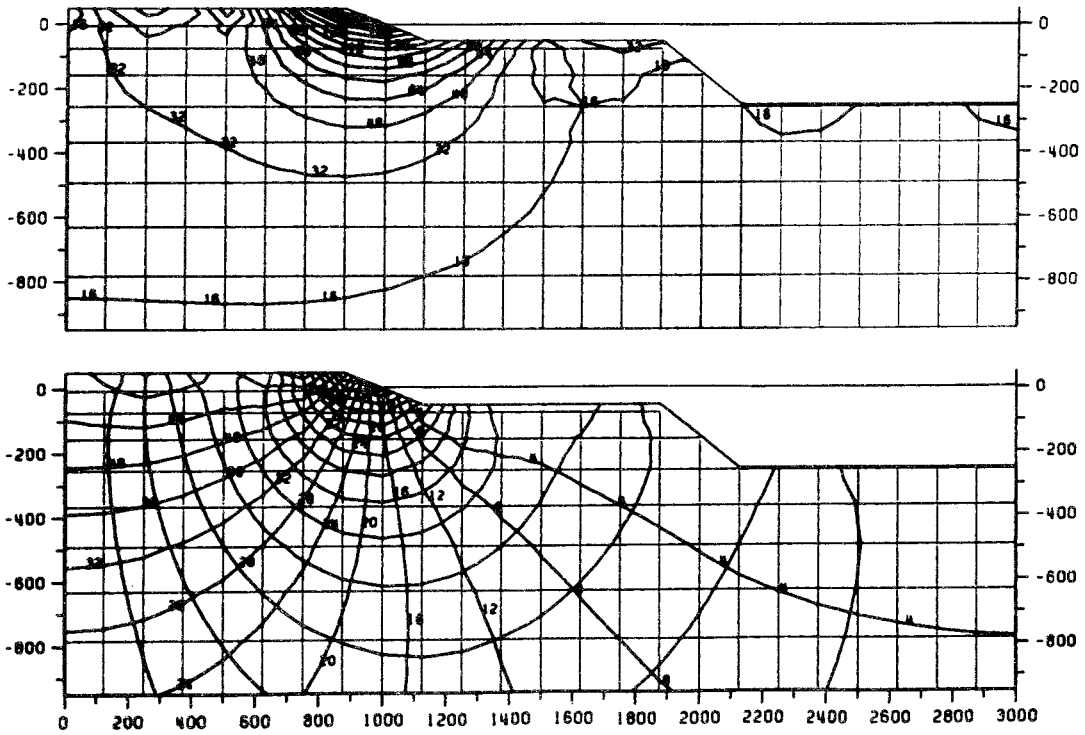

fig 6
exempel 6
Ia IIa IIIc
a = 100
b = 300

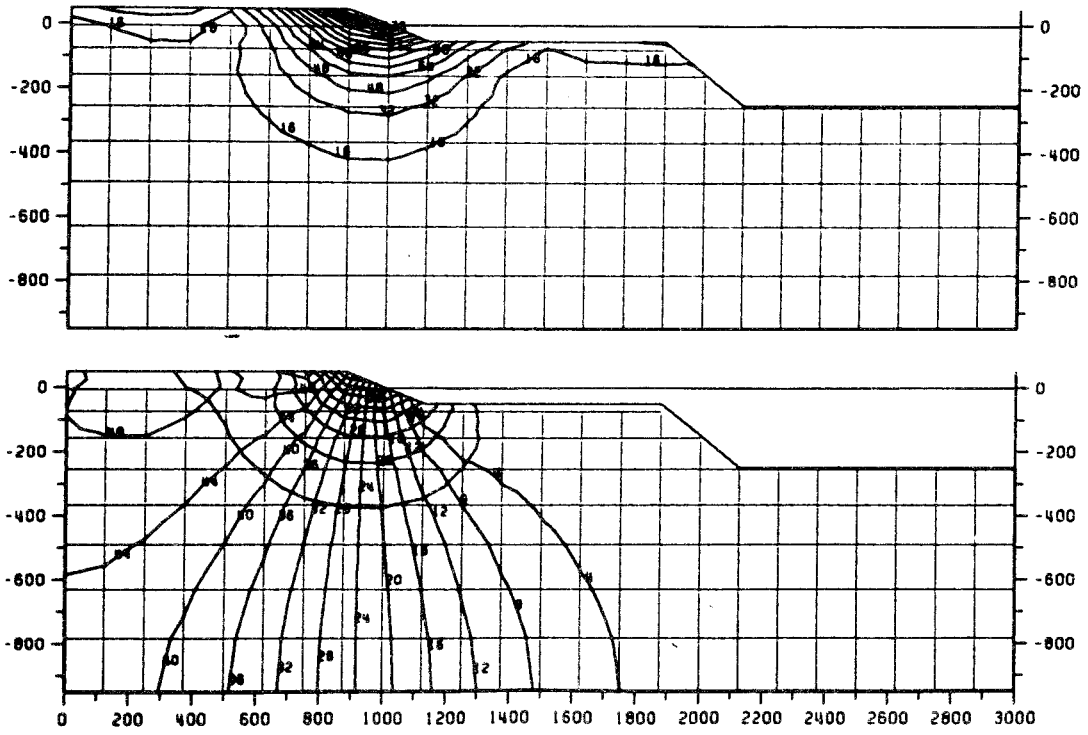

fig 7
exempel 7
Ia IIb IIIa
c = 75

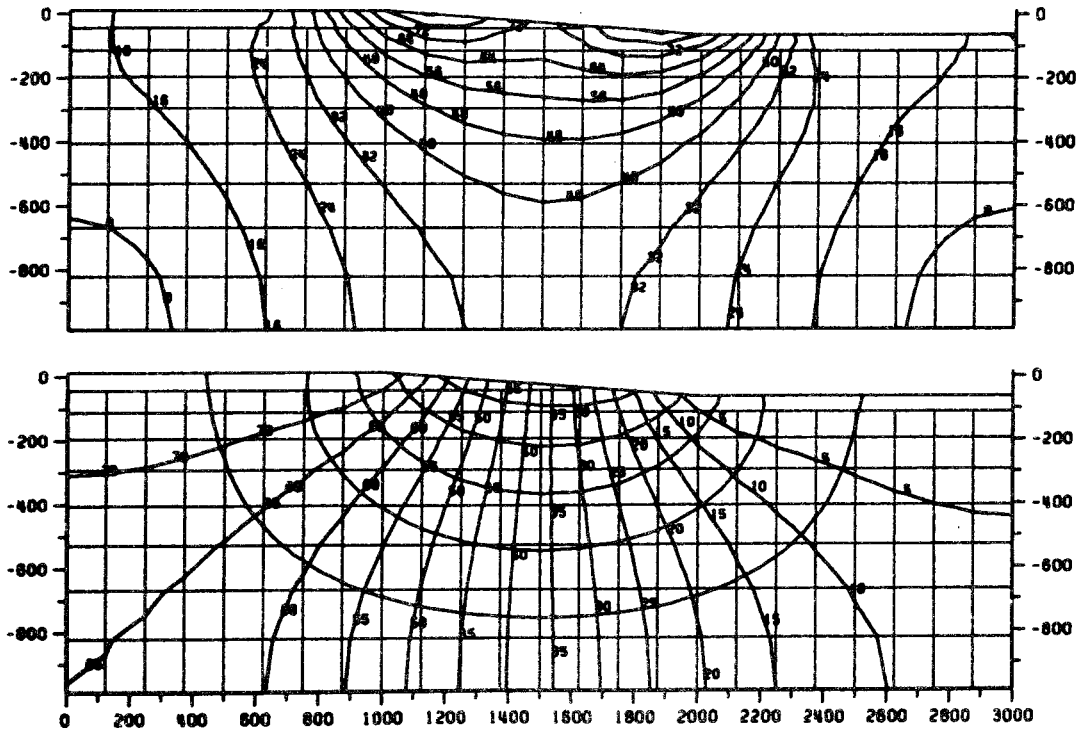

fig 8
exempel 8
Ia IIb IIIb
c = 75

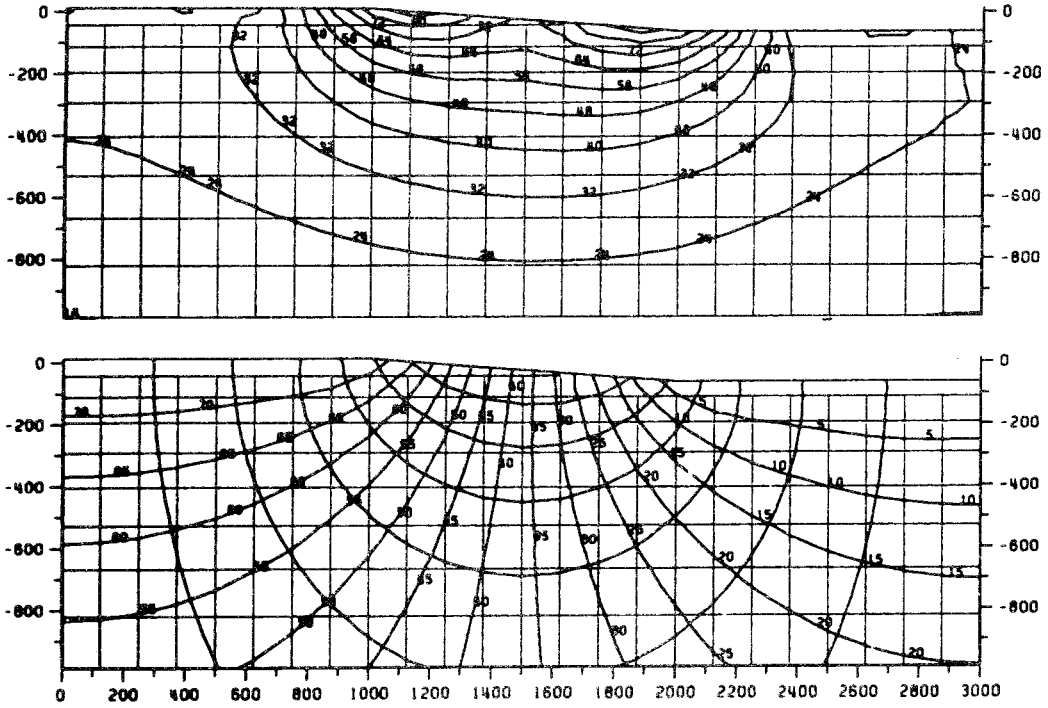

fig 9
exempel 9
Ia IIb IIIc
c = 75

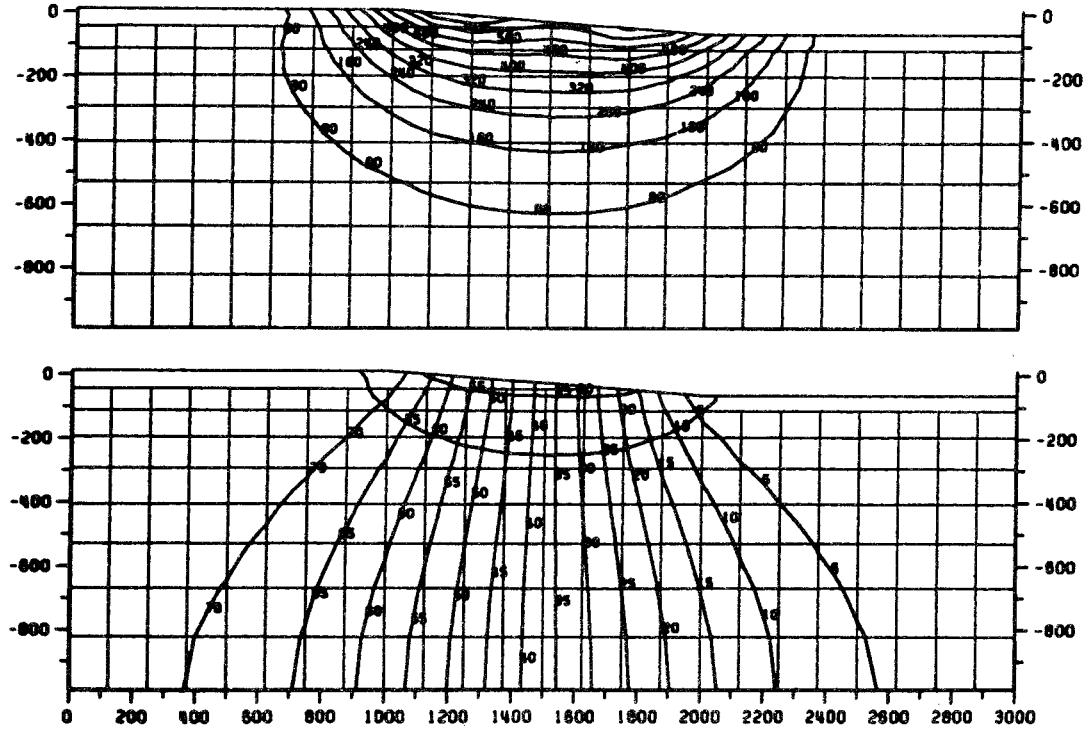

fig 10
exempel 10
Ia IIb IIIa
c = 150

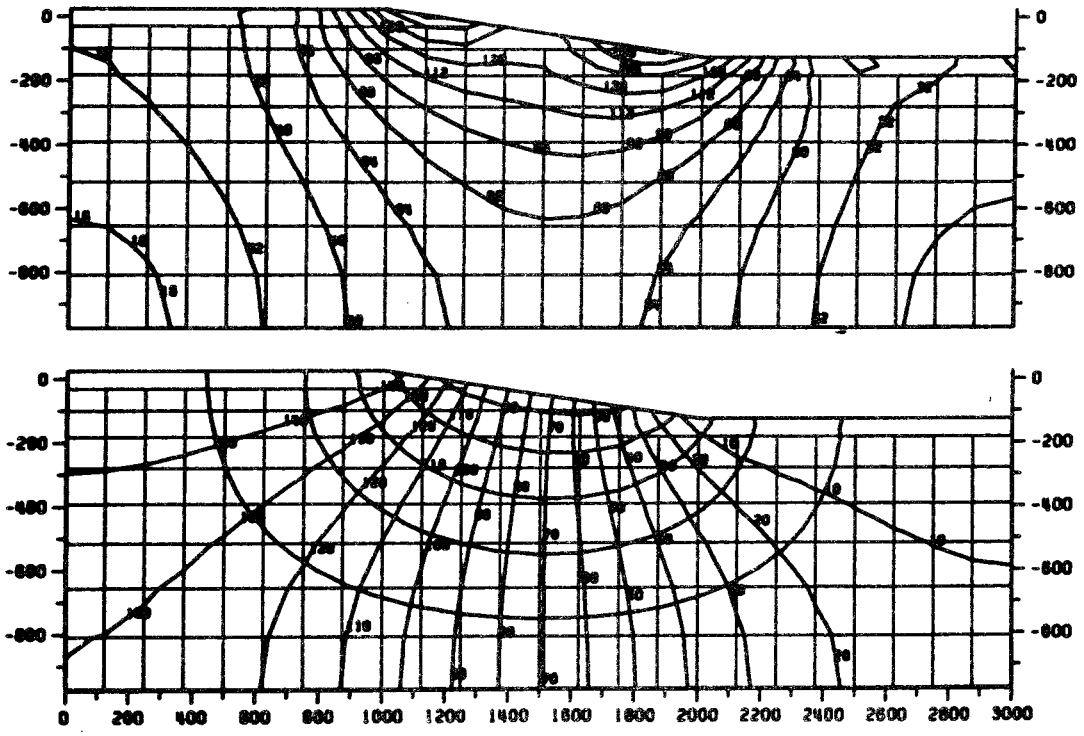

fig 11
exempel 11
Ia IIb IIIb
c = 150

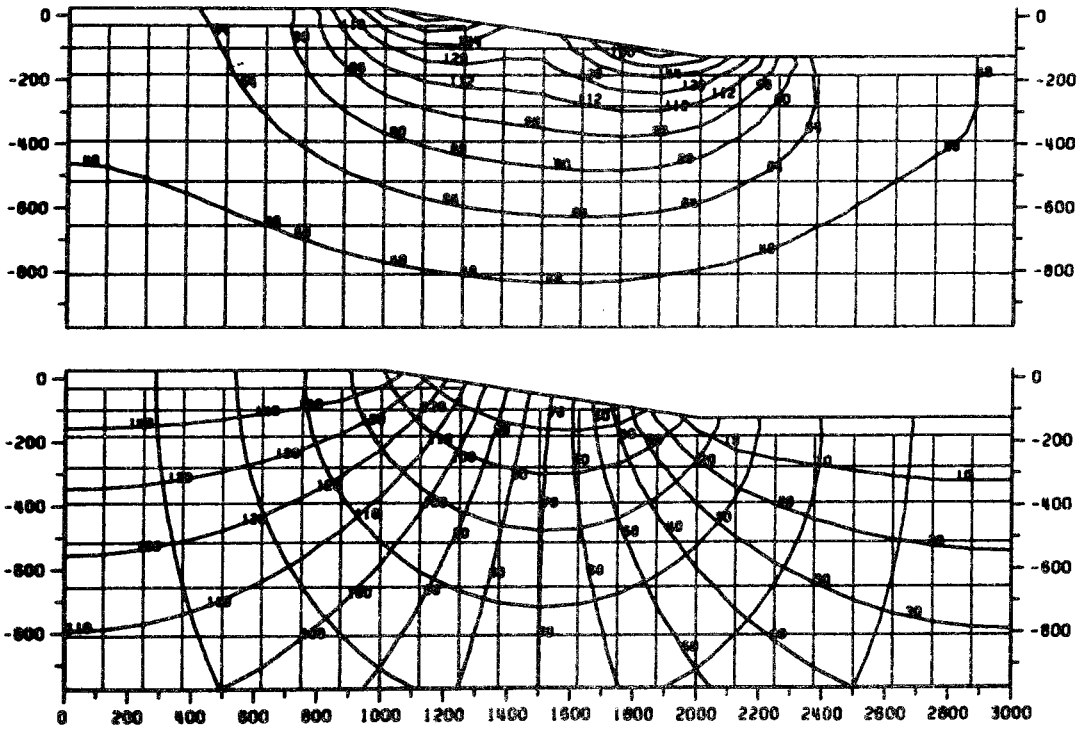

fig 12
exempel 12
Ia IIb IIIc
c = 150

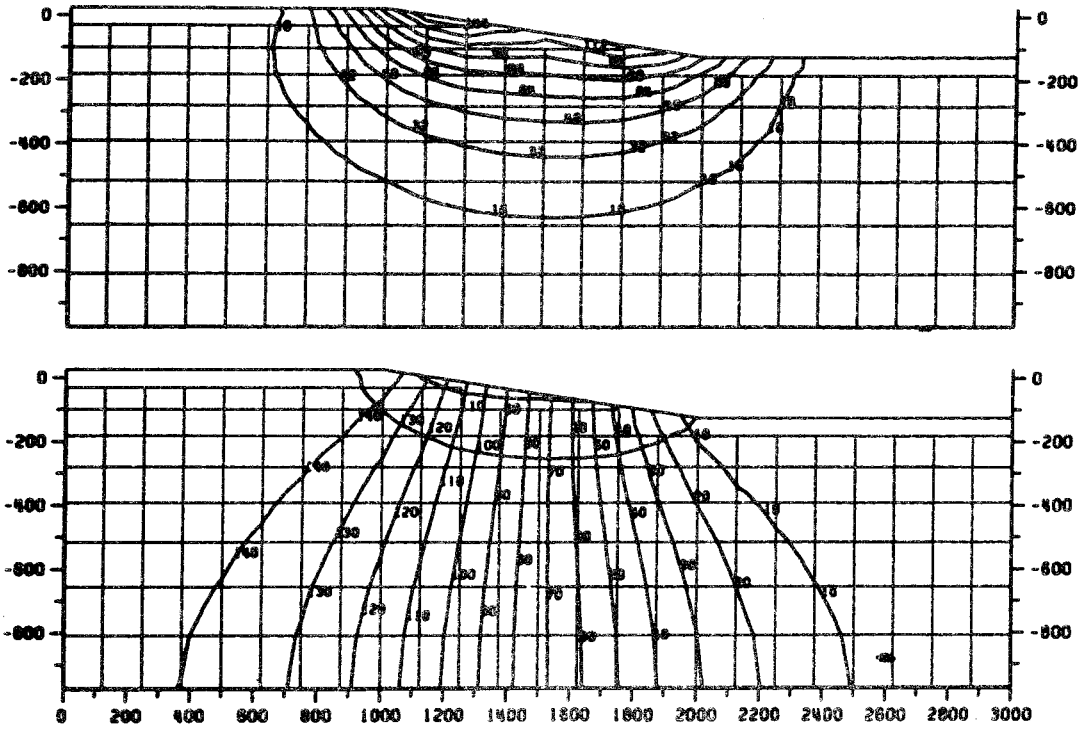

fig 13
exempel 13
Ib IIa IIIa
a = 50
b = 150

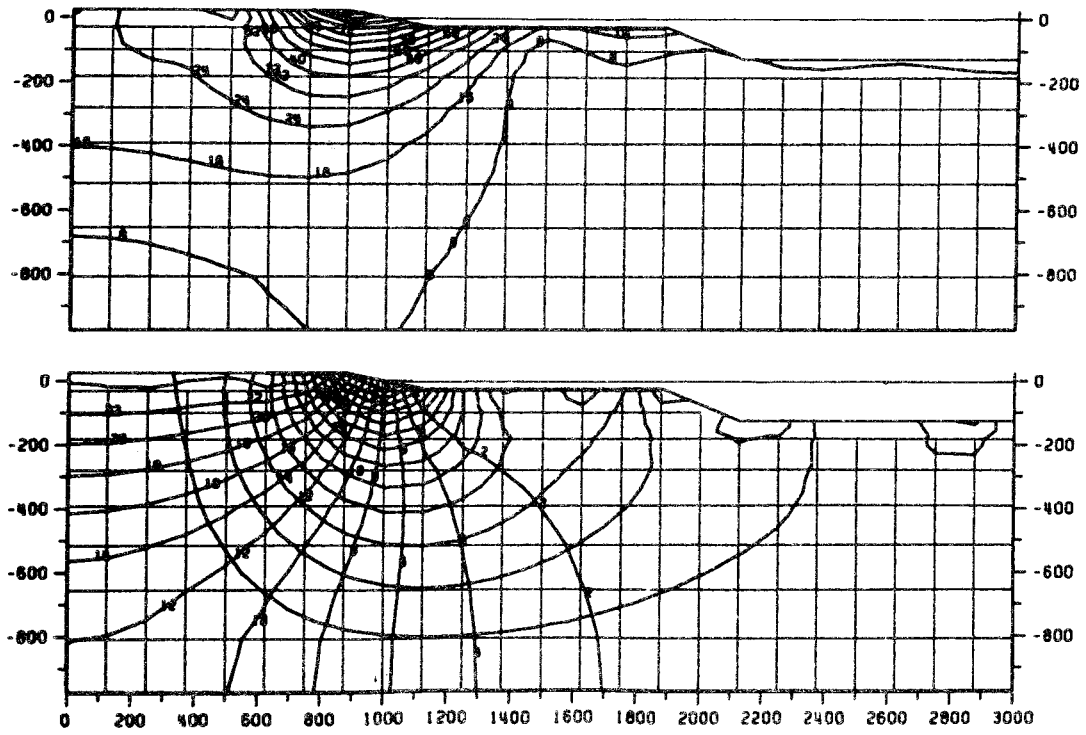

fig 14
exempel 14
Ib IIa IIIb
a = 50
b = 150

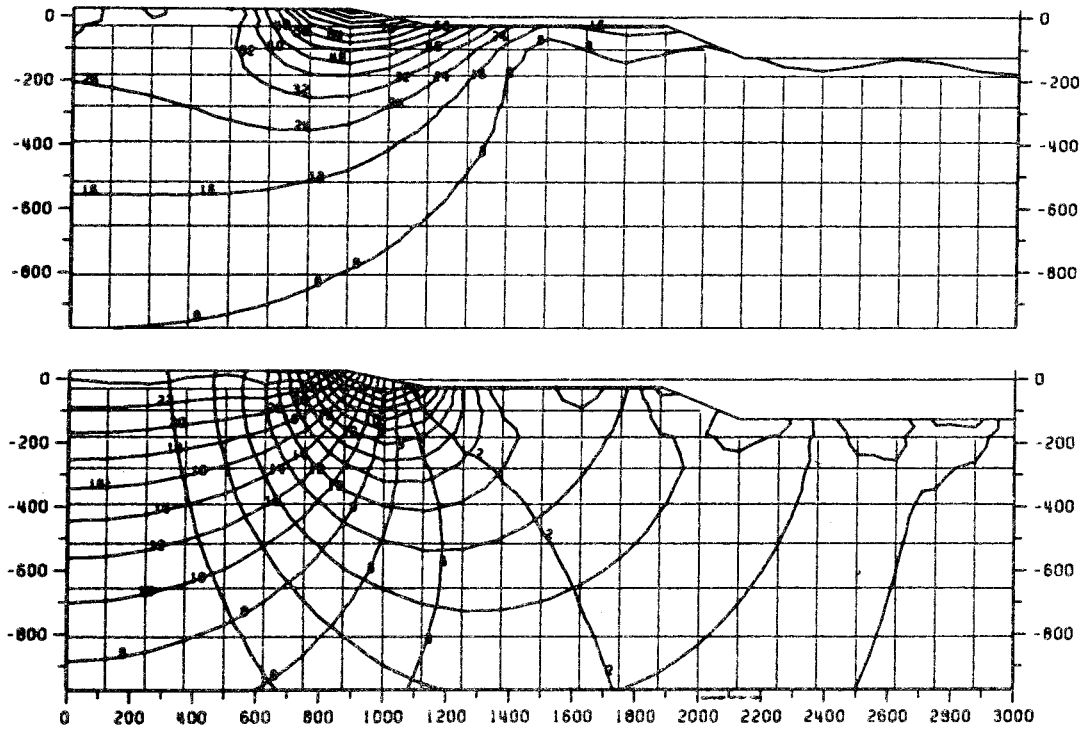

fig 15
exempel 15
Ib IIa IIIc
a = 50
b = 150

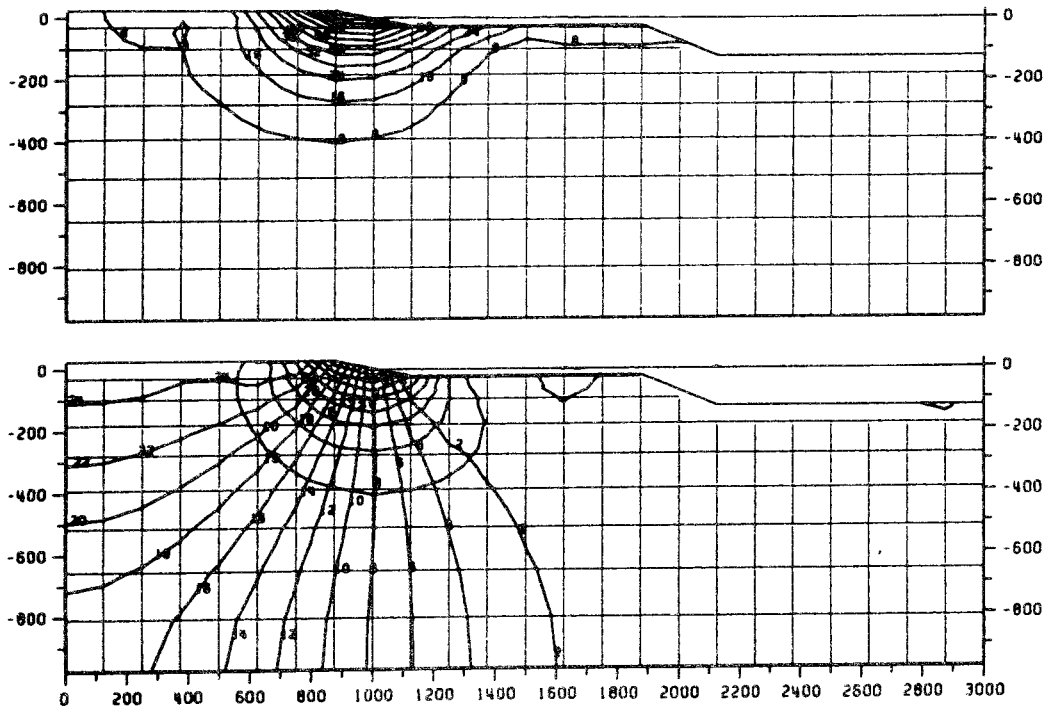

fig 16
exempel 16
Ib IIa IIIa
a = 100
b = 300

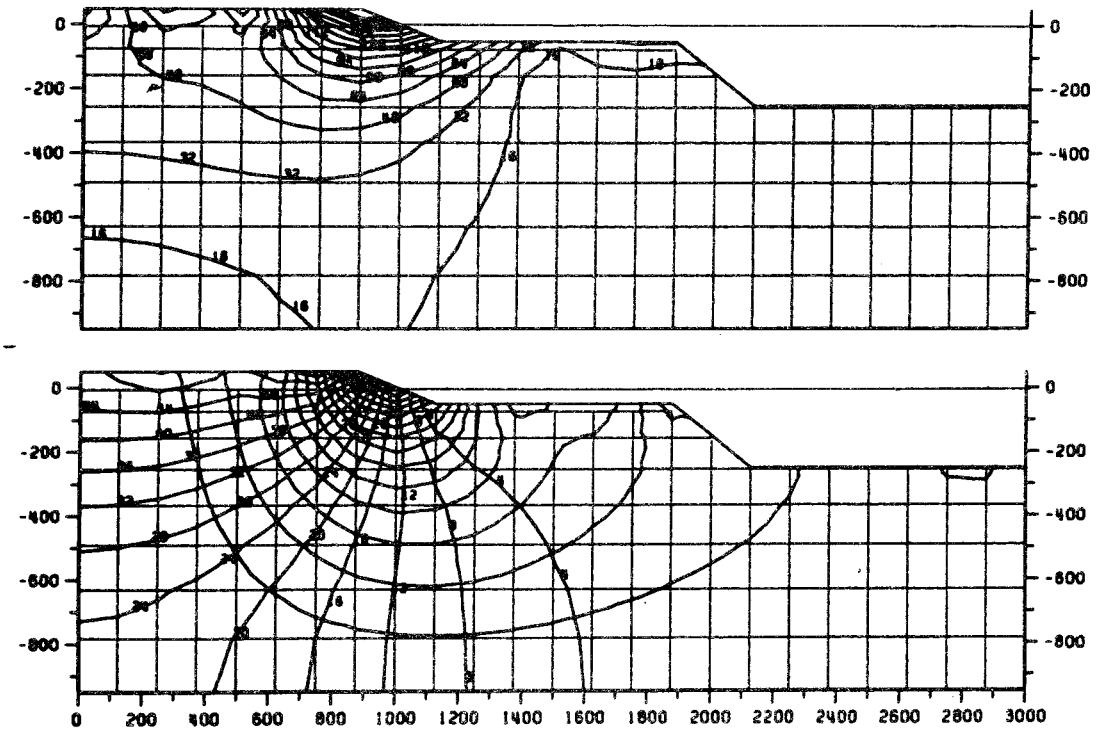

fig 17
exempel 17
Ib IIa IIIb
a = 100
b = 300

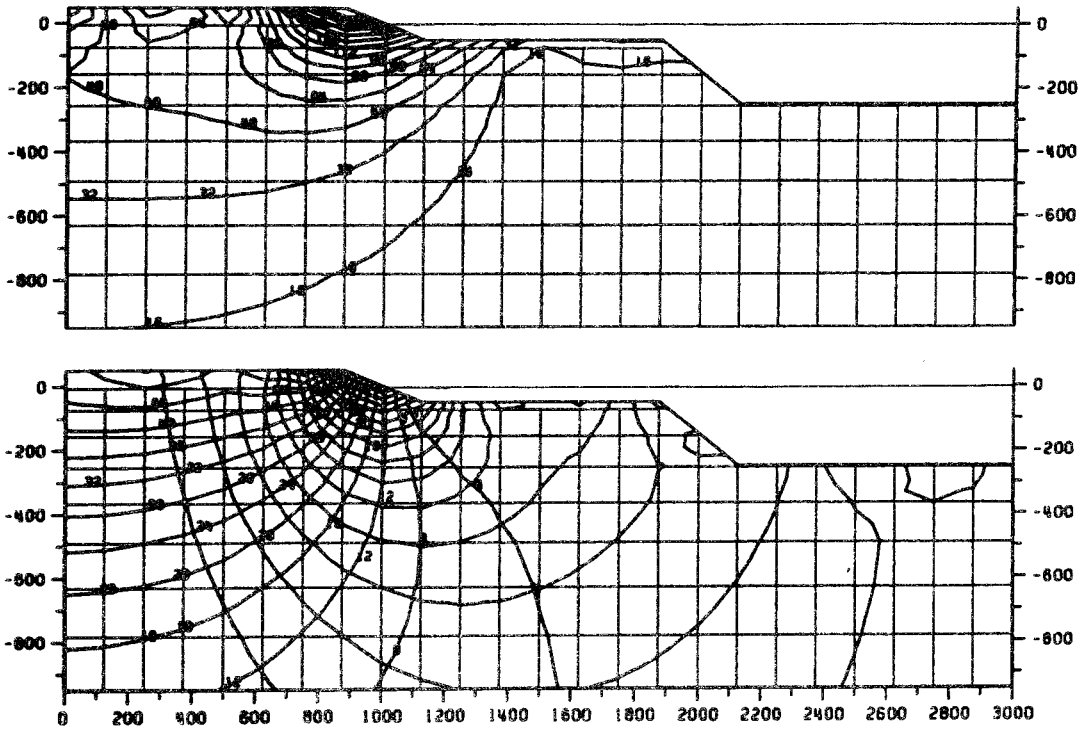

fig 18
exempel 18
Ib IIa IIIc
a = 100
b = 300

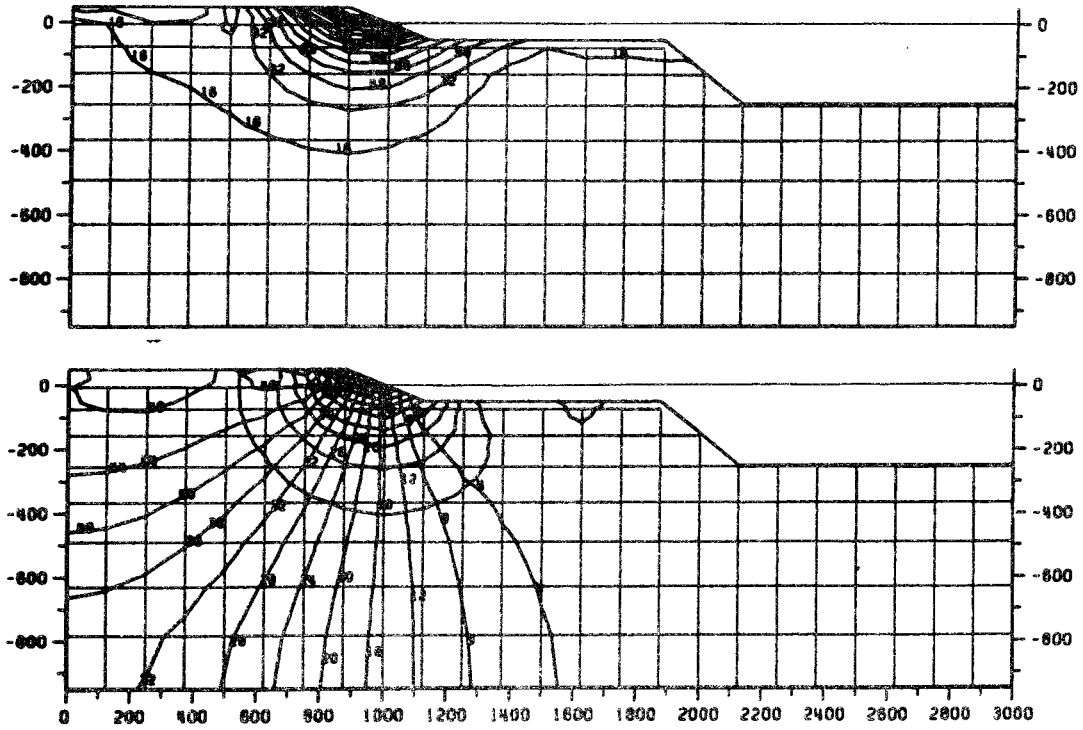

fig 19
exempel 19
Ib IIb IIIa
c = 75

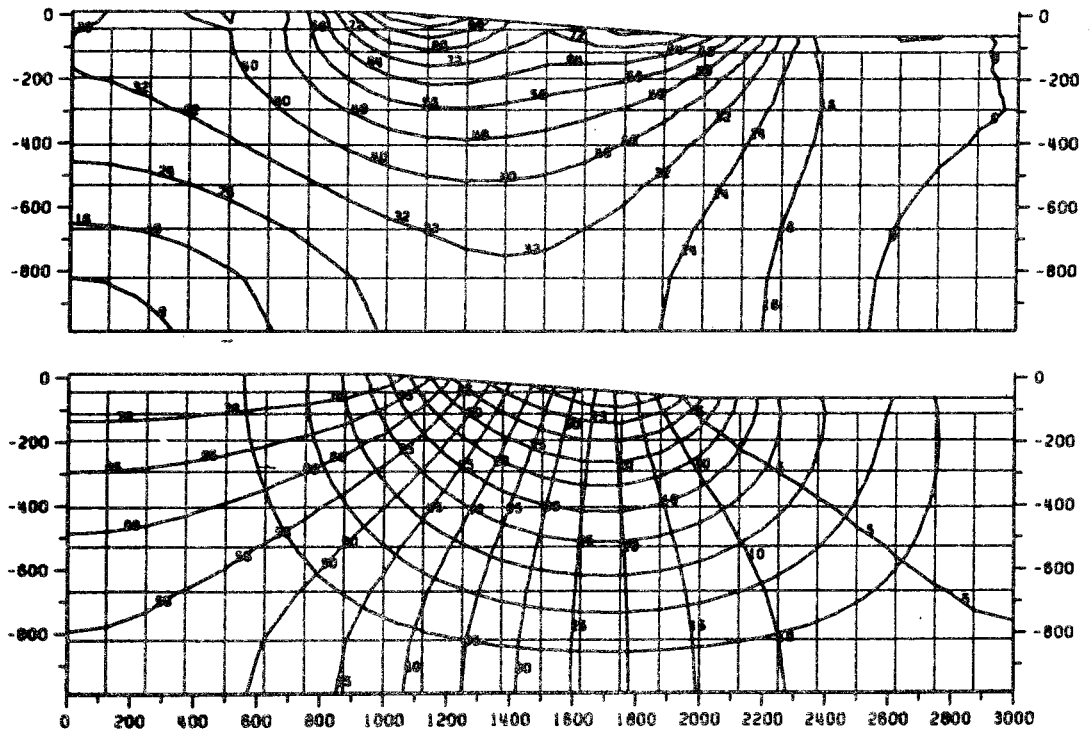

fig 20
exempel 20
Ib IIb IIIb
c = 75

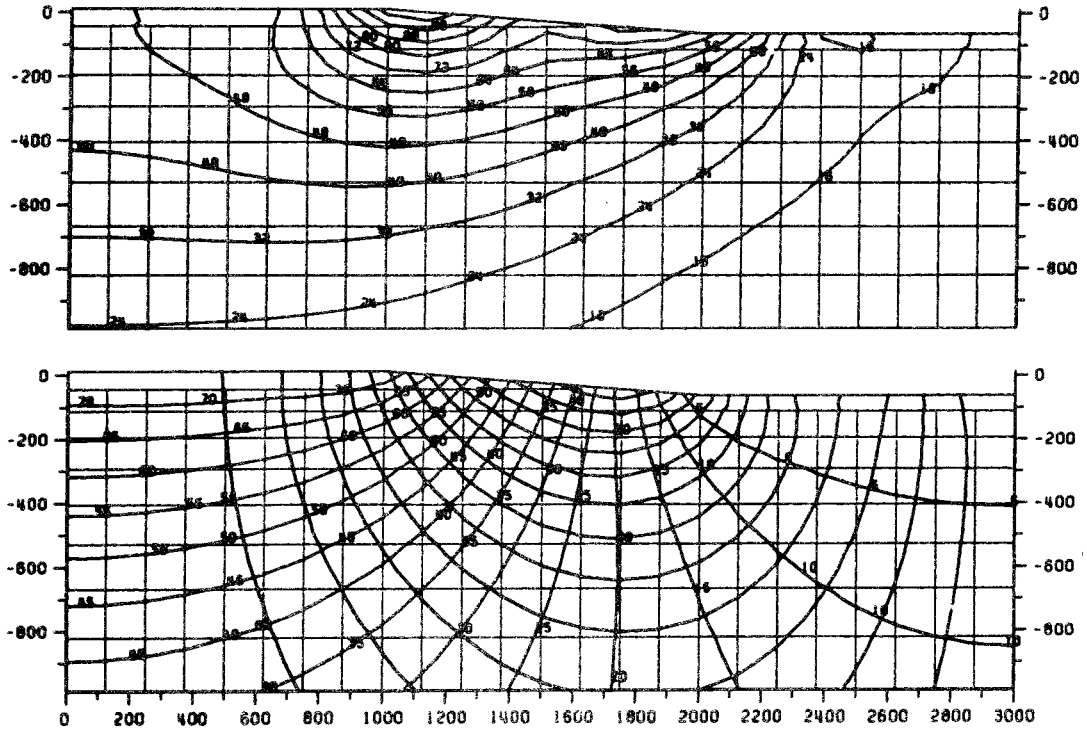

fig 21
exempel 21
Ib IIb IIIc
c = 75

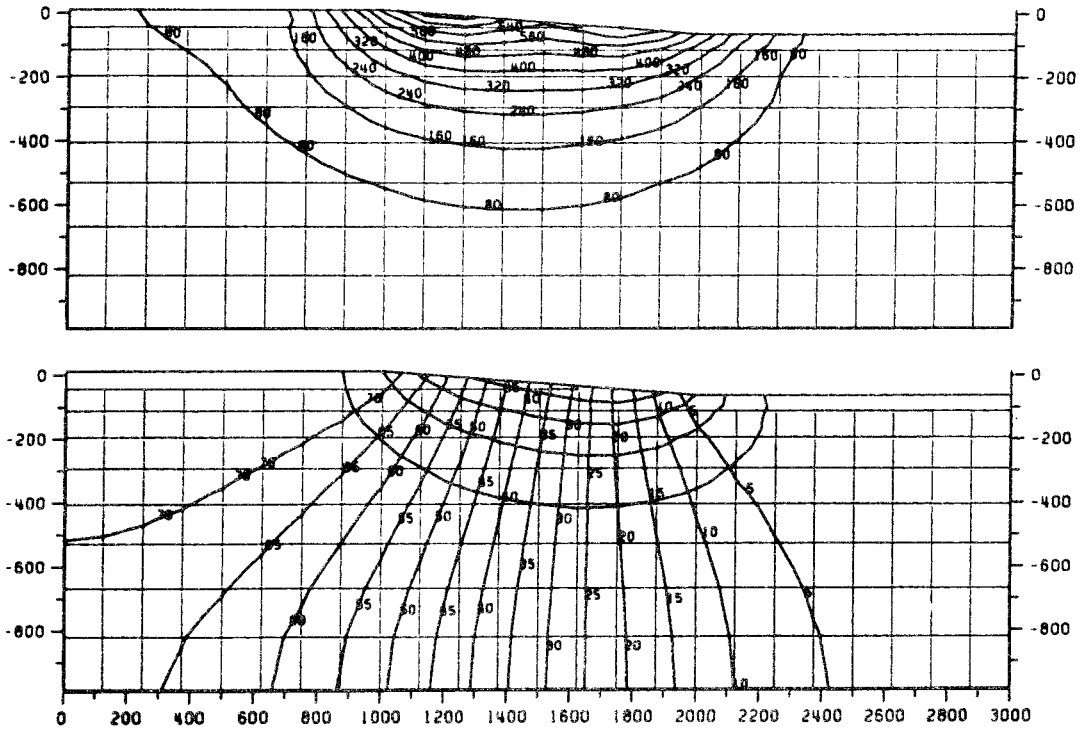

fig 22
exempel 22
Ib IIb IIIa
c = 150

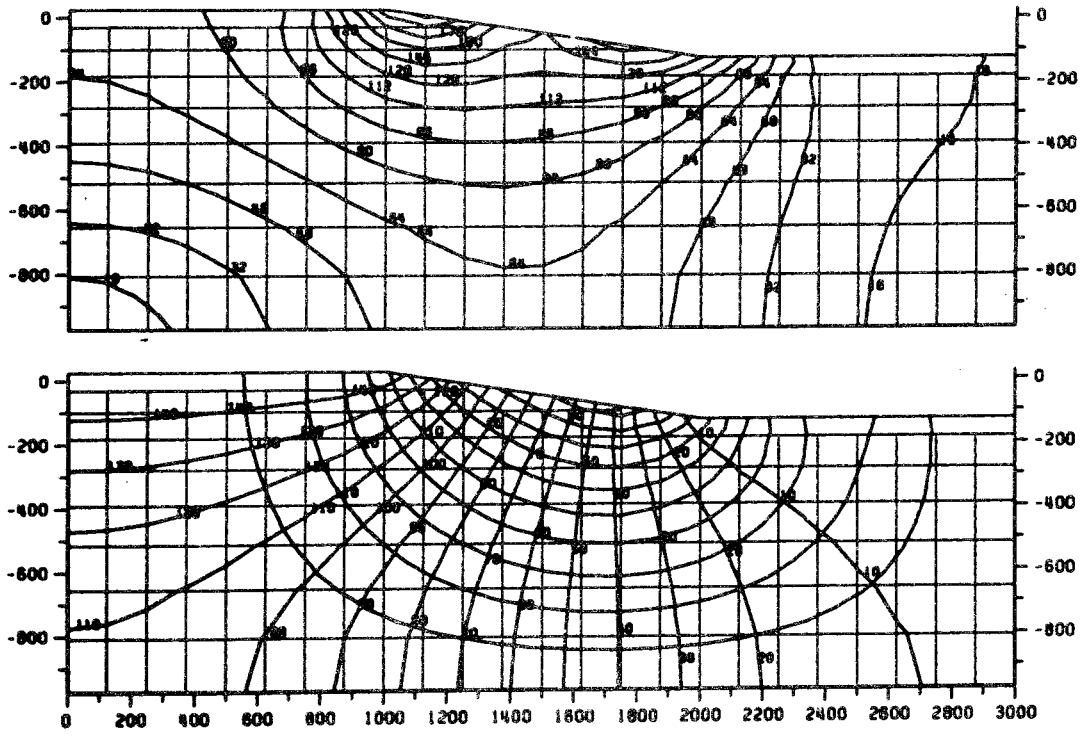

fig 23
exempel 23
Ib IIb IIIb
c = 150

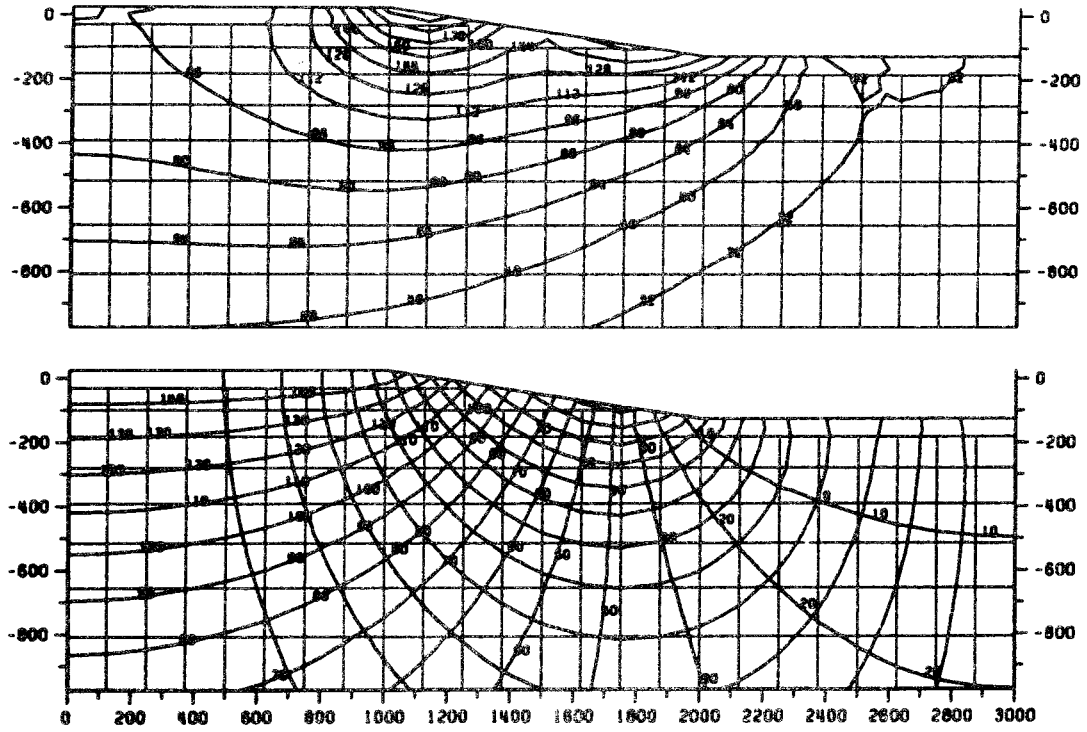

fig 24
exempel 24
Ib IIb IIIc
c = 150

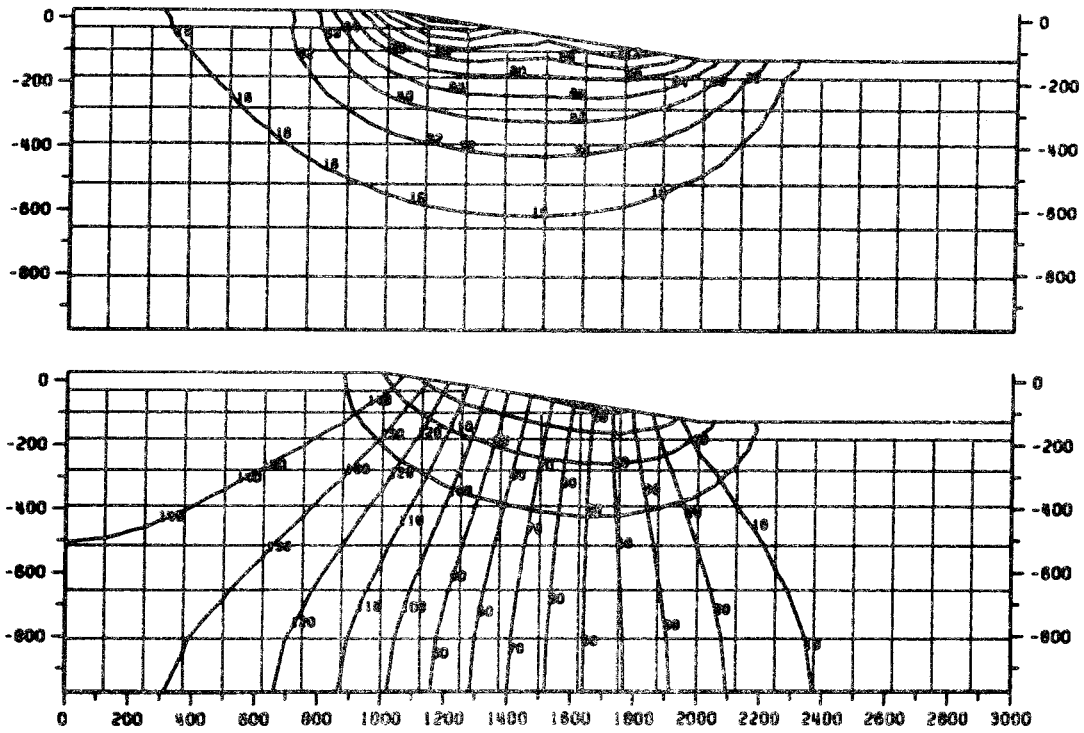

Table 1. Specific flow at left and right bottom corners fig. 25

Multiply by 10^{-9} to obtain dimensions $m^3/(m^2s)$

0	125	250	375	500	625	2375	2500	2625	2750	2875	3000	x-axis grid line number
Example 1.												
9.0	9.3	10.	12.	14.	16.	3.1	2.1	1.1	1.4	2.1	2.3	6
7.2	7.5	8.3	9.7	11.	13.	2.6	1.9	1.5	1.4	1.5	1.5	7
5.0	5.4	6.4	7.9	9.5	11.	2.3	1.8	1.4	1.2	1.0	.97	8
2.6	3.2	4.7	6.4	8.1	9.8	2.2	1.7	1.2	.89	.62	.50	9
0.0	2.0	3.9	5.8	7.7	9.3	2.1	1.6	1.2	.75	.37	0.0	10
Example 2.												
13.	13.	14.	15.	16.	17.	5.7	4.8	3.9	4.0	4.9	5.3	6
12.	12.	12.	13.	13.	14.	4.9	4.5	4.2	4.2	4.4	4.5	7
10.	10.	10.	10.	11.	11.	4.5	4.2	4.1	4.0	4.1	4.1	8
8.4	8.4	8.5	8.6	8.7	8.7	4.1	3.9	3.8	3.7	3.7	3.7	9
6.8	6.8	6.9	6.9	6.9	6.8	3.6	3.5	3.4	3.4	3.4	3.4	10
Example 3.												
1.5	1.7	2.1	2.9	4.1	5.6	.48	.24	.11	.34	.45	.43	6
1.0	1.2	1.5	2.0	2.7	3.6	.26	.13	.07	.13	.16	.15	7
.58	.69	.94	1.3	1.7	2.1	.17	.11	.086	.076	.068	.061	8
.24	.33	.53	.76	1.0	1.2	.11	.083	.060	.043	.029	.021	9
0.0	.14	.28	.43	.58	.72	.071	.051	.036	.024	.012	0.0	10
Example 3b.												
.12	.15	.25	.41	.71	1.2	.072	.069	.062	.10	.11	.088	6
.059	.078	.12	.20	.33	.49	.017	.006	.008	.020	.023	.017	7
.023	.033	.055	.088	.13	.18	.005	.002	.002	.004	.004	.003	8
.006	.011	.020	.031	.045	.060	.002	.001	.001	.001	.000	.000	9
0.0	.002	.006	.009	.013	.018	.000	.000	.000	.000	.000	0.0	10

0	125	250	375	500	625	2375	2500	2625	2750	2875	3000	x-axis grid line number
Example 8.												
24.	24.	24.	25.	27.	29.	29.	27.	25.	24.	23.	23.	6
22.	22.	23.	23.	24.	26.	26.	24.	23.	22.	22.	22.	7
20.	20.	21.	21.	22.	23.	23.	22.	21.	20.	20.	20.	8
18.	18.	18.	18.	19.	20.	20.	19.	18.	18.	18.	18.	9
15.	16.	16.	16.	16.	17.	17.	16.	16.	16.	15.	15.	10
Example 9.												
1.2	1.4	1.8	2.4	3.4	4.7	4.3	3.0	2.2	1.6	1.1	1.0	6
.9	1.0	1.3	1.8	2.5	3.4	3.2	2.3	1.6	1.2	.9	.7	7
.5	.6	.9	1.2	1.7	2.3	2.2	1.6	1.1	.8	.5	.4	8
.2	.3	.5	.7	1.1	1.4	1.4	1.0	.7	.4	.3	.2	9
0.0	.1	.2	.4	.6	.8	.8	.6	.4	.2	.1	0.0	10
Example 10.												
25.	26.	28.	32.	37.	44.	41.	33.	28.	24.	21.	20.	6
20.	21.	24.	28.	33.	40.	38.	31.	25.	21.	18.	17.	7
14.	16.	19.	24.	30.	36.	35.	27.	21.	17.	14.	13.	8
7.	10.	14.	20.	26.	33.	32.	25.	18.	13.	8.	7.	9
0.0	6.	12.	18.	25.	32.	31.	23.	17.	11.	5.	0.0	10
Example 11.												
49.	50.	51.	53.	56.	60.	59.	54.	51.	49.	46.	45.	6
46.	46.	47.	49.	51.	54.	54.	50.	48.	46.	44.	44.	7
42.	42.	43.	44.	45.	47.	48.	45.	43.	42.	41.	41.	8
37.	38.	38.	39.	40.	41.	41.	40.	38.	37.	37.	37.	9
33.	33.	33.	33.	34.	35.	35.	34.	33.	33.	32.	32.	10

0	125	250	375	500	625	2375	2500	2625	2750	2875	3000	x-axis grid line number
Example 12.												
2.7	3.0	3.8	5.1	7.2	9.9	8.0	5.5	4.1	2.9	2.0	1.7	6
1.9	2.2	2.8	8.9	5.4	7.3	6.3	4.4	3.1	2.2	1.6	1.4	7
1.2	1.4	1.9	2.7	3.7	5.5	4.4	3.2	2.2	1.5	1.1	.90	8
.50	.70	1.1	1.7	2.3	3.1	2.9	2.1	1.4	.93	.56	.40	9
0.0	.30	.62	.98	1.4	1.9	1.7	1.2	.84	.52	.24	0.0	10
Example 13.												
16.	16.	16.	17.	18.	20.	1.6	.86	.18	.88	1.4	1.5	6
12.	12.	13.	13.	14.	15.	1.2	.81	.59	.67	.80	.85	7
8.7	8.9	9.3	9.9	10.	11.	1.1	.83	.65	.56	.51	.49	8
4.5	4.7	5.5	6.5	7.5	8.3	1.1	.80	.60	.43	.30	.24	9
0.0	1.7	3.3	4.8	6.2	7.3	1.0	.78	.56	.37	.18	0.0	10
Example 14.												
19.	20.	20.	20.	21.	21.	2.3	1.6	.91	1.3	2.1	2.4	6
16.	16.	16.	17.	17.	16.	1.7	1.5	1.3	1.4	1.6	1.7	7
13.	13.	13.	13.	13.	12.	1.5	1.4	1.3	1.3	1.4	1.4	8
10.	10.	10.	10.	9.8	9.3	1.3	1.3	1.2	1.2	1.2	1.2	9
8.0	8.0	7.8	7.6	7.3	6.8	1.2	1.1	1.1	1.1	1.1	1.1	10
Example 15.												
3.3	3.5	3.8	4.5	5.5	6.7	.34	.19	.18	.35	.42	.39	6
2.2	2.3	2.5	2.9	3.5	4.0	.15	.060	.053	.11	.13	.12	7
1.2	1.3	1.4	1.7	2.0	2.3	.10	.065	.052	.054	.050	.045	8
.49	.54	.68	.86	1.0	1.2	.068	.049	.037	.028	.020	.014	9
0.0	.14	.28	.42	.55	.65	.042	.030	.022	.015	.008	0.0	10

0	125	250	375	500	625	2375	2500	2625	2750	2875	3000	x-axis grid line numb
Example 15b.												
.30	.33	.44	.63	.96	1.4	.065	.071	.064	.10	.11	.08	6
.14	.16	.21	.30	.42	.57	.013	.006	.010	.022	.023	.017	7
.059	.066	.088	.12	.16	.20	.004	.001	.002	.004	.004	.003	8
.016	.020	.028	.039	.052	.064	.001	.001	.000	.001	.000	.000	9
0.0	.003	.007	.010	.014	.018	.000	.000	.000	.000	.000	0.0	10
Example 16.												
33.	34.	35.	36.	38.	41.	4.	3.	2.	3.	4.	5.	6
26.	26.	27.	28.	29.	30.	2.	.	.	1.	1.	2.	7
17.	18.	19.	20.	21.	22.	1.	1.	.	.	.	.	8
9.	9.	11.	13.	15.	16.	1.	1.	.	.	.	.	9
0.0	3.	6.	9.	12.	14.	1.	1.	.	.	.	0.0	10
Example 17.												
40.	41.	41.	42.	43.	44.	6.	3.	1.	3.	5.	6.	6
34.	34.	34.	34.	34.	34.	3.	2.	1.	2.	3.	3.	7
27.	27.	27.	27.	26.	25.	3.	2.	2.	2.	2.	2.	8
21.	21.	21.	20.	19.	18.	2.	2.	2.	2.	2.	2.	9
16.	16.	15.	15.	14.	13.	2.	2.	2.	2.	2.	2.	10
Example 18.												
7.5	7.8	8.7	10.	12.	14.	1.4	1.5	1.4	1.8	1.9	1.7	6
4.9	5.1	5.6	6.5	7.7	8.9	.41	.29	.31	.51	.56	.50	7
2.7	2.8	3.2	3.7	4.4	5.0	.16	.36	.78	1.4	1.5	1.4	8
1.1	1.2	1.5	1.9	2.3	2.6	.10	.064	.055	.058	.048	.037	9
0.0	.31	.63	.93	1.2	1.4	.068	.046	.036	.029	.017	0.0	10

0	125	250	375	500	625	2375	2500	2625	2750	2875	3000	x-axis grid line number
Example 19.												
26.	26.	27.	28.	31.	33.	15.	12.	10.	8.	7.	7.	6
21.	21.	22.	23.	25.	28.	13.	11.	8.	7.	6.	6.	7
15.	15.	16.	18.	20.	22.	12.	9.	7.	6.	4.	4.	8
8.	8.	10.	12.	14.	17.	11.	9.	6.	4.	3.	2.	9
0.0	3.	6.	9.	12.	15.	11.	8.	6.	3.	1.	0.0	10
Example 20.												
40.	40.	41.	42.	43.	44.	17.	15.	14.	13.	13.	13.	6
37.	37.	37.	38.	38.	39.	15.	14.	13.	12.	12.	12.	7
32.	33.	33.	33.	33.	33.	13.	12.	11.	11.	11.	11.	8
28.	28.	28.	28.	28.	28.	11.	10.	10.	10.	9.	9.	9
23.	23.	23.	23.	23.	23.	9.	9.	8.	8.	8.	8.	10
Example 21.												
3.3	3.4	3.8	4.5	5.5	6.9	3.3	2.3	1.6	1.1	.8	.7	6
2.3	2.4	2.7	3.2	3.9	4.8	2.5	1.7	1.2	.8	.6	.5	7
1.3	1.4	1.6	2.0	2.5	3.0	1.7	1.2	.8	.5	.4	.3	8
.5	.6	.8	1.1	1.4	1.7	1.1	.8	.5	.3	.2	.1	9
0.0	.1	.3	.5	.7	.9	.6	.4	.3	.1	.	0.0	10
Example 22.												
52.	52.	54.	57.	62.	68.	29.	23.	19.	16.	14.	13.	6
42.	43.	45.	48.	52.	57.	27.	21.	17.	14.	12.	11.	7
30.	31.	33.	36.	40.	45.	25.	19.	14.	11.	9.	8.	8
16.	17.	20.	24.	30.	35.	23.	17.	12.	8.	5.	4.	9
0.0	6.	12.	18.	25.	31.	22.	17.	11.	7.	3.	0.0	10

0	125	250	375	500	625	2375	2500	2625	2750	2875	3000	x-axis grid line number
Example 23.												
82.	82.	83.	85.	87.	90.	35.	31.	29.	27.	26.	25.	6
75.	75.	76.	77.	78.	80.	32.	29.	26.	25.	24.	24.	7
66.	67.	67.	67.	68.	68.	28.	25.	24.	23.	22.	22.	8
57.	57.	57.	57.	57.	57.	23.	22.	21.	20.	19.	19.	9
48.	48.	48.	48.	47.	47.	19.	18.	17.	17.	17.	16.	10
Example 24.												
6.9	7.2	8.0	9.4	11.	14.	6.2	4.2	3.0	2.1	1.4	1.1	6
4.8	5.0	5.7	6.7	8.1	10.	4.9	3.4	2.3	1.6	1.1	.97	7
2.9	3.0	3.5	4.2	5.2	6.4	3.5	2.4	1.6	1.1	.76	.63	8
1.2	1.4	1.7	2.3	2.9	3.7	2.2	1.6	1.1	.68	.40	.28	9
0.0	.36	.74	1.1	1.6	2.1	1.4	.95	.63	.38	.18	0.0	10

fig 32

example 1

K = 0.000 001

ϕ = 0.001

Lines of equal times of flow to surface

times in years

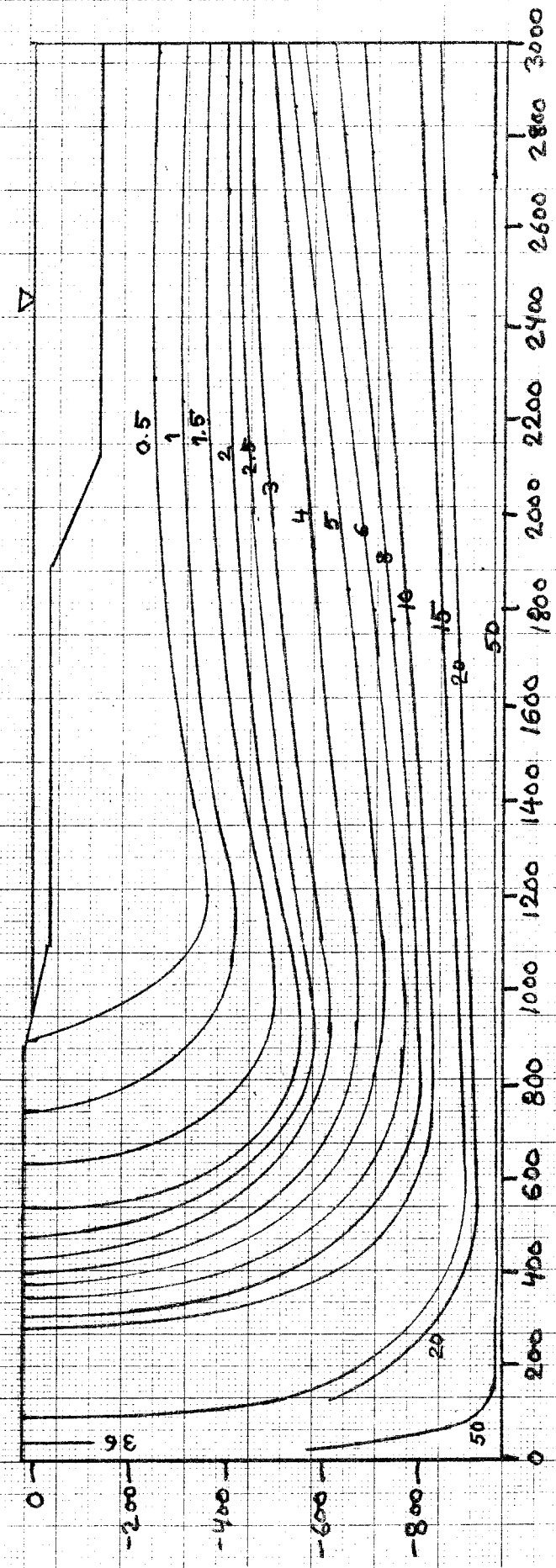

fig 33
example 2

K = 0.000 001
ϕ = 0.001

Lines for equal times of flow to surface

times in years

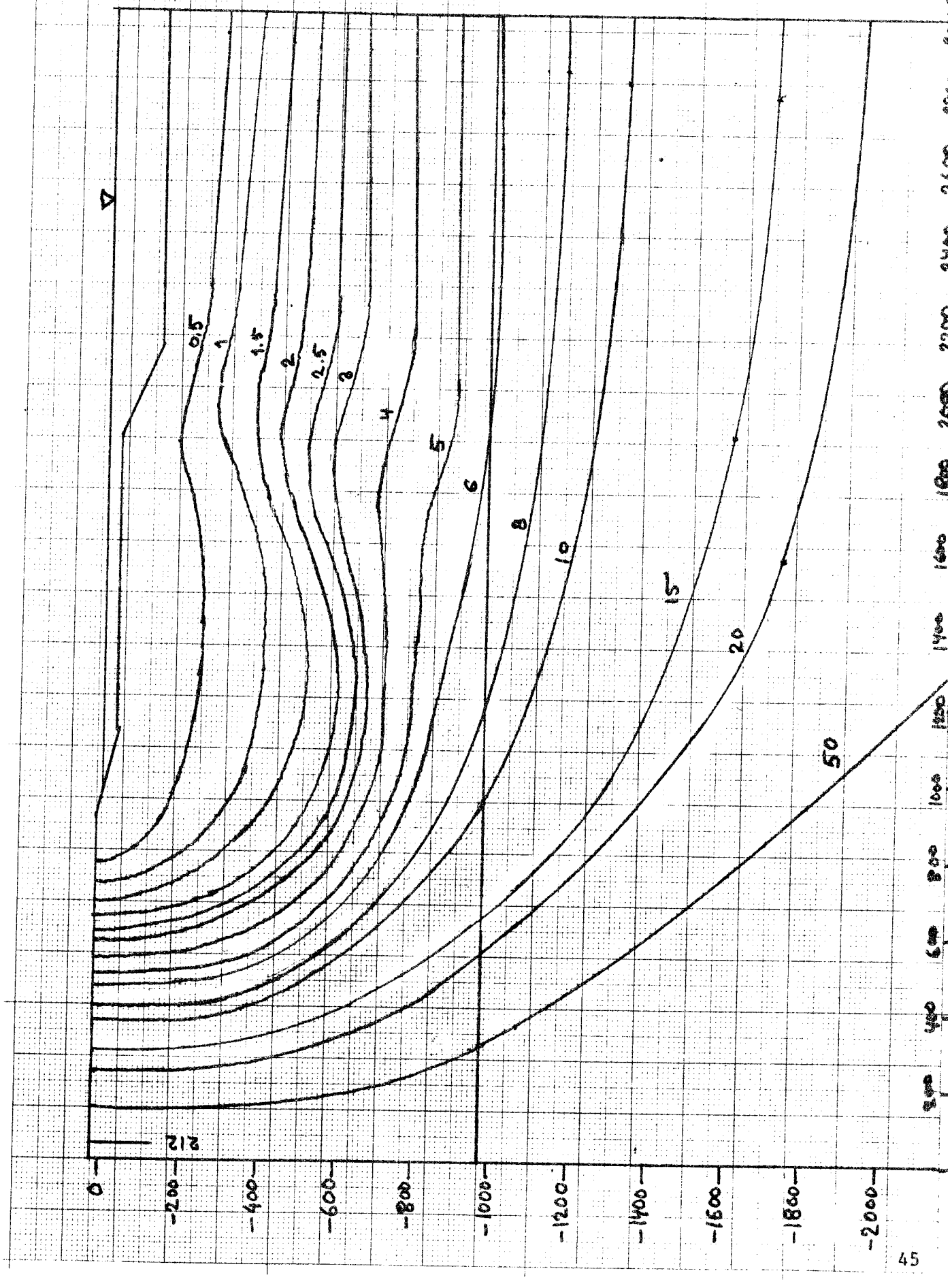

SELTE ⊗
4441

fig 34

example 3

$K = 0.000\ 001 \cdot 10^{0.0013z}$

Lines of equal times of flow to surface

times in years

$\phi = 0.001$

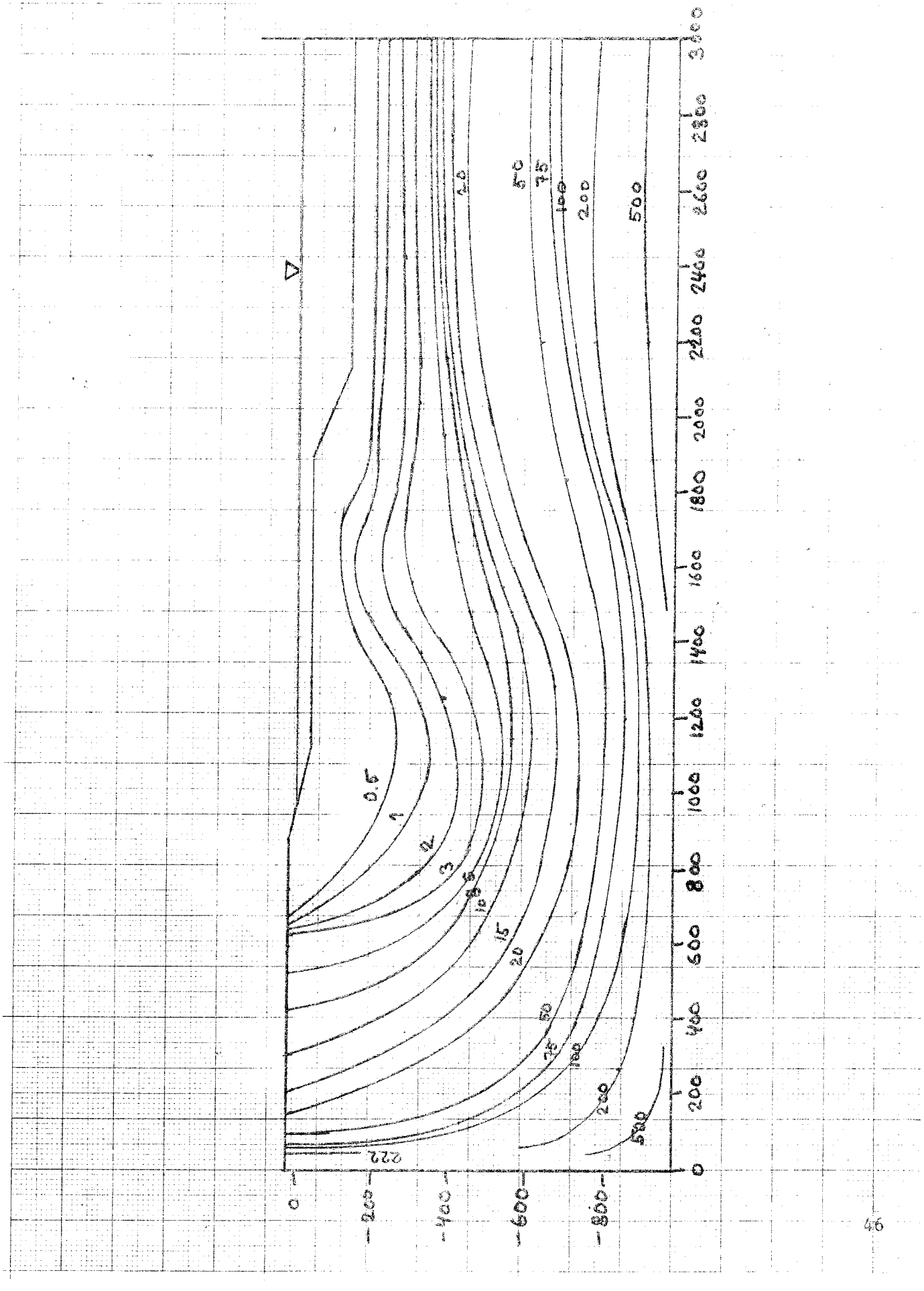

fig 35

example 3b

Lines of equal times of flow to surface

times in years

$K = 0.000\ 001 \cdot 10^{0.0030z}$

$\phi = 0.001$

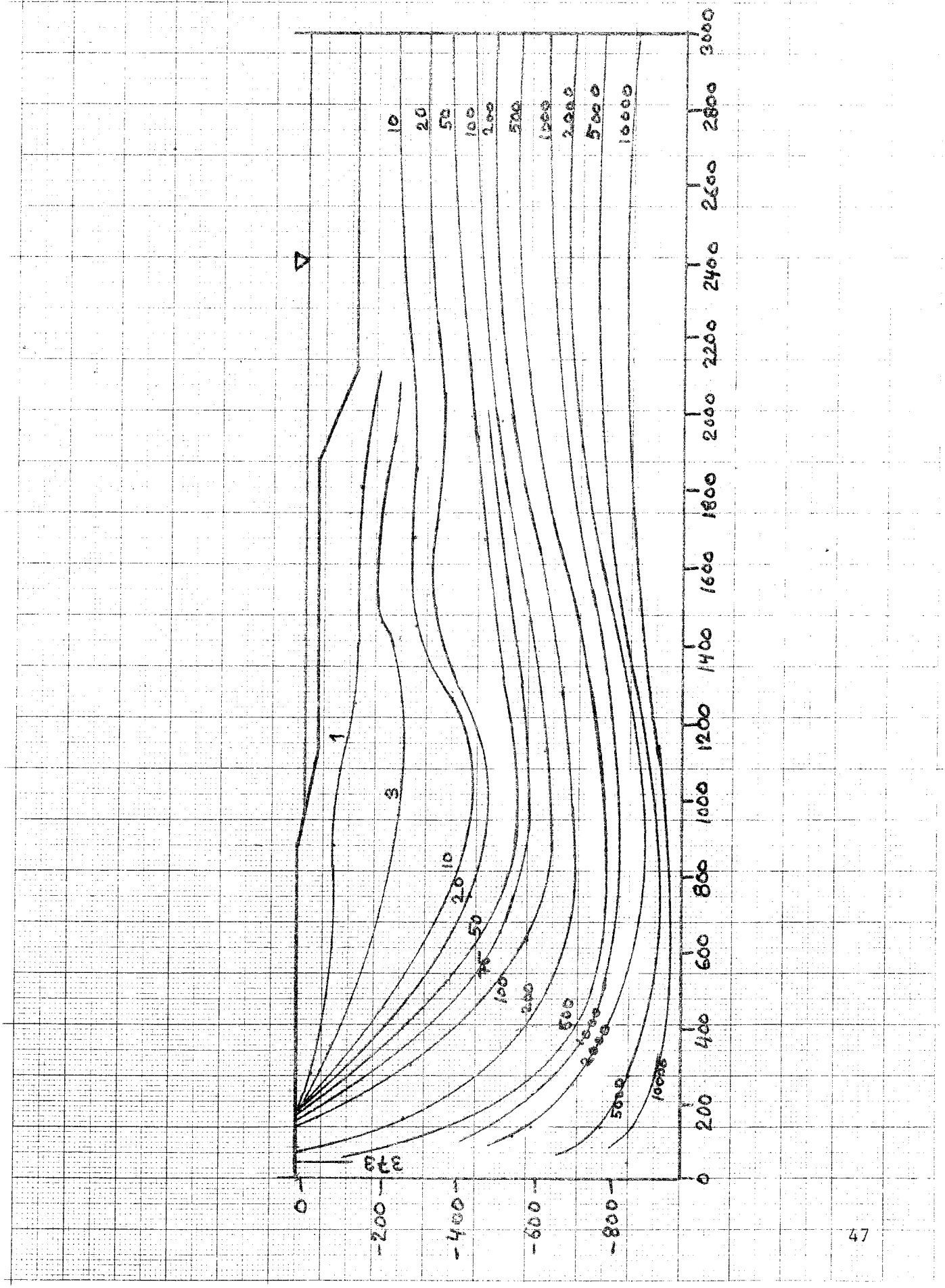

fig 36
example 7

K = 0.000 001
ϕ = 0.001

Lines of equal times of flow to surface

times in years

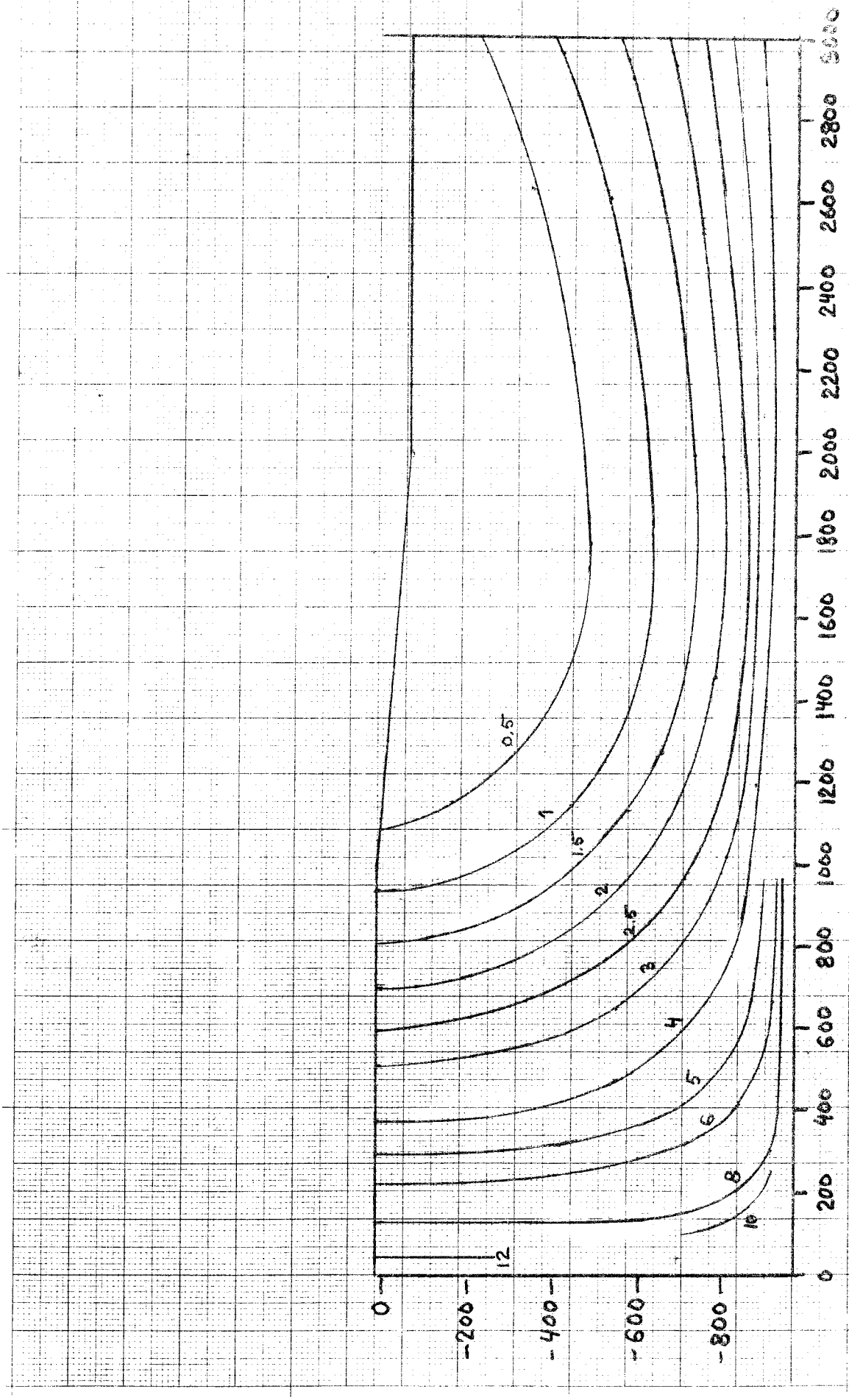

fig 37

example 15

$K = 0.000\ 001 \cdot 10^{0.0013z}$

$\phi = 0.001$

Lines of equal times of flow to surface

times in years

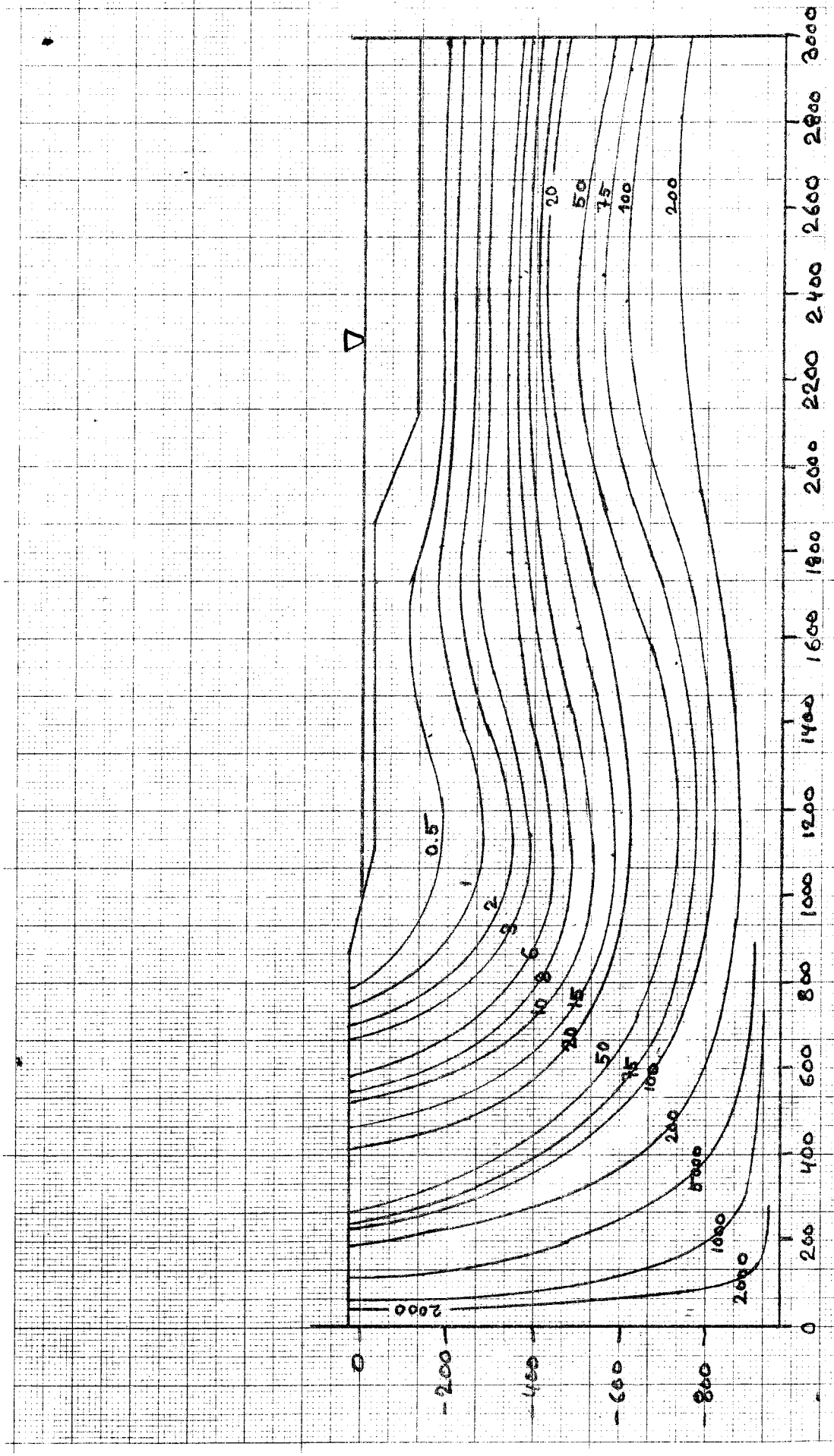

fig 38

example 15b

List of equal times of flow to surface

$K = 0.000\ 001 \cdot 10^{0.0030z}$

$\phi = 0.001$

times in years

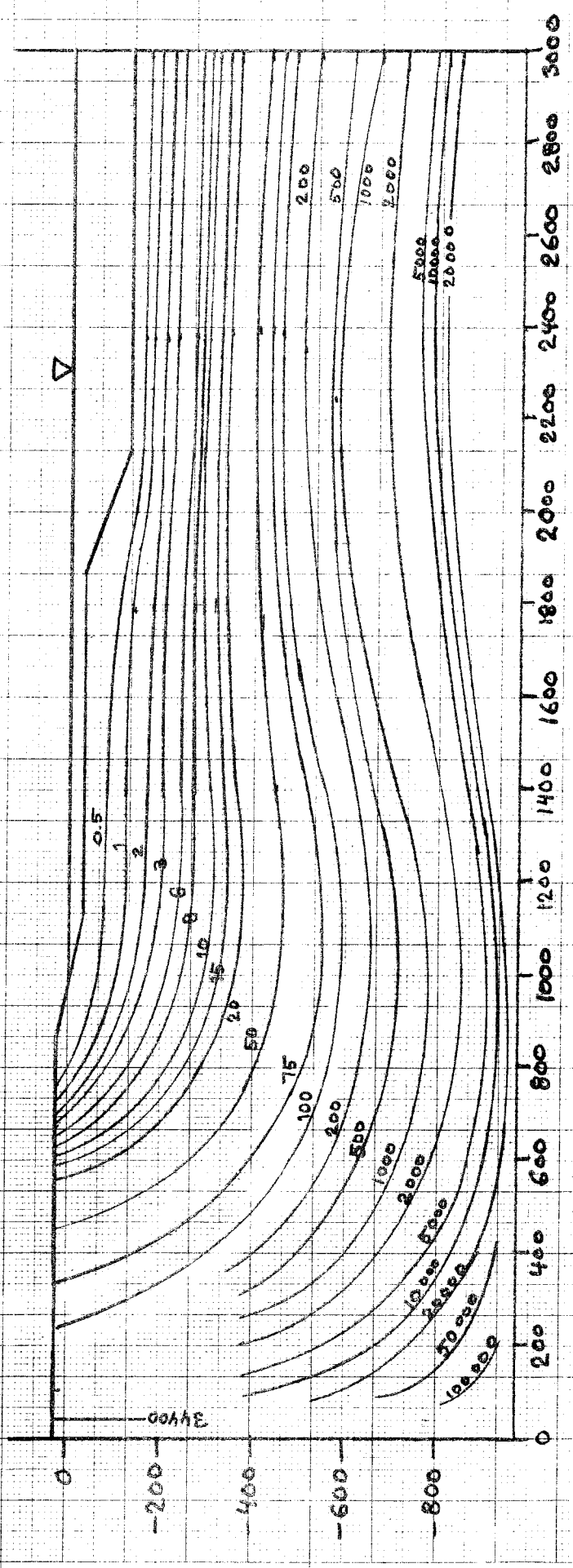

fig 39 - 40

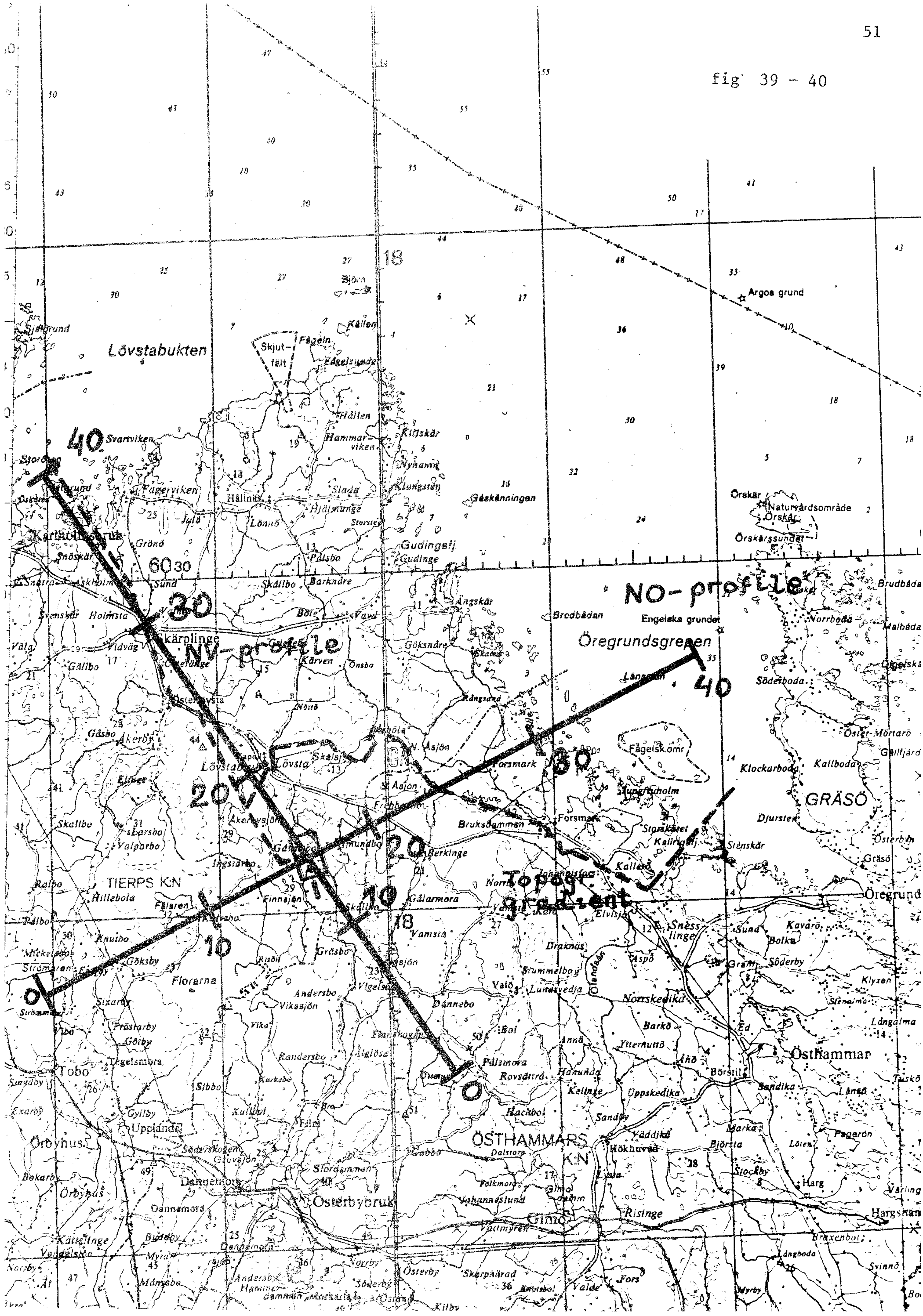
NV-profile
NO-profile
Topogr. gradient
Lövstabukten
Öregrundsgrepen
GRÄSÖ
TIERPS K:N
ÖSTHAMMARS K:N
Östhammar
Öregrund
Forsmark
Skärplinge
Gimo
Österbybruk
Dannemora
Örbyhus

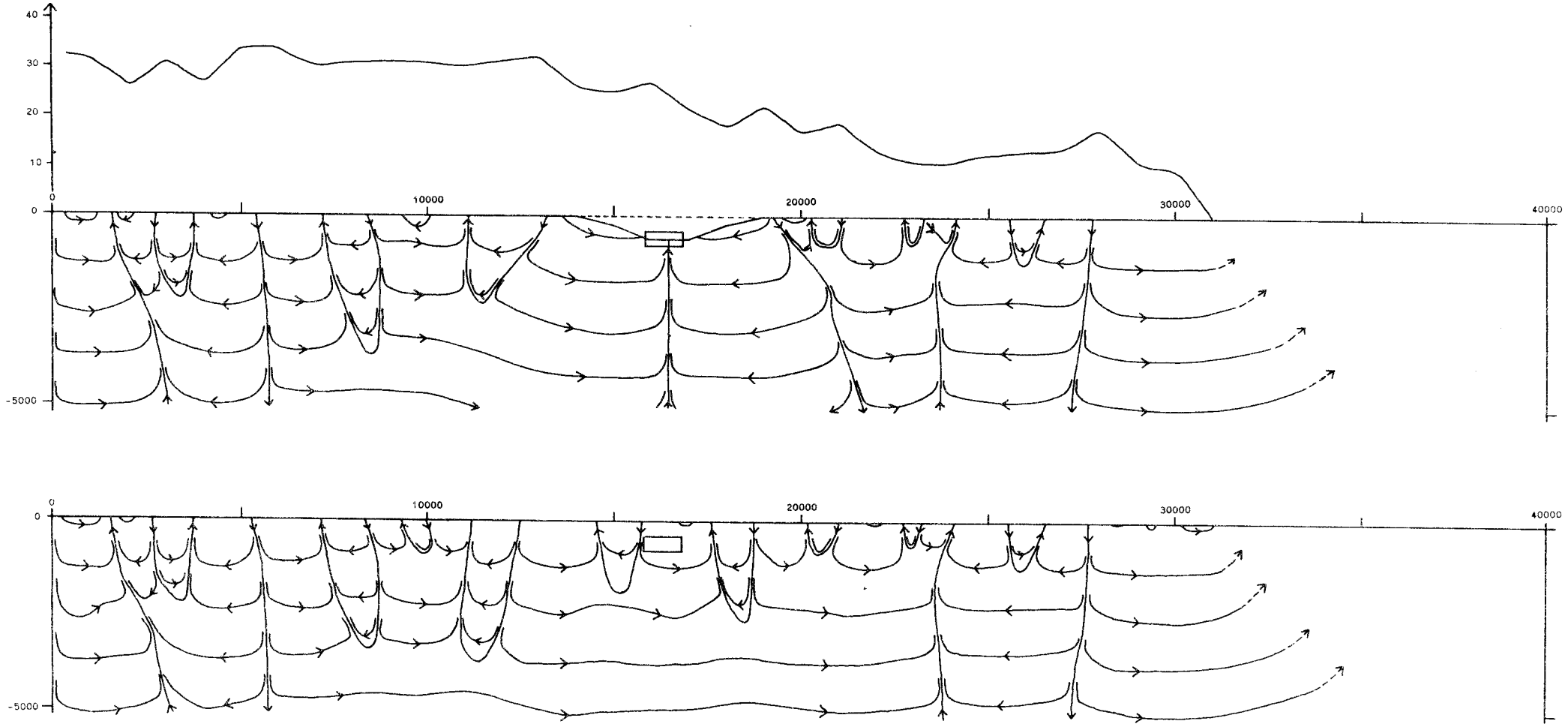

Fig 41. At top: NE-profile. $K = 0.000001 \cdot 10^{0.0030z}$
No bottom
Groundwater level lowered to a depth of 600 metres around a repository

Fig 42a. At bottom: NE-profile. $K = 0.000001 \cdot 10^{0.0030z}$
No bottom
Groundwater level not lowered

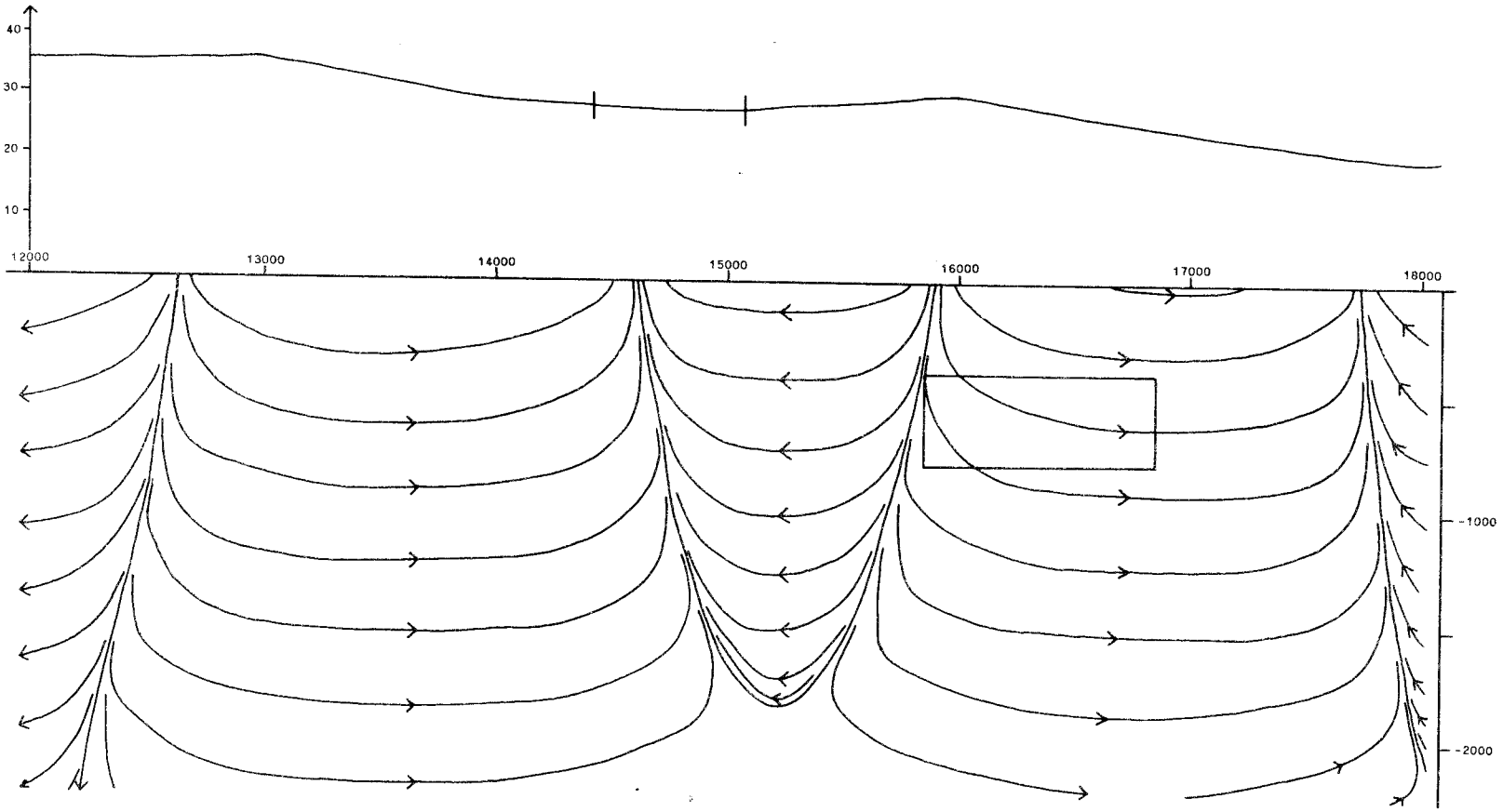

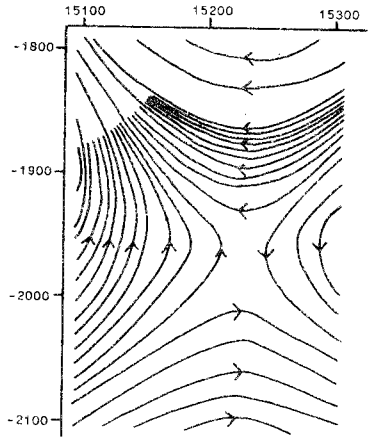

Fig. 42b. At left: special from fig. 42a.

Fig. 42c. At right: special from fig. 42b.

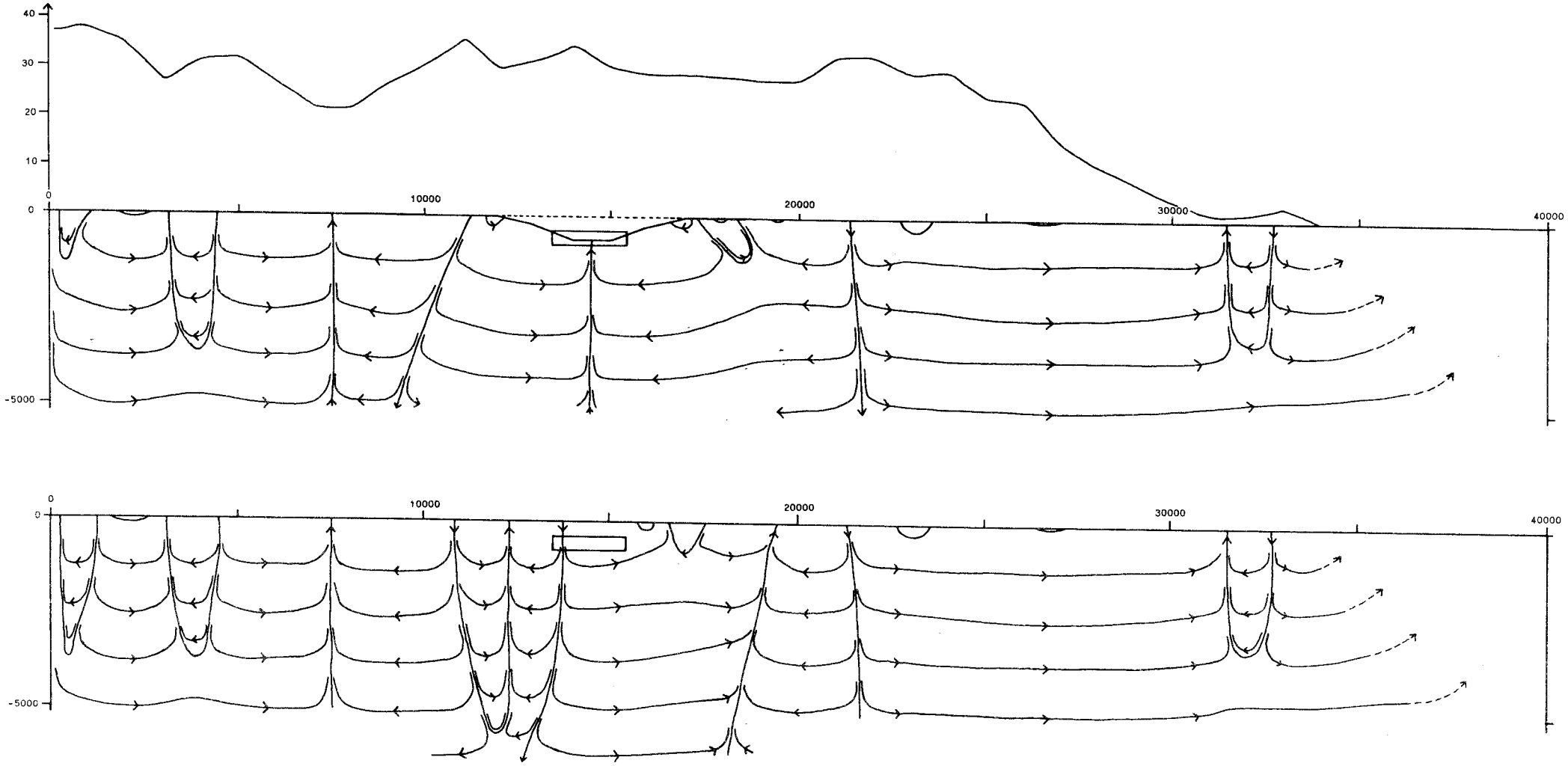

Fig 43. At top: NW-profile. $K = 0.000001 \cdot 10^{0.0030z}$
No bottom
Groundwater level lowered to a depth of 600 metres around a repository

Fig 44. At bottom: NW-profile. $K = 0.000001 \cdot 10^{0.0030z}$
No bottom
Groundwater level not lowered

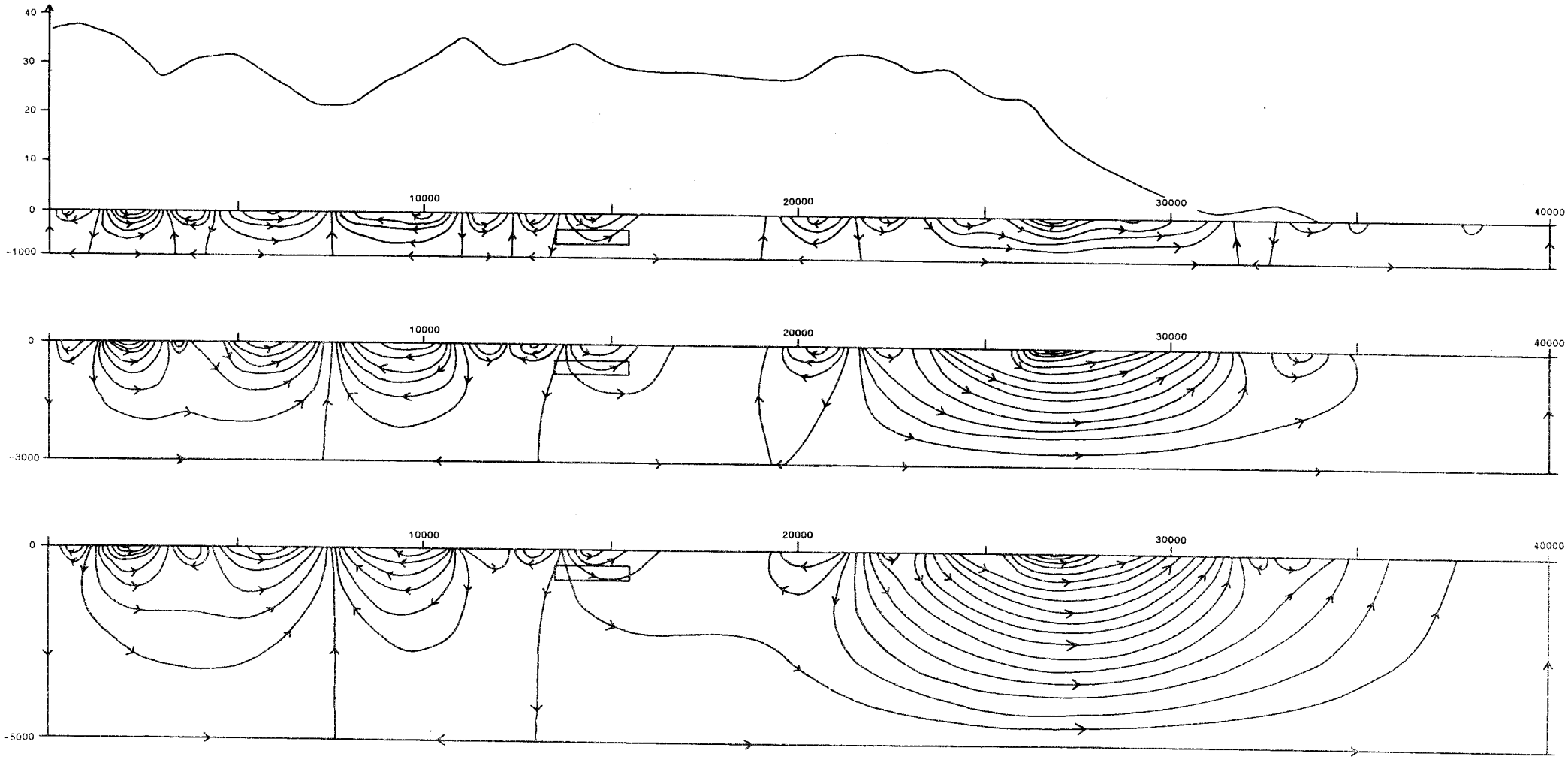

Fig. 45. NW-profile. K = 0.000001 Impervious bottom at 1000 metres depth (at top)
3000 metres depth (centre)
5000 metres depth (at bottom)

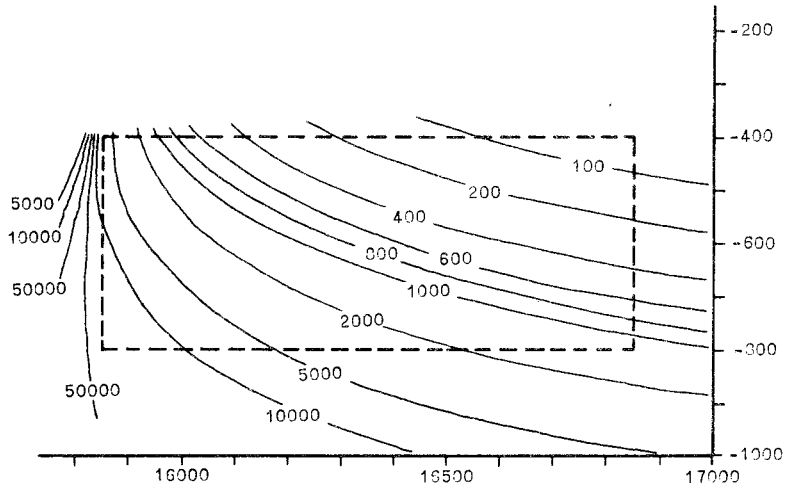

Fig 46. FINNSJÖN NE-profile
Groundwater not lowered
Time needed for flow to ground surface (years)
$K = 0.000001 \cdot 10^{0.0030z}$ $\phi = 0.001$

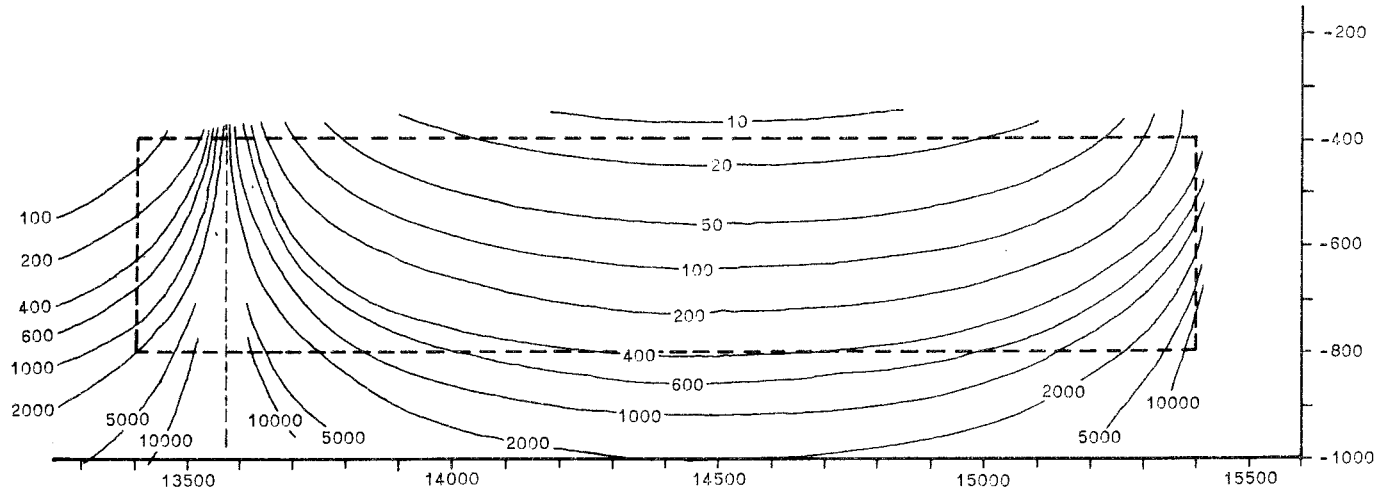

Fig 47. FINNSJÖN NW-profile
Groundwater not lowered
Time needed for flow to ground surface (years)
$K = 0.000001 \cdot 10^{0.0030z}$ $\phi = 0.001$

APPENDIX

Analytical solutions for groundwater flow obeying Darcy's law.

According to Darcy, groundwater flow in an isotropic medium obeys

$$\vec{q} = -K \cdot \nabla\varphi \tag{1}$$

If the water is considered incompressible, we also have the following law of continuity:

$$\nabla \cdot \vec{q} = 0 \tag{2}$$

The permeability K is supposed to vary only with z, so that K=K(z) and $K_z = K'(z)$. Relations (1) and (2) give

$$\varphi_{xx} + \varphi_{yy} + \varphi_{zz} + (K'/K)\varphi_z = 0 \tag{3}$$

If K is constant we obtain the Laplace-equation, but this is of no further significance.

The solutions given in the following are essentially 2-dimensional. The first case considers flow in the x-z-plane when the geometry is degenerate in the y-dimension, the second flow in the r-z-plane (cylindrical coordinates) when the geometry is symmetrical around the z-axis.

The introduction of the boundary conditions for equation (3) is facilitated by using the streamfunction ψ. ψ can be constructed in the following way: We assume a function $\alpha(x,z)$ such that

$$\psi_x = \alpha \cdot \varphi_z \tag{4}$$

In order that the equipotential lines and the streamlines be orthogonal, we must have

$$\nabla\psi \cdot \nabla\varphi = 0 \tag{5}$$

which immediately gives

$$\psi_z = -\alpha \cdot \varphi_x \tag{6}$$

Calculation of the second derivatives gives

$$\begin{aligned} &\varphi_{xx} + \varphi_{zz} + (\alpha_x/\alpha)\varphi_x + (\alpha_z/\alpha)\varphi_z = 0 \\ &\psi_{xx} + \psi_{zz} - (\alpha_x/\alpha)\psi_x - (\alpha_z/\alpha)\psi_z = 0 \end{aligned} \tag{7}$$

We see that φ and ψ satisfy the same equation (the Laplace-equation) only if α is a constant. If the equation for φ is given, we can determine α by identifying coefficients.

Case 1. 2-dimensional flow

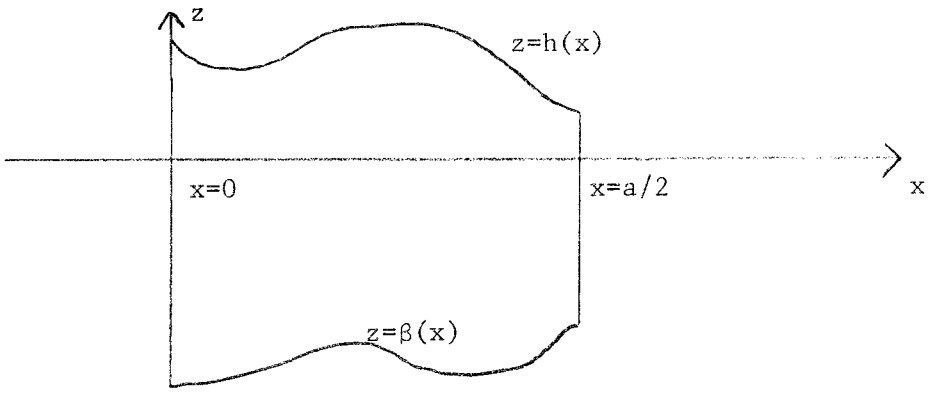

The 2-dimensional flow implies $\varphi=\varphi(x,z)$ and $\varphi_{yy}=0$. We assume a solution $\varphi(x,z)=f(x)g(z)$ which gives

$$\frac{g''(z)}{g(z)} + \frac{K'(z)}{K(z)}\frac{g'(z)}{g(z)} = -\frac{f''(x)}{f(x)} = \omega^2 \tag{8}$$

where the constant ω^2 is due to the fact that a variation of x does not affect the left side of the equation. (8) gives us the following equations:

$$f''(x) + \omega^2 f(x) = 0 \tag{9}$$

$$g''(z) + \frac{K'(z)}{K(z)} g'(z) - \omega^2 g(z) = 0 \tag{10}$$

Although solutions of (10) are known for several functions K(z), we will only consider the case $K(z) = c\cdot e^{2\mu z}$. (9) and (10) then give

$$\varphi(x,z) = e^{-\mu z}\,[C\, e^{\eta z} + D\, e^{-\eta z}][\cos \omega x + B \sin \omega x] \tag{11}$$

$$\eta = (\omega^2+\mu^2)^{1/2}$$

We also obtain $\alpha_x/\alpha = 0$; $\alpha_z/\alpha = 2\mu$ and $\alpha = c\cdot e^{2\mu z}$ from which we conclude that if $\omega \neq 0$

$$\psi(x,z) = ce^{\mu z}[\frac{\mu-\eta}{\omega} C\, e^{\eta z} + \frac{\mu+\eta}{\omega} D\, e^{-\eta z}][\sin \omega x - B \cos \omega x] \tag{12}$$

If $\omega = 0$, we have

$$\psi(x,z) = 2\mu c D x$$

We can now introduce the boundary conditions. $x = 0$, $x = a/2$ and $z = \beta(x)$ are all parts of the same streamline. Assuming $\psi(0,z) = 0$ we must have $B = 0$. $\psi(a/2,z) = 0$ then gives $\omega = \omega_k = 2k\pi/a$ for all natural numbers $k \neq 0$. If $k = 0$ we have $D = 0$. We finally obtain the general solution as a linear combination of the given solutions for different ω_k:

$$\varphi(x,z) = e^{-\mu z} \sum_{k=0}^{\infty} [C_k e^{\eta_k z} + D_k e^{-\eta_k z}] \cos \omega_k x$$

$$\psi(x,z) = ce^{\mu z} \sum_{k=1}^{\infty} \frac{1}{\omega_k} [(\mu-\eta_k)C_k e^{\eta_k z} + (\mu+\eta_k)D_k e^{-\eta_k z}] \sin \omega_k x \qquad (13)$$

$$\eta_k = (\omega_k^2 + \mu^2)^{1/2}$$

$$D_o = 0$$

Introducing the boundaryconditions at the top and the bottom gives

$$\varphi[x,h(x)] = \alpha(x)$$

$$\psi[x,\beta(x)] = 0 \qquad (14)$$

If $h(x)$, $\alpha(x)$ and $\beta(x)$ are known for $x=x_j$, $j=1,2,\ldots,m$, we can use the fact that the sums for φ and ψ must converge to obtain an approximate solution. Writing

$$\varphi_N[x_j,h(x_j)] = \sum_{k=0}^{N} a_{jk}C_k + \sum_{k=0}^{N} b_{jk}D_k = \alpha(x_j)$$

$$\psi_N[x_j,\beta(x_j)] = \sum_{k=1}^{N} c_{jk}C_k + \sum_{k=1}^{N} d_{jk}D_k = 0 \qquad (15)$$

we obtain a system of linear equations in C_k and D_k which can be solved under certain conditions. If these conditions are favorable, and if the convergence of the sums (13) is fast enough, the approximation will be good.

Extra difficulties are introduced when $|\beta(x)|$ is large. In this case we use a horisontal bottom $\beta(x) = \beta$. $\psi[x,\beta(x)]$ then becomes an ordinary fourierseries which sums to zero giving

$$D_k = -\frac{\mu-\eta_k}{\mu+\eta_k} C_k e^{2\eta_k \beta} \qquad k \neq 0 \qquad (16)$$

Substituting (16) into (13) and taking the limit $\beta \to -\infty$ gives

$$\varphi_\infty(x,z) = e^{-\mu z} \sum_{k=0}^{\infty} C_k e^{\eta_k z} \cos \omega_k x$$
$$\psi_\infty(x,z) = ce^{\mu z} \sum_{k=1}^{\infty} \frac{\mu-\eta_k}{\omega_k} C_k e^{\eta_k z} \sin \omega_k x \qquad (17)$$

The coefficients C_k are determined in the same way as before, i.e. by solving the equation

$$\varphi_{\infty N}[x_j, h(x_j)] = \sum_{k=0}^{N} a_{jk} C_k = \alpha(x_j) \qquad (18)$$

Case 2. Flow symmetrical around the z-axis

Introducing cylindrical coordinates, equation (3) is transformed into

$$\varphi_{rr} + \varphi_{zz} + \frac{1}{r}\varphi_r + \frac{K'(z)}{K(z)}\varphi_z = 0 \qquad (19)$$

Following the procedure of case 1, we assume a solution $\varphi(r,z) = f(r)g(z)$ giving the two equations

$$f''(r) + \frac{1}{r} f'(r) + \omega^2 f(r) = 0 \qquad (20)$$

$$g''(z) + \frac{K'(z)}{K(z)} g'(z) - \omega^2 g(z) = 0 \qquad (21)$$

As in case 1 we only consider $K(z) = c \cdot e^{2\mu z}$. Solving (20) and (21), we obtain

$$\varphi(r,z) = e^{-\mu z}[C\, e^{\eta z} + D\, e^{-\eta z}][J_o(\omega r) + B\, N_o(\omega r)]$$
$$\eta = (\omega^2+\mu^2)^{1/2} \qquad (22)$$

where J_o and N_o are Bessel- and Neumann functions. We can immediately reject N_o by setting $B = 0$ as N_o is infinite on the z-axis. Equations (7) and (19) give $\alpha_r/\alpha = 1/r$; $\alpha_z/\alpha = 2\mu$ and $\alpha = cre^{2\mu z}$ from which we conclude that if $\omega \neq 0$

$$\psi(r,z) = -ce^{\mu z}[\frac{\mu-\eta}{\omega} C e^{\eta z} + \frac{\mu+\eta}{\omega} D e^{-\eta z}] r J_1(\omega r) \qquad (23)$$

If $\omega = 0$ we have

$$(r,z) = -c\mu D r^2$$

As we want a finite potential when z tends to the negative infinity, we put D = 0 when $\omega = 0$. Assuming $\psi(a/2,z) = 0$, we obtain $\omega = \omega_k$ = = the k:th root $J_1(\omega_k) = 0$. Both $J_o(\omega_k r)$ and $J_1(\omega_k r)$ can be shown to be orthogonal on the interval (0,1) relative r. We obtain the general solution as

$$\varphi(r,z) = e^{-\mu z} \sum_{k=0}^{\infty} [\, C_k e^{\eta_k z} + D_k e^{-\eta_k z} \,] J_o(\omega_k r)$$

$$\psi(r,z) = ce^{\mu z} \sum_{k=1}^{\infty} \frac{1}{\omega_k} [\, (\mu-\eta_k) C_k e^{\eta_k z} + (\mu+\eta_k) D_k e^{-\eta_k z} \,] r J_1(\omega_k r) \qquad (24)$$

$$\eta_k = (\omega_k^2 + \mu^2)^{1/2}$$

$$D_o = 0$$

Comparing with the results of case 1, we notice that we can obtain (24) from (13) simply by replacing $\cos \omega x$ by $J_o(\omega r)$ and $\sin \omega x$ by $r J_1(\omega r)$. In determining the coefficients C_k and D_k we proceed as in case 1.

Anisotropic flow

In this case K in (1) is a tensor. We will only consider the case when K is diagonal and a function of z only:

$$K = \begin{bmatrix} a(z) & 0 \\ 0 & c(z) \end{bmatrix}$$

In this case equation (3) becomes

$$\varphi_{xx} + (c/a)\varphi_{zz} + (c'/a)\varphi_z = 0$$

where c' is the derivative of c(z). A transformation of the z-axis according to $u = z\sqrt{\xi}$ gives

$$\varphi_{xx} + (c/a)\xi\varphi_{uu} + (c'/a)\sqrt{\xi}\varphi_u = 0$$

$\xi = a/c$ puts this equation in the same form as (3):

$$\varphi_{xx} + \varphi_{uu} + \frac{c'}{c\sqrt{\xi}} \varphi_u = 0$$

We conclude that if we want to solve a problem with a permeability relation $a(z) = \xi \cdot c(z)$ with $\mu = \mu_0$ over a region $x_1<x<x_2$, $z_1<z<z_2$, we solve the corresponding isotropic problem with $\mu = \mu_0\sqrt{\xi}$ over the region $x_1<x<x_2$, $z_1/\sqrt{\xi} < z < z_2/\sqrt{\xi}$.

1978.05.18

INVESTIGATIONS OF GROUNDWATER FLOW IN ROCK AROUND REPOSITORIES FOR NUCLEAR WASTE

II. Local groundwater depression around a repository

Roger Thunvik
Royal Institute of Technology
Stockholm
Sweden

Introduction

Future plans for the ultimate storage of waste obtained from nuclear plants call for underground repositories in bedrock deep beneath the surface of the ground. Since most hardrock formations are fractured water will flow into the repositories during the period of construction and operation of the storage facilities.

In a study of groundwater flow under undisturbed conditions in an unconfined aquifer, one can ordinarily assume that the groundwater table will follow the topography. This is based on an assumption that the precipitation will be sufficient to replenish the aquifer continuously. However, human intervention such as the pumping out of water from tunnels and the like during construction can have a considerable effect on the groundwater level. It is therefore of interest to determine the variation with time and space of the groundwater table and, if the intervention is to continue throughout a long period of time, to determine the water table at steady state flow conditions.

It is the purpose of this investigation to study the variation in time of the groundwater table as a function of hydraulic conductivity, porosity and accretion to the groundwater table due to precipitation.

Assumptions

The present investigation has been based on a proposal which calls for a system of parallel, horizontal storage tunnels. The distance between two adjacent tunnels is about 25 metres (centre to centre). Each tunnel has a cross-section of 3.5 x 3.5 metres and a length of up to 1000 metres. It is assumed that the groundwater flow in the area around the tunnels can be considered two-dimensional since the characteristic length of the tunnels is large. Alternatively, the flow in intersecting vertical fracture zones (where the flow can also be considered two-dimensional) can be studied.

In the initial stage the groundwater table coincides with the surface of the ground which is assumed to be horizontal, i.e. $\eta(x,0)=h_1$ (see Figure 2). Moreover, it is assumed that grounwater accretion attributable to percolation is evenly distributed in both time and space. If the groundwaterlevel were to rise high enough to create surface pools, it is assumed that they would either run off or evaporate.

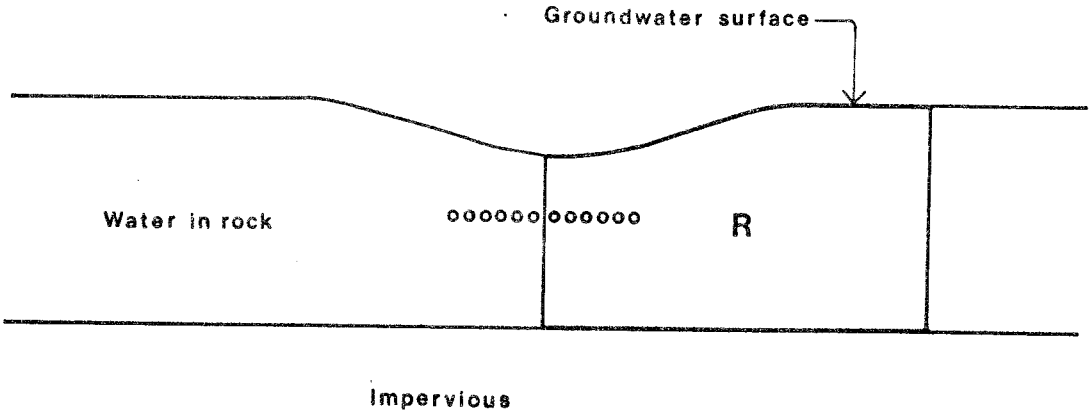

Figure 1. Crosss-section of rock being drained, showing tunnels and region R in Figure 2.

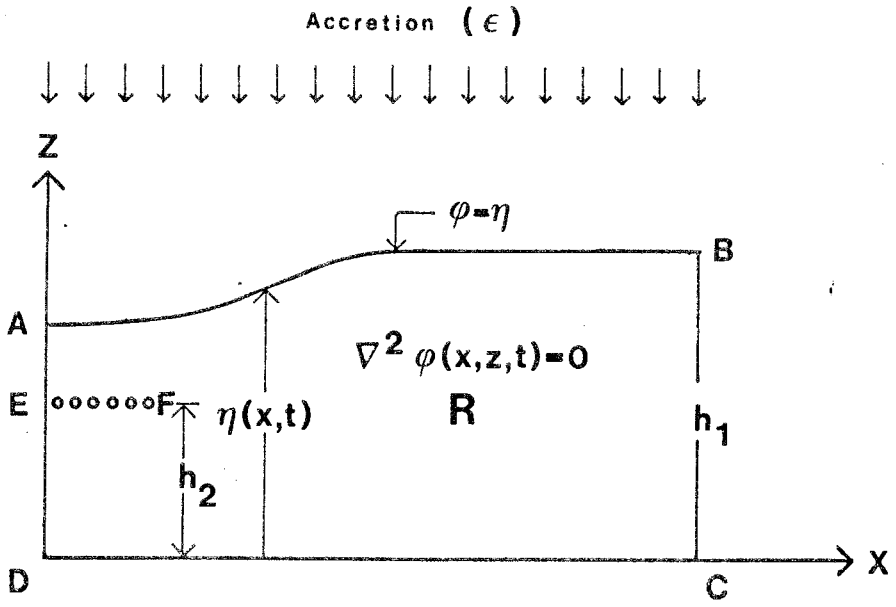

Figure 2. Geometry of the flow domain. Region R is a two-dimensional vertical cross-section.

Mathematical formulation of the problem

The flow is assumed to obey Darcy's law which, together with the continuity equation for a homogeneous, isotropic, incompressible medium and incompressible fluid flow gives the Laplace equation

$$\nabla^2\varphi(x,z,t)=0 \tag{1}$$

where φ is piezometric head ($=p/\gamma + z$), p is pressure, γ is specific weight of the fluid, t is time, x and z are co-ordinates in a Cartesian co-ordinate system. The following boundary conditions are applied to equation (1) (see Figure 2):

(i) Unsteady phreatic surface (A-B)

$$\frac{\phi}{K}\frac{\partial \eta(x,t)}{\partial t} - \frac{\partial \varphi}{\partial x}\frac{\partial \eta}{\partial x} + \frac{\partial \varphi}{\partial z} + \frac{\varepsilon}{K} = 0 \tag{2}$$

where ϕ is porosity, η is elevation of the phreatic surface above a reference plane and ε is net accretion to the phreatic surface.

(ii) Streamline (B-C)

$$\frac{\partial \varphi}{\partial x} = 0 \tag{3}$$

(iii) Streamline (C-D)

$$\frac{\partial \varphi}{\partial z} = 0 \tag{4}$$

(iv) Streamline (A-D)

$$\frac{\partial \varphi}{\partial x} = 0 \tag{5}$$

(v) Constant piezometric head at the tunnel boundaries (E-F)

$$\varphi = \frac{p_g}{\gamma} + z \tag{6}$$

p_g is air pressure in the tunnels.

The complete problem to be solved thus consists of (1)-(6) inclusive, with $\eta(x,0)$ given and x,z and t as independent variables. As the system of equations is highly non-linear a numerical technique was used to solve the problem.

The boundary condition for the bottom C-D is obtained by considering it impervious. For D-A the boundary condition is obtained by assuming that the flow domain is symmetrical around D-A, which can thus be treated as a streamline. This also applies to B-C which can be assumed to be a symmetry line to a number of adjacent tunnel systems. Because of the symmetry in the flow domain, only a limited part (R in Figure 1) of the entire flow domain has to be studied reducing the required calculations. At the upper boundary A-B, as well as in the tunnels along E-F, atmospheric pressure prevails.

One practical step that can be taken in connection with the calculation is to introduce the parameter ε_d which is defined as

$$\varepsilon_d = \frac{\varepsilon}{K} \tag{7}$$

In addition the following applies

$$\varepsilon_d \leq 1 \tag{8}$$

That is to say, the accretion to the groundwater surface attributable to percolation (ε) cannot exceed the actual value of the hydraulic conductivity (K). It is also practical to introduce the following transformation to dimensionless time

$$t_d = \frac{K}{\phi} t \tag{9}$$

The advantage of these transformations is that the number of calculation cases can be limited and that the selection of time steps suitable for the calculations is facilitated. The latter is a valuable feature if the time scale varies widely for different calculation cases.

The parameters which will determine the result of this calculation are hydraulic conductivity (K), porosity (ϕ) and the groundwater accretion (ε).

Numerical examples with comments

Several numerical examples have been carried out to illustrate the fluctuation of the groundwater surface using the above model. The results are presented both in graphic and tabular form.

The flow domain in the examples has the folloing dimensions (see Figure 2):

D-C : 3000 metres

B-C : 1000 metres

D-E : 500 metres

E-F : 20 tunnels, each with a cross-section of 3.5 x 3.5 metres and with a distance of 25 metres between the centres of adjacent tunnels. Atmospheric pressure (p_g=0) is assumed to prevail in the tunnels, i.e. $\varphi=h_2$.

Qualitatively, the results depend on the value of the accretion ε_d to the phreatic surface. In all cases presented a standard value of the porosity of ϕ=0.001 was chosen.

It is of interest to note that the results obtained for each value of ε_d can be applied to several different paired combinations of K and ε. For example ε_d=0.16, aside from the time scale, is equivalent to (ε=50,K=10^{-8}), (ε=5,K=10^{-9}), (ε=0.5,K=10^{-10}) etc. Consequently, the examples have been built up primarily around a number of different values of ε_d while keeping all the other conditions constant.

The actual values of ε_d and the corresponding values of ε and K are presented in Table 1.

		ε_d				
		0	0.08	0.16	0.32	0.48
K (m/s)	10^{-6}	0	2500	5000	10000	15000
	10^{-7}	0	250	500	1000	1500
	10^{-8}	0	25	50	100	150
	10^{-9}	0	2.5	5	10	15
	10^{-10}	0	0.25	0.5	1	1.5

Table 1. Vertical accretion to the groundwater table ($\varepsilon=\varepsilon_d K$ (mm/year)) relative to the K value and ε_d.

The drop of the groundwater table naturally takes place most rapidly in the area just above the tunnels. Table 2 presents the drawdown of the groundwater table at the centre line (i.e. A-E in Figure 2) as a function of time (t_d). Table 3 presents times (t) for the drop of the groundwater table down to the tunnel system as a function of K and ε.

The lateral extent of the drawdown of the groundwater table depends upon the value of ε_d. This is illustrated by the graphical displays that accompany the examples.

In example 1 ($\varepsilon_d=0$), the extent of the drawdown is infinite provided the horizontal extent of the flow area is assumed to be infinte. At $t_d=1000$ the drawdown in the example is about 50 metres at B-C in Figure 2 ($t_d=1000$, $\phi=0.001$ corresponds to K values (m/s) of 10^{-6}, 10^{-7}, 10^{-8}, 10^{-9} and 10^{-10} to the following values of t (years): 0.03, 0.3, 3, 30 and 300 respectively.

	Example				
	1	2	3	4	5
t_d	ε_d=0	ε_d=0.08	ε_d=0.16	ε_d=0.32	ε_d=0.48
0	0	0	0	0	0
100	-96	-87	-79	-63	-47
200	-192	-176	-160	-127	-95
300	-289	-265	-240	-191	-142
400	-385	-353	-321	-256	-191
500	-477	-440	-401	-321	-239
550	-500				
600		-500	-476	-385	-287
650			-500		
700				-447	-336
800				-500	-384
900					-429
1000					-472
1100					-500

Table 2. Drawdown (m) above the tunnels (A-E in Figure 2) as a function of time t_d.

Example

		1		2		3		4		5	
		ε_d=0	t_d=550	ε_d=0.08	t_d=600	ε_d=0.16	t_d=650	ε_d=0.32	t_d=800	ε_d=0.48	t_d=1100
		ε	t	ε	t	ε	t	ε	t	ε	t
K	10^{-6}	0	0.017	2500	0.019	5000	0.02	10000	0.025	15000	0.035
	10^{-7}	0	0.17	250	0.19	500	0.2	1000	0.25	1500	0.35
	10^{-8}	0	1.7	25	1.9	50	2	100	2.5	150	3.5
	10^{-9}	0	17	2.5	19	5	20	10	25	15	35
	10^{-10}	0	170	0.25	190	0.5	200	1	250	1.5	350

Table 3. Times t (years) for the groundwater table to drop to the tunnelsystem for different values of ε (mm/year) and K (m/s).

In the other examples, the extent of the drawdown is limited. Groundwater accretion in these cases is thus sufficient to fill the aquifer up to the ground surface beyond a certain distance from the tunnel system. Figure 3 shows the extent of the drawdown as a function of ε_d.

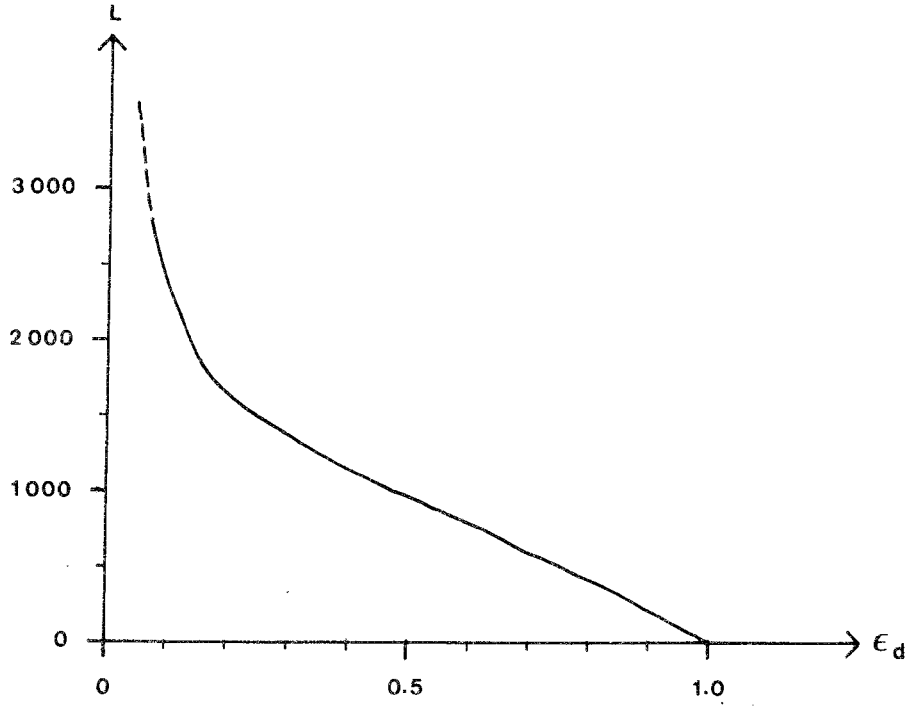

Figure 3. Lateral extent (L) of the drawdown of the groundwater table as a function of ε_d.

The examples are presented graphically in Figure 4-9. These diagrams show the gradual drawdown of the groundwater surface at equal time intervals (Δt_d). Moreover the piezometric head (φ) is illustrated by means of isolines having the following values: -50, -100, -200, -250, -300, -350, -400 and -450 metres (however the isolines in Figure 7b are limited to -100, -200, -300 and -400 metres).

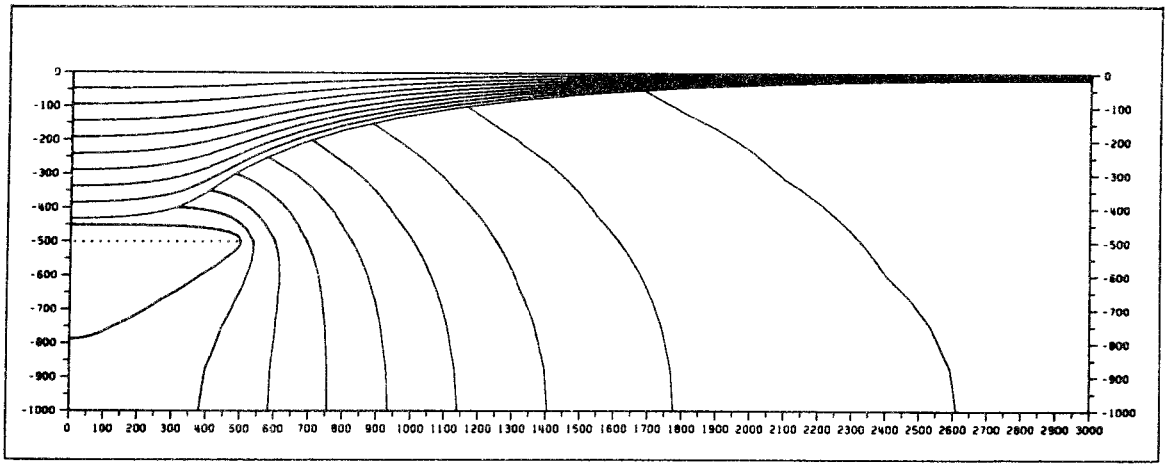

a

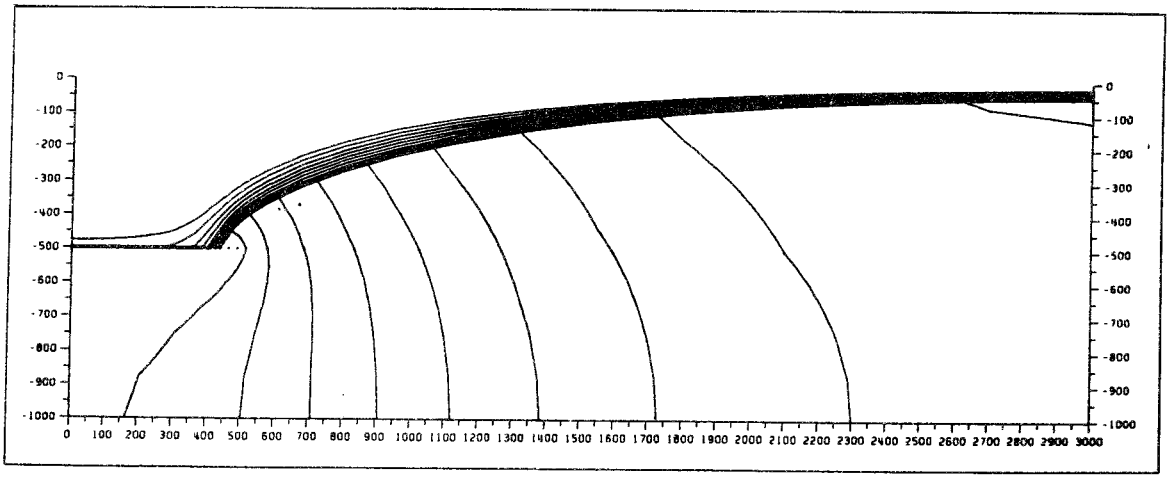

b

Figur 4. Example 1

$\varepsilon_d=0$

$\Delta t_d=50$

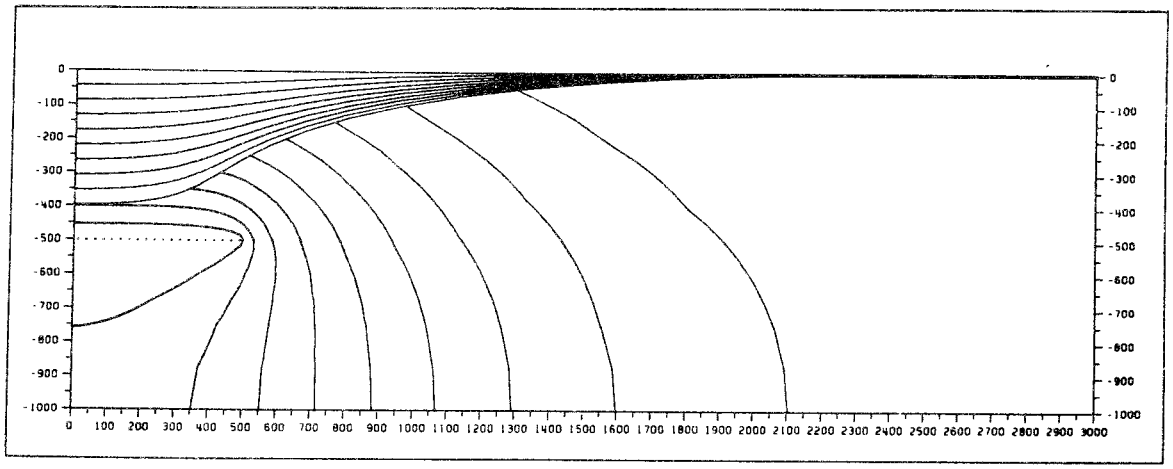

a

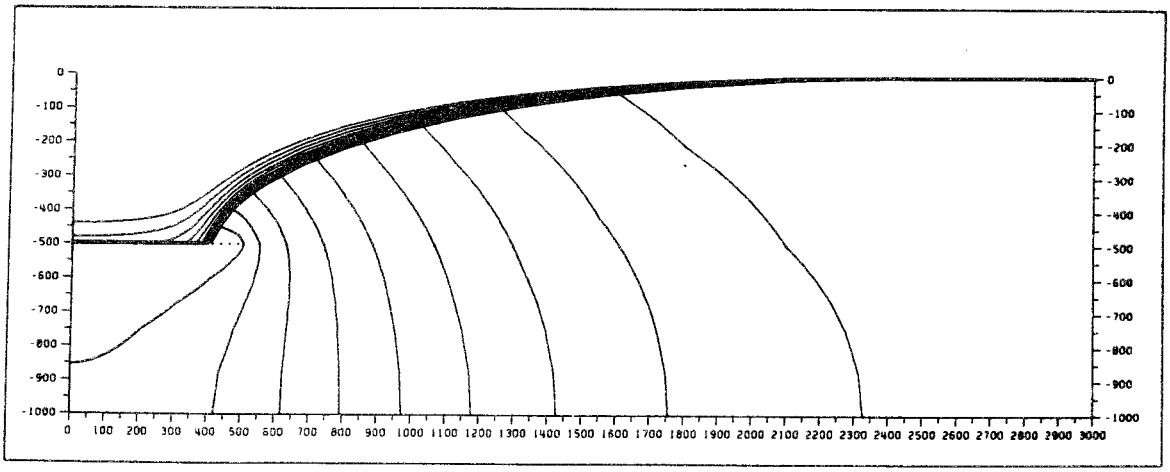

b

Figur 5. Example 2

ε_d=0.08

Δt_d=50

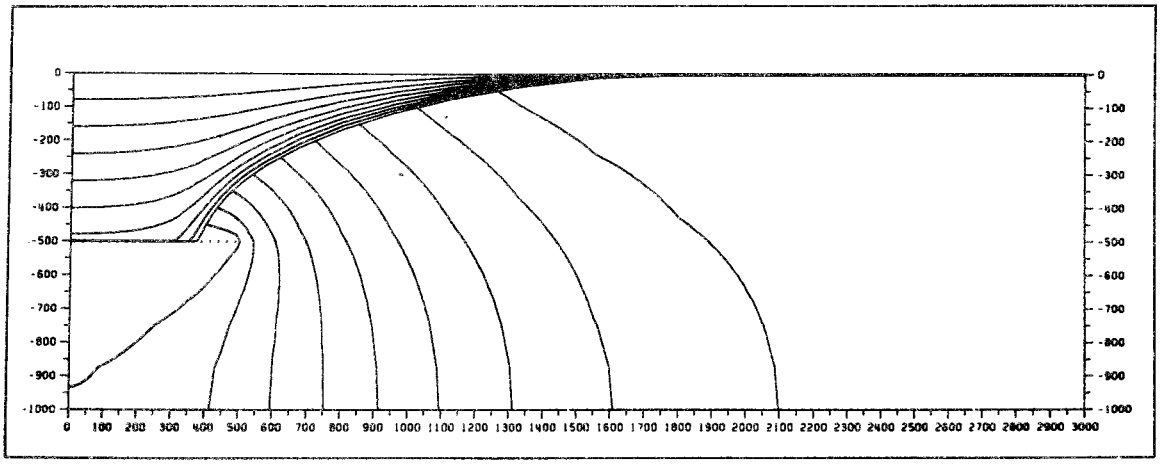

a

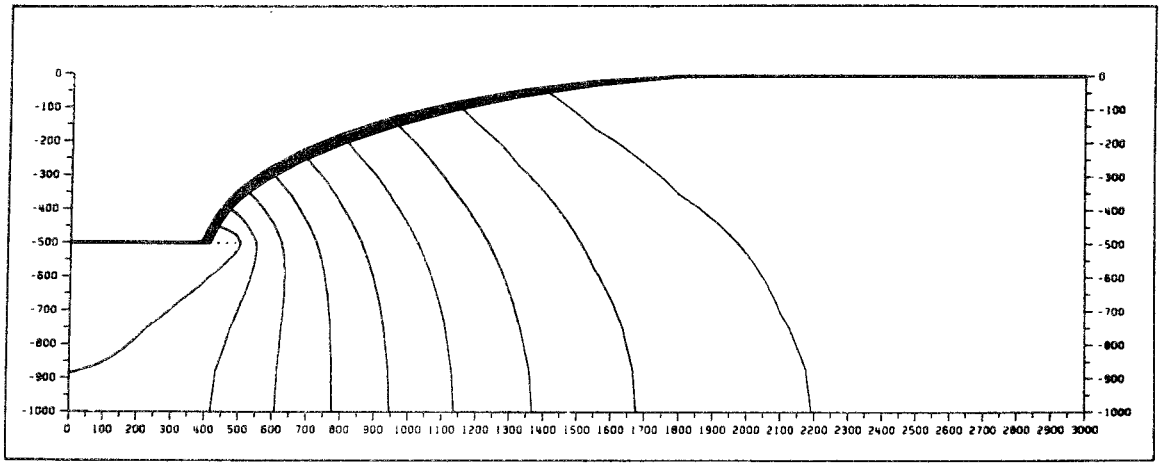

b

Figur 6. Example 3

ε_d=0.16

Δt_d=100

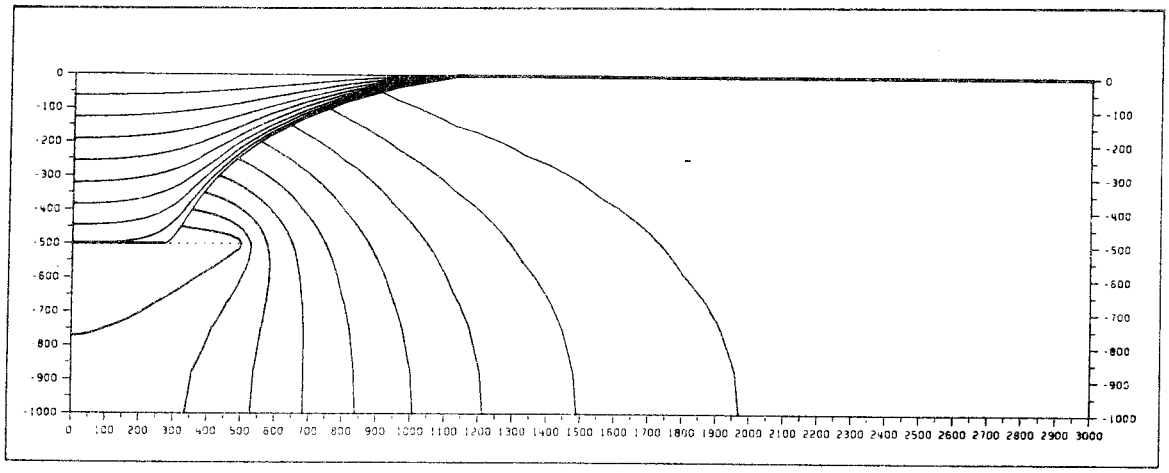

a

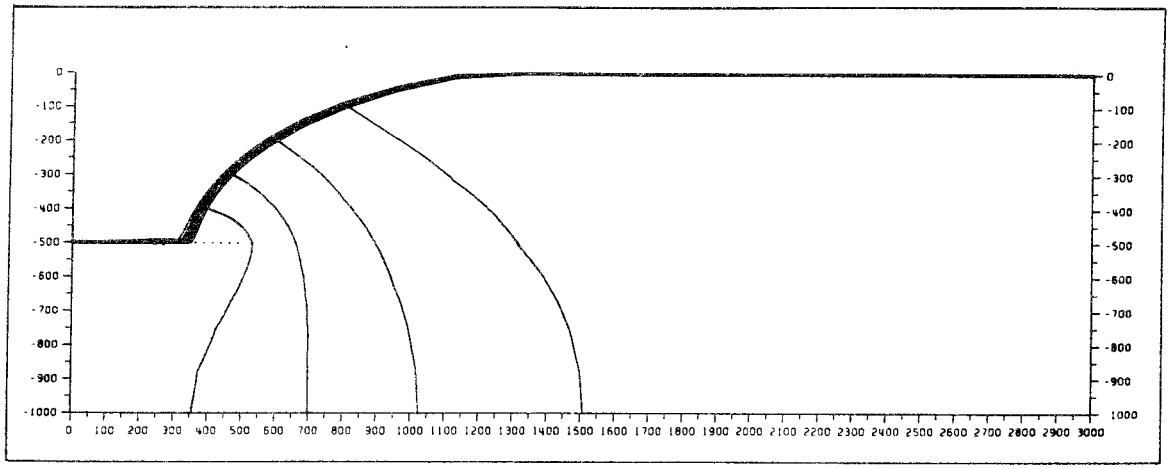

b

Figur 7. Example 4

ε_d=0.32

Δt_d=100

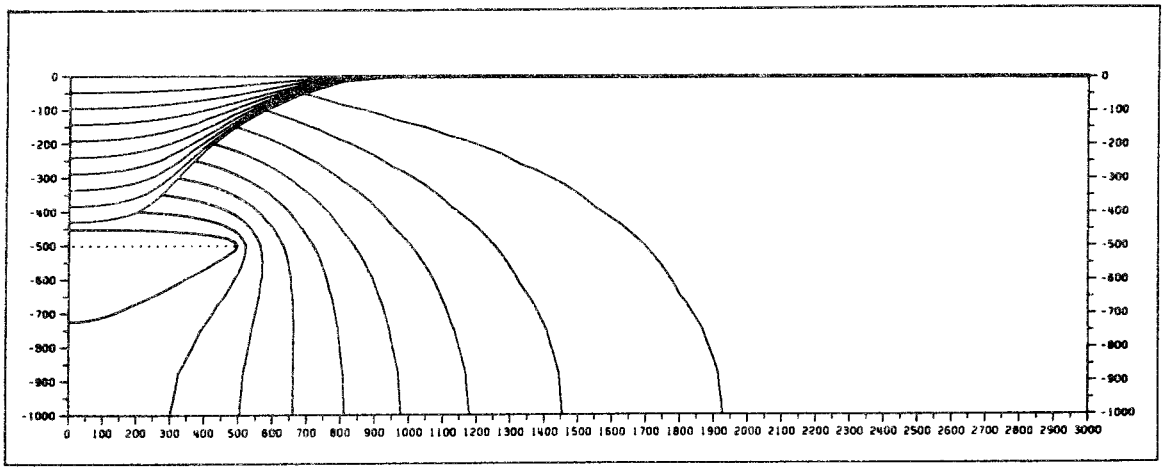

a

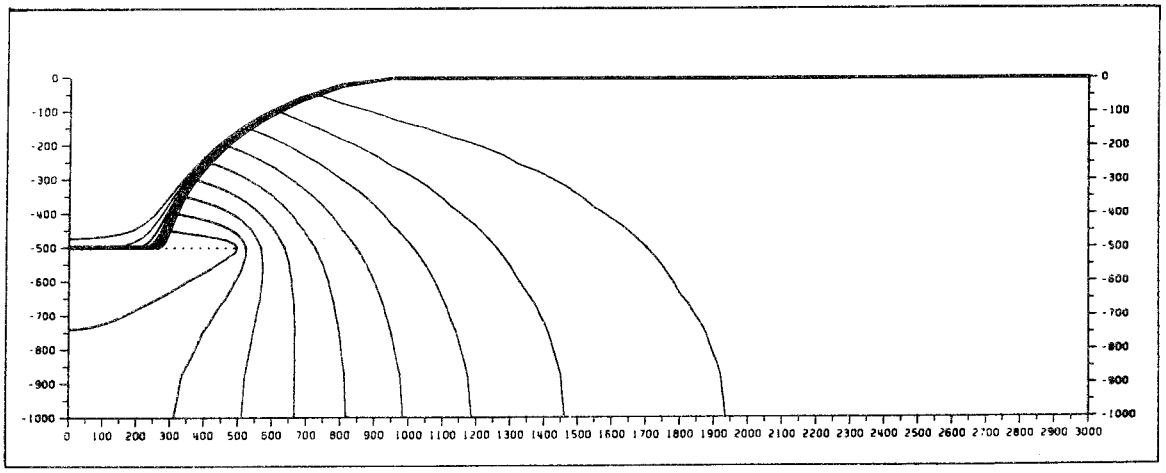

b

Figur 8. Example 5

ε_d=0.48

Δt_d=100

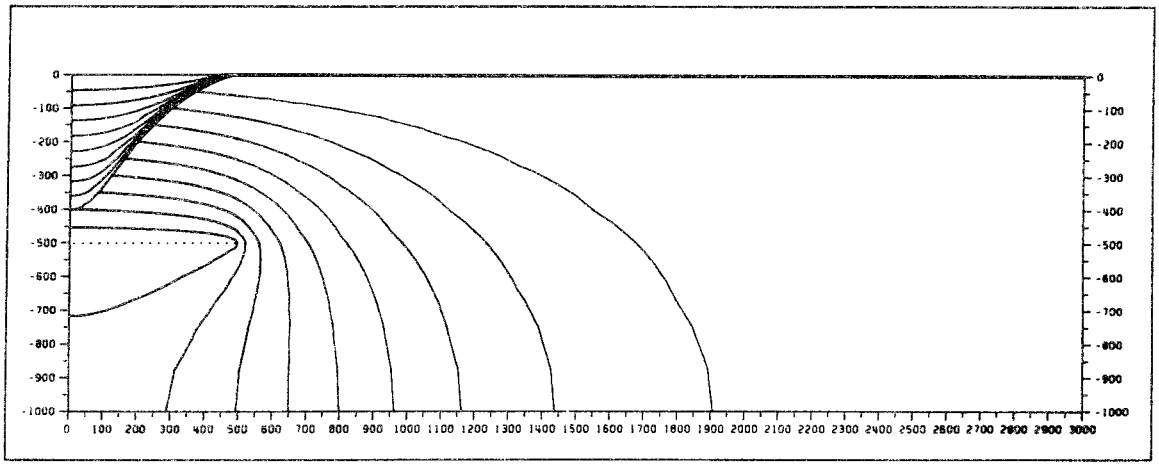

a

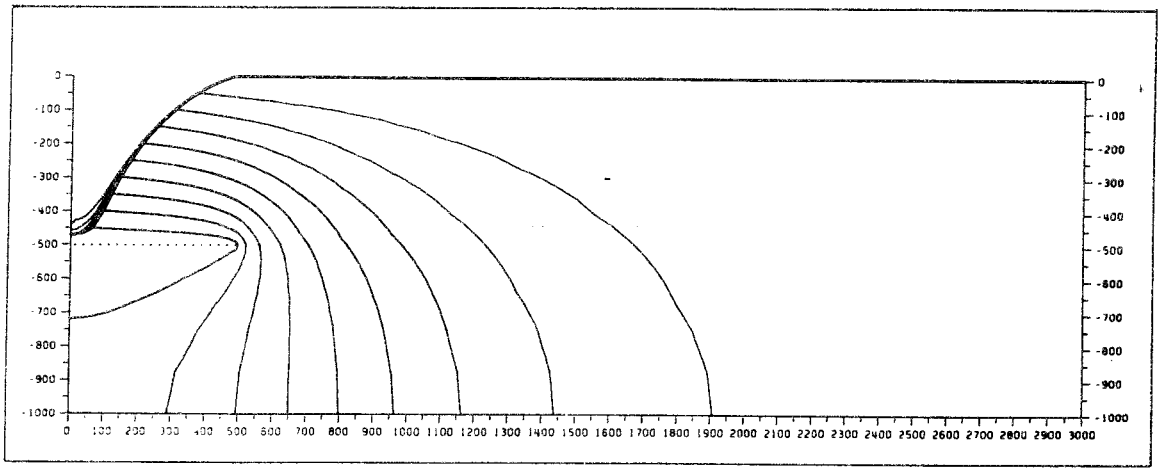

b

Figur 9. Example 6

ε_d=0.80

Δt_d=300

1978.05.18

INVESTIGATIONS OF GROUNDWATER FLOW IN ROCK AROUND REPOSITORIES FOR NUCLEAR WASTE

III. Three Dimensional Model of Groundwater Flow governed by Topography

John Stokes
Roger Thunvik
Royal Institute of Technology
Stockholm, Sweden

Three dimensional model of groundwater flow governed by topography.

The questions discussed in section I were essentially two dimensional in character (see page I.2). A two dimensional model was natural in this investigation. The questions were also easy to approach with an analytic method. On the other hand new questions have arizen, partly due to the obtained results, which demand a more powerful model:

a) In a two dimensional model the plane-parallel geometry will give flowtimes to the surface which generally are too short. The local topography will have too large an effect on the groundwater flow. On the other hand the axisymmetrical model will give the opposite effect. Time intervals for flow times obtained in this way are eften so large that they are of limited value. A three-dimensional model would give better possibilities to determine the flowtimes.

b) The analytical approach given in section I limits the choice of K-values to a variation with depth. This method also restricts the model to continuously varying K-values. It is not possible to study the effects of fracture zones on groundwater flow with this approach. With a numerical model it is at least in principle possible to introduce K-values varying in on arbitrary way in space. In the field several fracture zones are often found to intersect under acute angles. In these cases the geometry of the fracture zones can be suspected to determine the groundwater flow to a high degree. All these problems demand a three dimensional model.

c) When giving a description of groundwater flow it is essential to know the K-variation in space. To obtain K-values is very expensive. It is also difficult to judge how large regions that can be represented by single measurements. It is desirable to use all available information as for instance age determinations of groundwater,

actual groundwater level instead of topography, etc., and determine the K-value from this information. This approach requires a fully developed three-dimensional model.

The model described in this section is a three-dimensional finite element model. The solution satisfies Darcy's law, where $\bar{\bar{K}}$ is a diagonal tensor in the coordinate system chosen:

$$\vec{q} = \bar{\bar{K}} \nabla\varphi$$

The solution is also governed by the equation of continuity

$$\nabla \cdot \vec{q} = 0$$

whence

$$\nabla \cdot (\bar{\bar{K}} \nabla\varphi) = 0$$

One of the boundaries is the groundwater table which coincides with topography. The heights are chosen to give a representative topography as the boundary conditions are only given at descrete points, see fig. 2a.

The modelled region is also bounded by vertical streamlines, i.e. no flow boundaries. The bottom is also bounded in the same way.

The model has been tested in the Finnsjön-region, see fig 1. and fig I. - 39 - 40. The geografic area is 30 km^2. The depth from the surface to the bottom is about 1500 metres. The three-dimensional region is divided into 5715 tetrahedric elements distributed in 5 horizontal layers. Each layer is 300 metres thick. The total number of nodes is 1230. After consulting the Swedish Geological Survey vertical fracture zones have been chosen according to fig.1. Due to numerical considerations the fracture zones were given a width of 50 metres. From a geological point of view this width is to large. This is compensated by

giving fracture zone-K-values which are 100 times larger than rock-K-values instead of 10000 times:

$K_1 = 10^{0.0030z-4}\ m^3/m^2s$ in the fracture zones

$K_2 = 10^{0.0030z-6}\ m^3/m^2s$ in the rock

where z is depth (negative downwards). This choice of K in the fracture zones means that same amount of water will flow through these as if they were 0.5 metres wide with a K-value 10000 times larger than that of the surrounding rock.

The true flow velocity in an arbitrary point is determined by $-\frac{1}{\phi}\bar{\bar{K}}\nabla\varphi$ when the potential φ has been computed for all nodes in the region. Here ϕ is the effective porosity and has been chosen as $\phi = 0.001$. In this way the results are comparable to those obtained in section I. Finally the flow-times from arbitrary points to the surface are obtained by numerical integration along the pathlines.

The intersections between the equipotential surfaces and the level surfaces 0, -500, -1000 and -1500 metres are presented in figs. 2a-d. It is seen in these figures that the region is divided into two parts by a line from SSE to NNW. To the west of this line water is flowing towards the fracture zone in Finnsjön, while water further to the east flows towards the marshes in the east half of the region.

The water flow from the 500-metre level has been studied to obtain a more detailed description of the flow pattern. Pathlines intersecting the 500 metre level at gridpoints 200 metres apart (in a regular mesh over the whole region) intersect the surface at the crosses shown in fig. 3. Pathlines starting or ending at the vertical boundaries have been excluded. The main direction of flow has been suggested by drawing straight lines between the starting point at - 500 metres and the surface discharge point for a few selected pathlines. The dashed lines show the boundaries of the discharge areas at the surface.

The times of flow along these pathlines have been computed. These times are presented in figure 4a where the digits denote years in exponents of ten (e.g. the curve marked with a digit 3 denotes a flowtime of 1000 years for water at points on this curve at the -500 metre level to reach the surface). Times for water at the groundsurface to reach the -500 metre level have also been computed. The results of this calculation are presented in figure 4b. The contour map in figure 4b shows that some particular areas with high ages can be distinguished. Two such areas are located to the left in figure 4b. A third area with high ages can be found near the boundary to the right in the figure. A comparison between figure 3 and 4b shows that areas with high ages are mainly represented as outflow areas and vice versa.

As mentioned earlier, the flowtimes from the 500-metre level to the surface were calculated for mesh points 200 metres apart. This distance is too large to give any details around the fracture zones. The groundwater level in the fracture zones was also chosen the same as in the immediate vicinity. This condition is not very realistic as the high K-value in the fracture zones relative the K-value in the rock tends to decrease the groundwater level.

In order to study the effects of a decreased water level in the fracture zones on the flowtimes, a number of synthetic examples were modelled. The dimensions of these models were 4242 * 6000 * 700 metres. The solutions were obtained by the method of finite elements (924 nodes and 3330 elements distributed in two layers). All the models were given a topography consisting of a linear slope: At the bottom of the figures the ground is at the 10-metre level, while it is at the zero metre level at the top. Outside the fracture zones the groundwater level is assumed to follow the topography. The fracture zones were given a width of 200 metres (the left fracture zone in the figures has a width of

100 metre due to symmetry). The water level in the fracture zones also varies linearly: At the bottom of the figures the water level is one metre below the ground, while it coincides with the ground level at the top of the figures. The K-values were chosen in the same way as in the Finnsjön-model:

$K_1 = 10^{0.0030z-4}$ m^3/m^2s in the fracture zones
$K_2 = 10^{0.0030z-6}$ m^3/m^2s in the surounding rock

The results are summarized in the three models shown in figures 6 - 8.

Figure 6 shows the effect of a single fracture zone parallel to the topographic gradient. The flowtimes are seen to be almost unaffected by the presence of a fracture zone already at a distance equal to the width of the fracture zone. In fact at this distance, the flowtimes are slightly longer than with no fracture zone. This is due to the focusing effect of the fracture zone: The water is near enough to be drawn towards the zone but yet so far away that it reaches the ground level before reaching the fracture zone. In this way the flow path will be longer than without a fracture-zone which, in this case, gives longer flowtimes.

Figure 7 shows the model with a fracture zone parallel to the topographic gradient and also one at right angles to this gradient. First of all the same general effects as discussed for fig. 6 can be seen. Also, the introduction of a fracture zone at right angles to the gradient tends to widen the zone with short flowtimes. Otherwise, this fracture zone seems to have a very small effect on the flowtimes. This is due to nearly all water flowing across the fracture zone and in to the rock on the other side.

Figure 8 again shows a model with a fracture zone parallel to the topographic gradient. There is also a fracture zone at an acute angle to the gradient. The flowtimes are completely unaffected by the acute fracture zone in the region with lower topography, while the flowtimes in the region with high topography are decreased due to the fact that water in this region does not reach the low topography region.

As an overall result, the following statements are concluded:
a) A fracture zone parallel to the topographic gradient does not affect the flowtimes in the surrounding rock.
b) A fracture zone not parallel to the topographic gradient shortens the flowtimes in regions where the ground level is higher than at the fracture zone. In regions where the ground is lower, the flowtimes are unaffected.

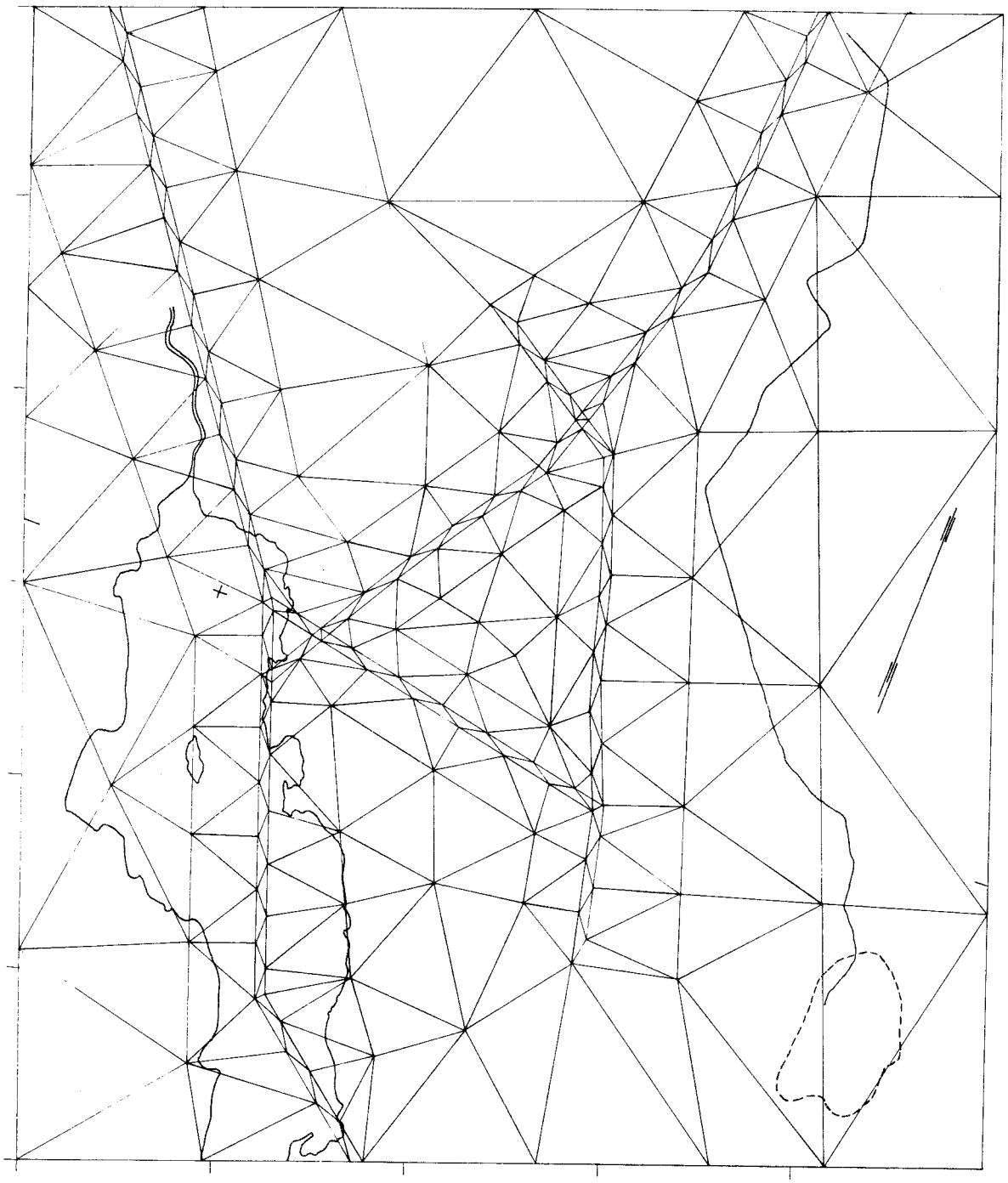

Figure 1. Map of the Finnsjön area.
The map also shows the element mesh used in the numerical model. The shaded area illustrates major fracture zones.

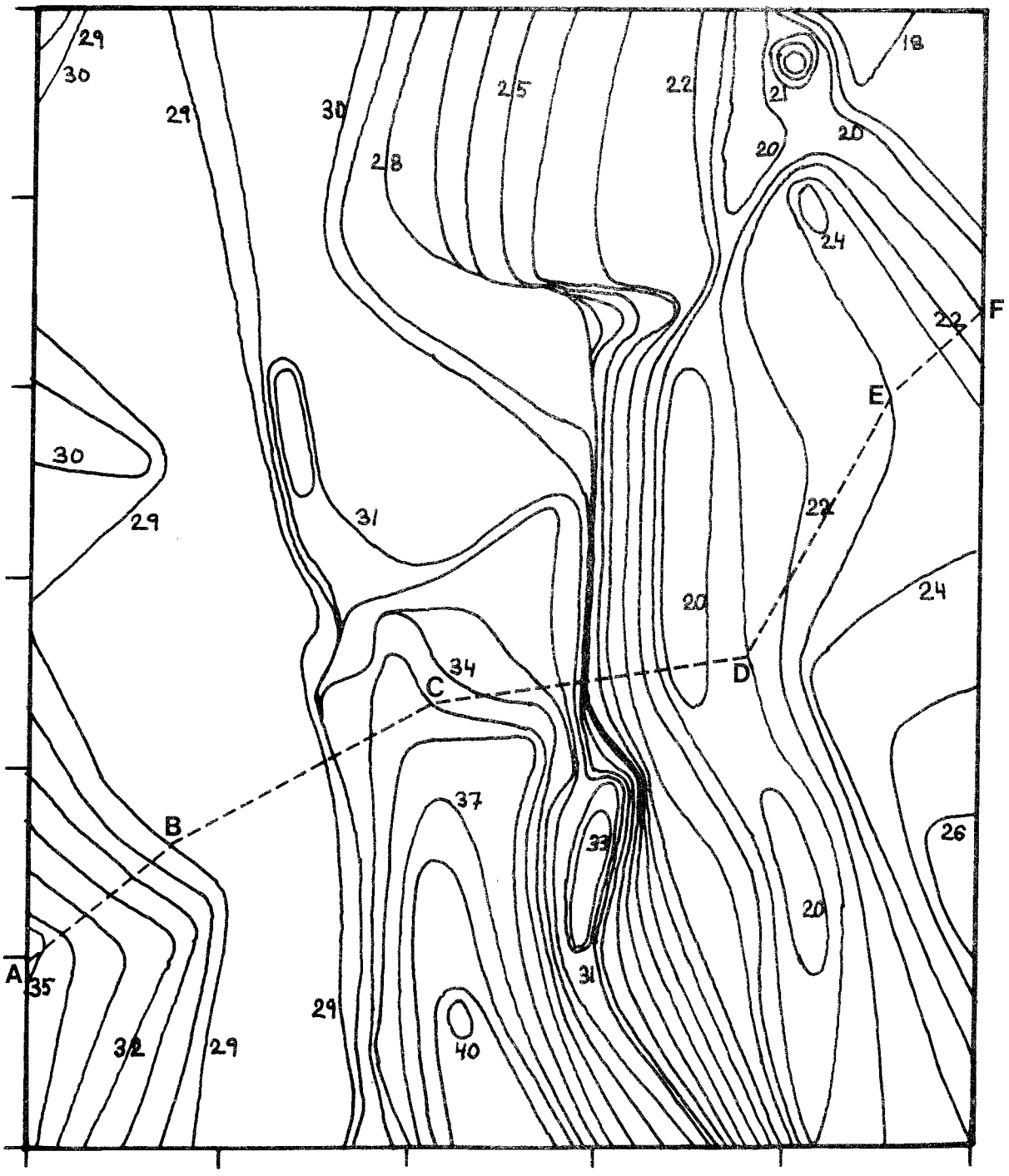

Figure 2a. Horizontal cross-section showing the piezometric head distribution at the zero metre level. The dashed line A-B-C-D-E-F shows the vertical profile shown in figure 5.

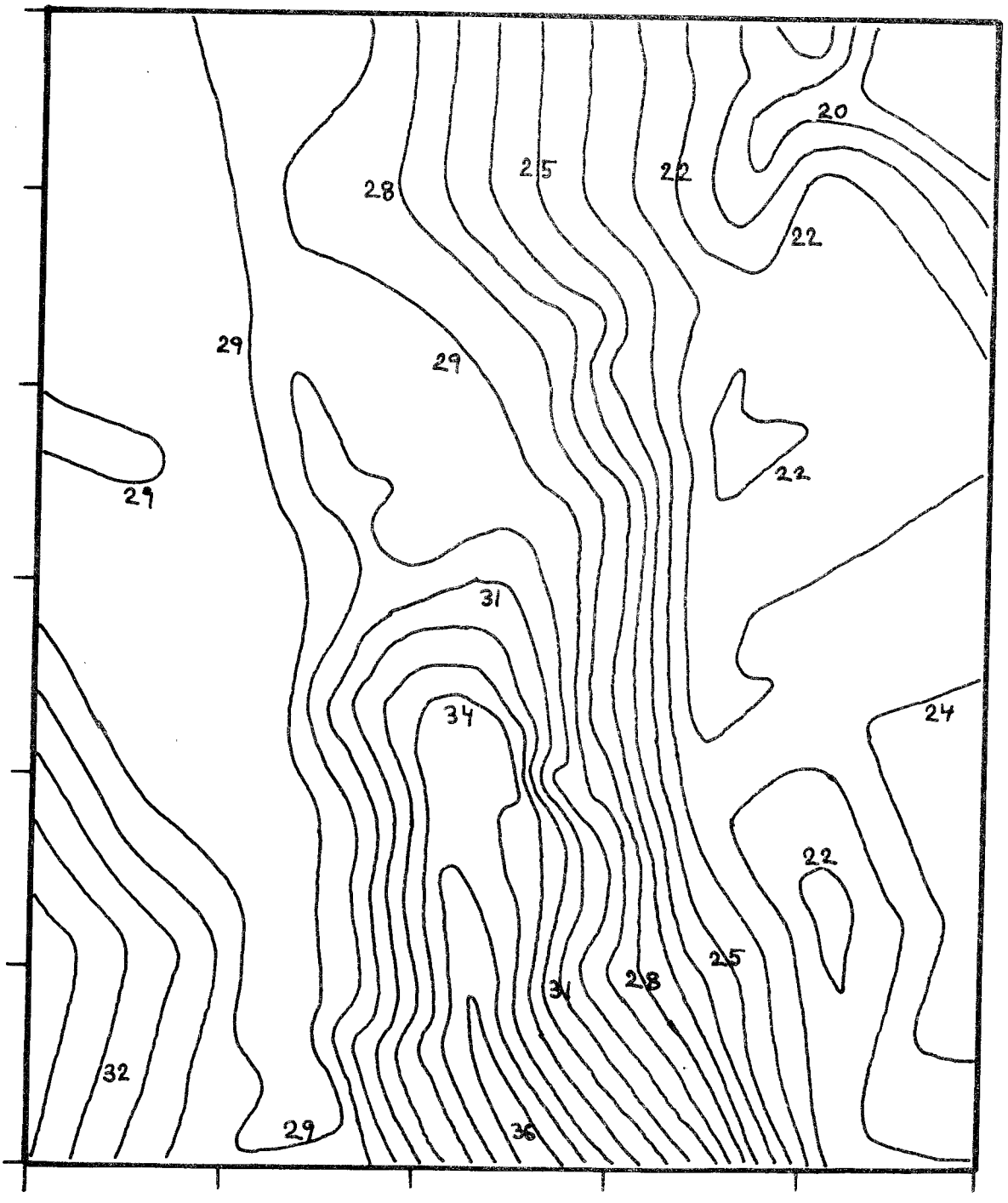

Figure 2b. Horizontal cross-section showing the piezometric head distribution at the - 500 metre level.

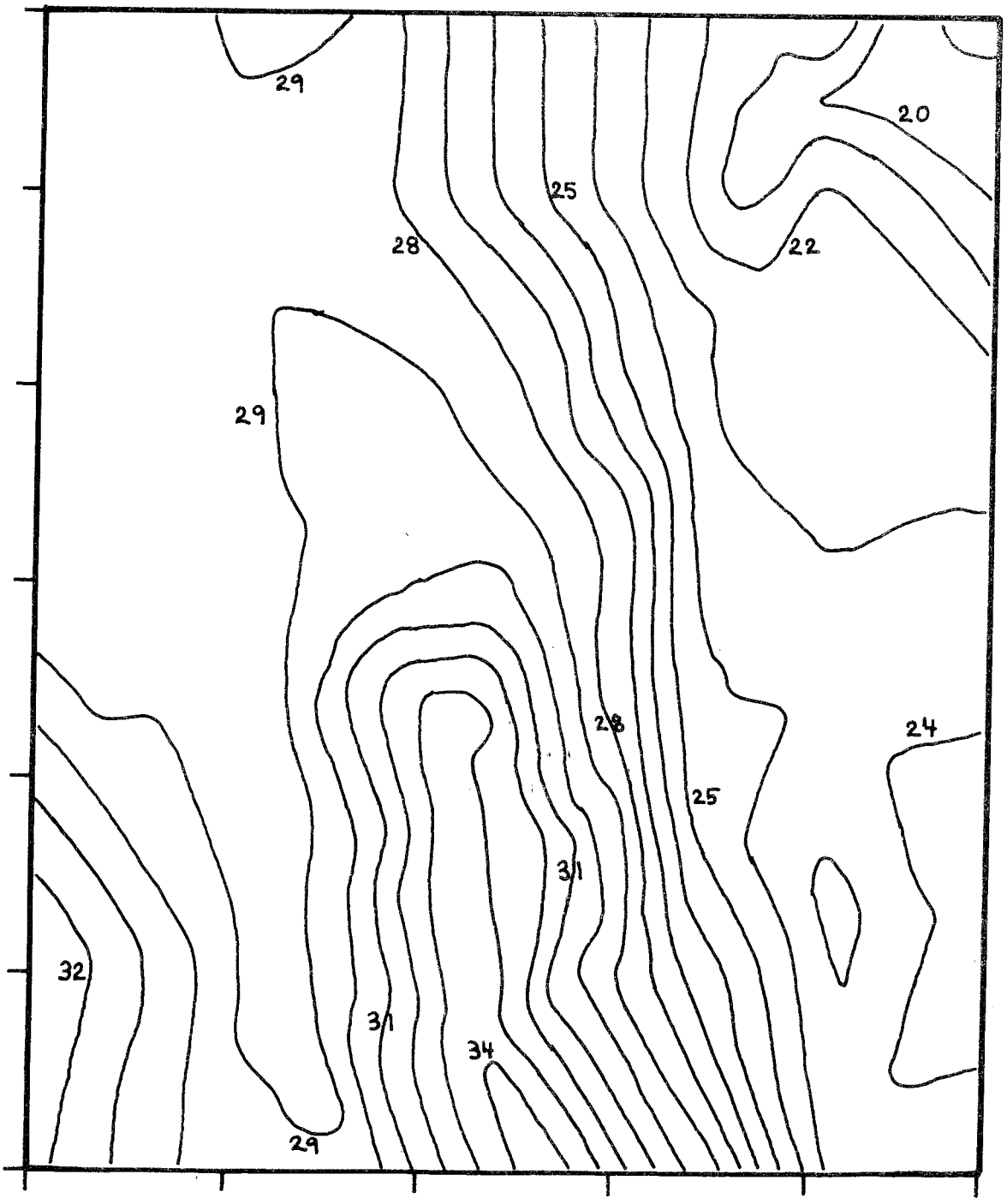

Figure 2c. Horizontal cross-section showing the piezometric head distribution at the - 1000 metre level.

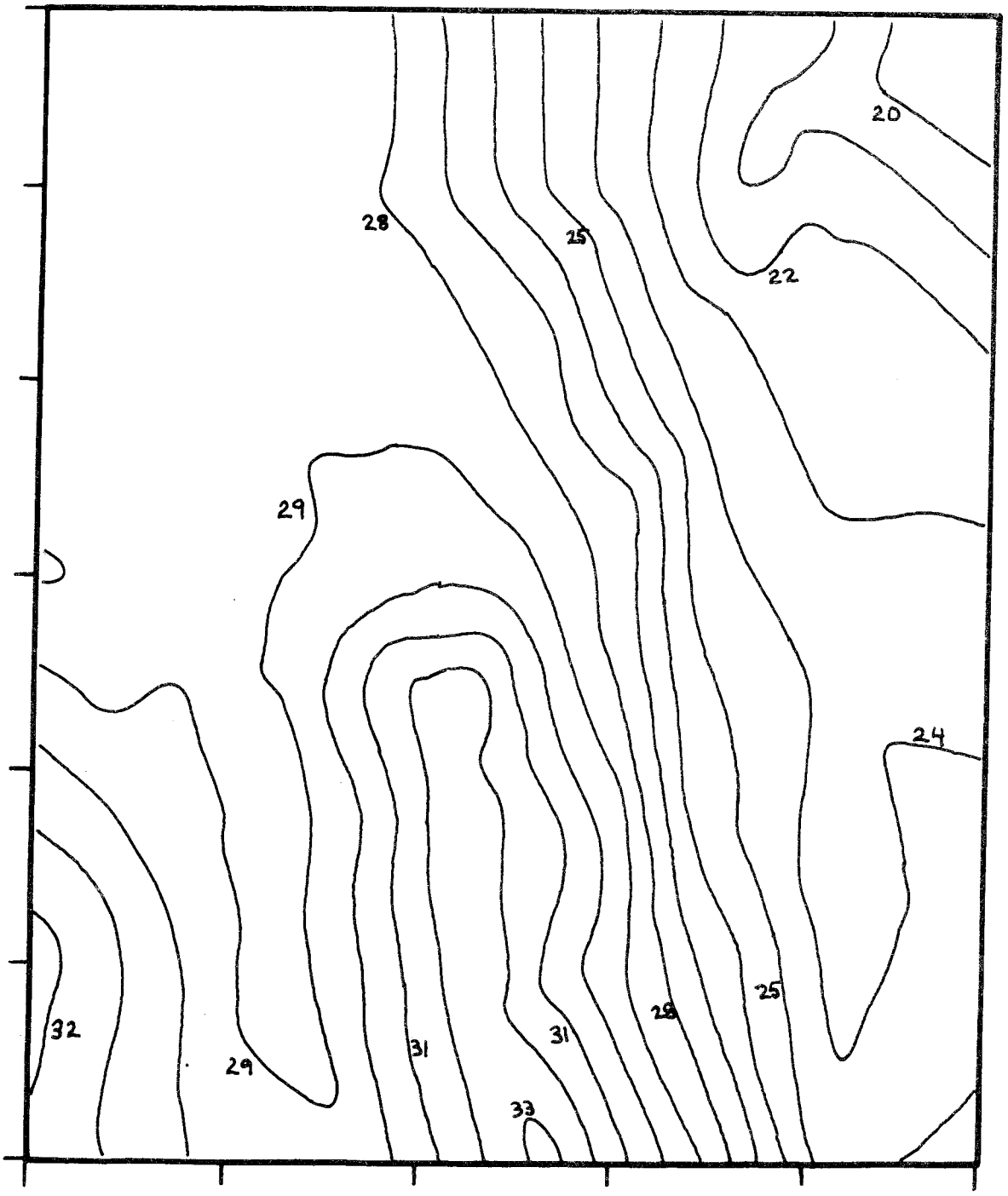

Figure 2d. Horizontal cross-section showing the piezometric head distribution at the - 1500 metre level.

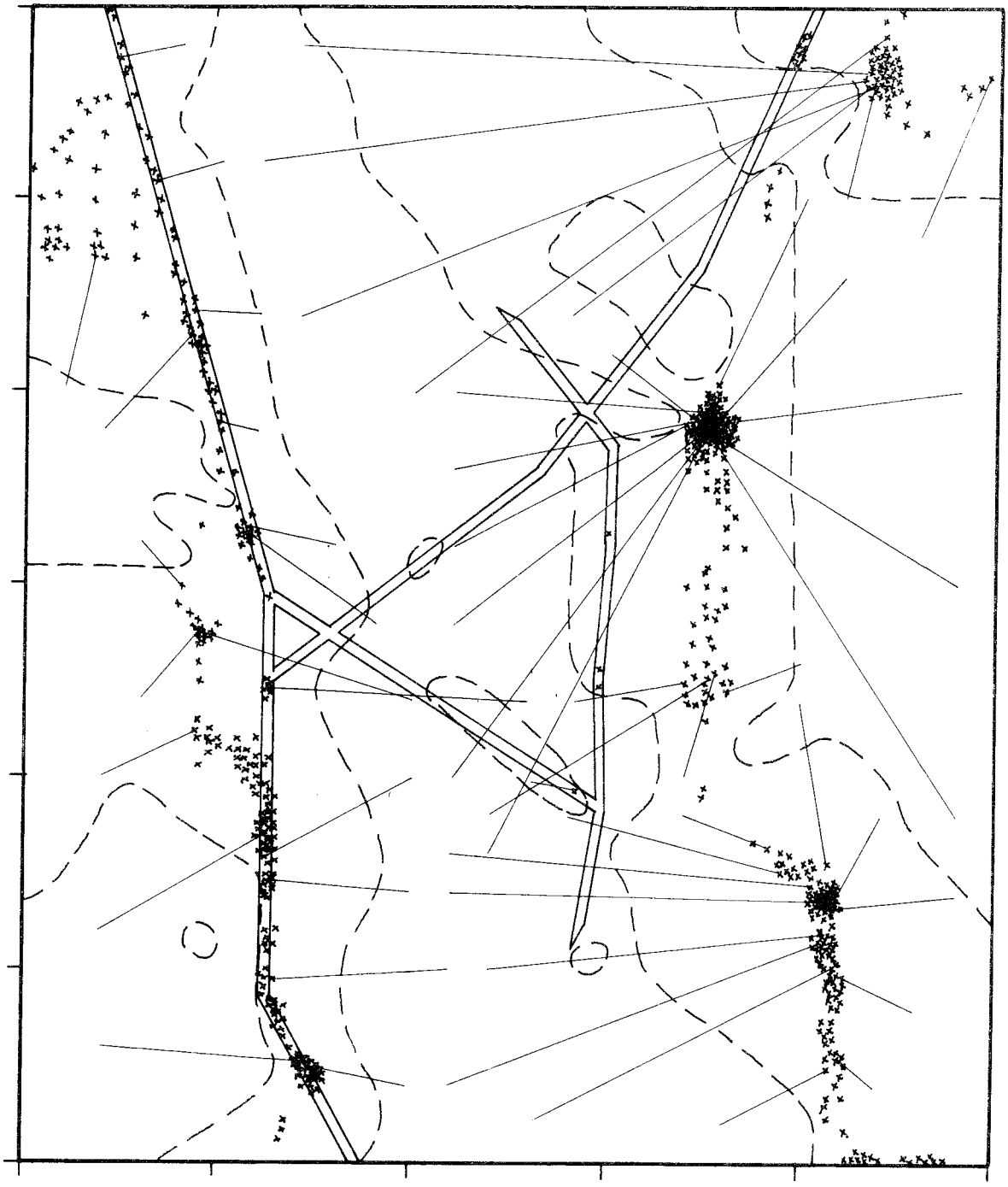

Figure 3. Spots with outflow of water from the - 500 metre level. Some of the outflow points are connected with their starting points at the - 500 metre level illustrating the main flow direction.
Dashed lines denote boundaries between inflow and outflow areas at the groundsurface.

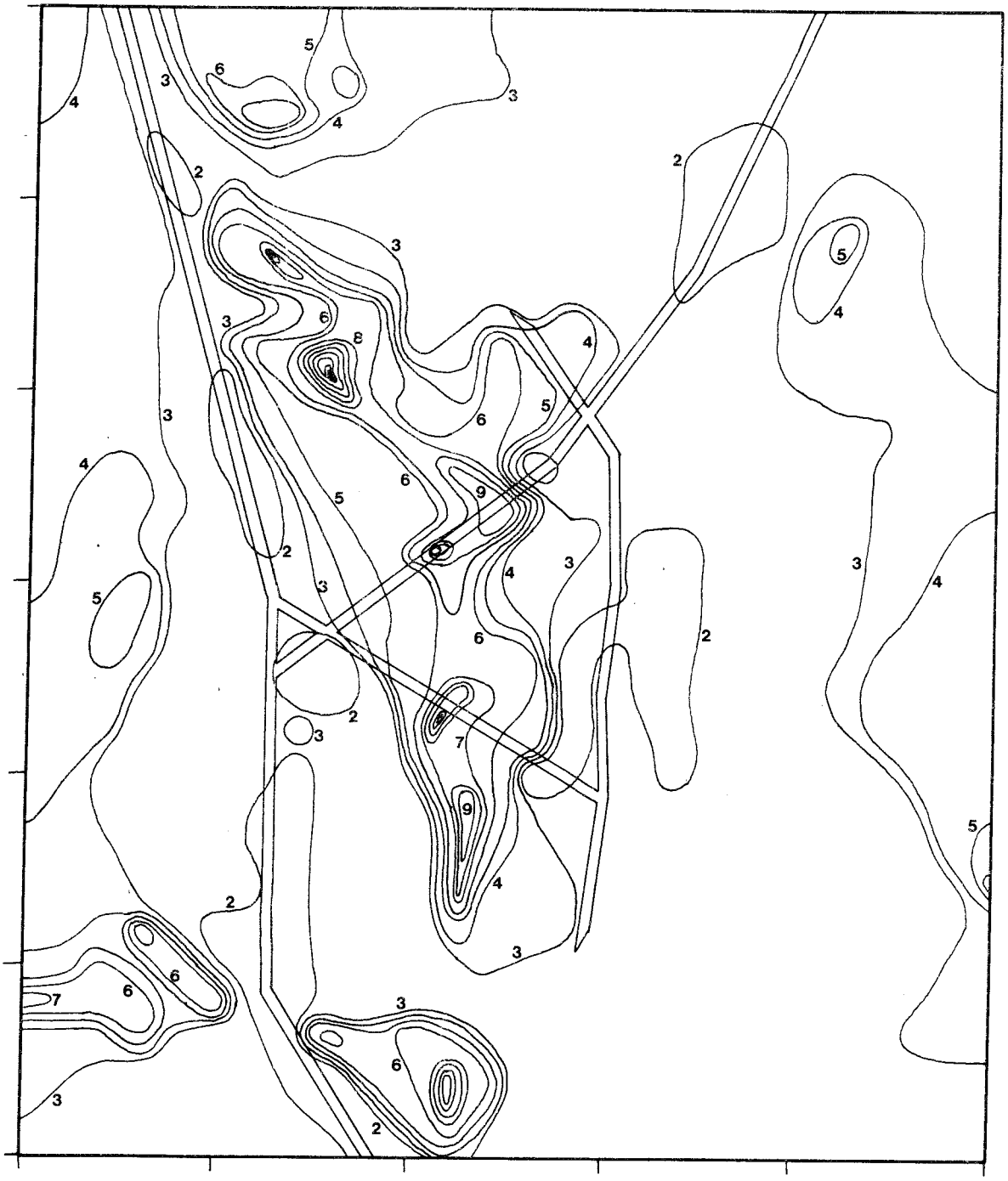

Figure 4a. Times for water at the -500 metre level to reach the groundsurface. Digits in the figure denote years in exponents of ten. E.g. the curve with a digit 3 implies a flow time of 1000 years for water at this line to reach the groundsurface from the - 500 metre level.

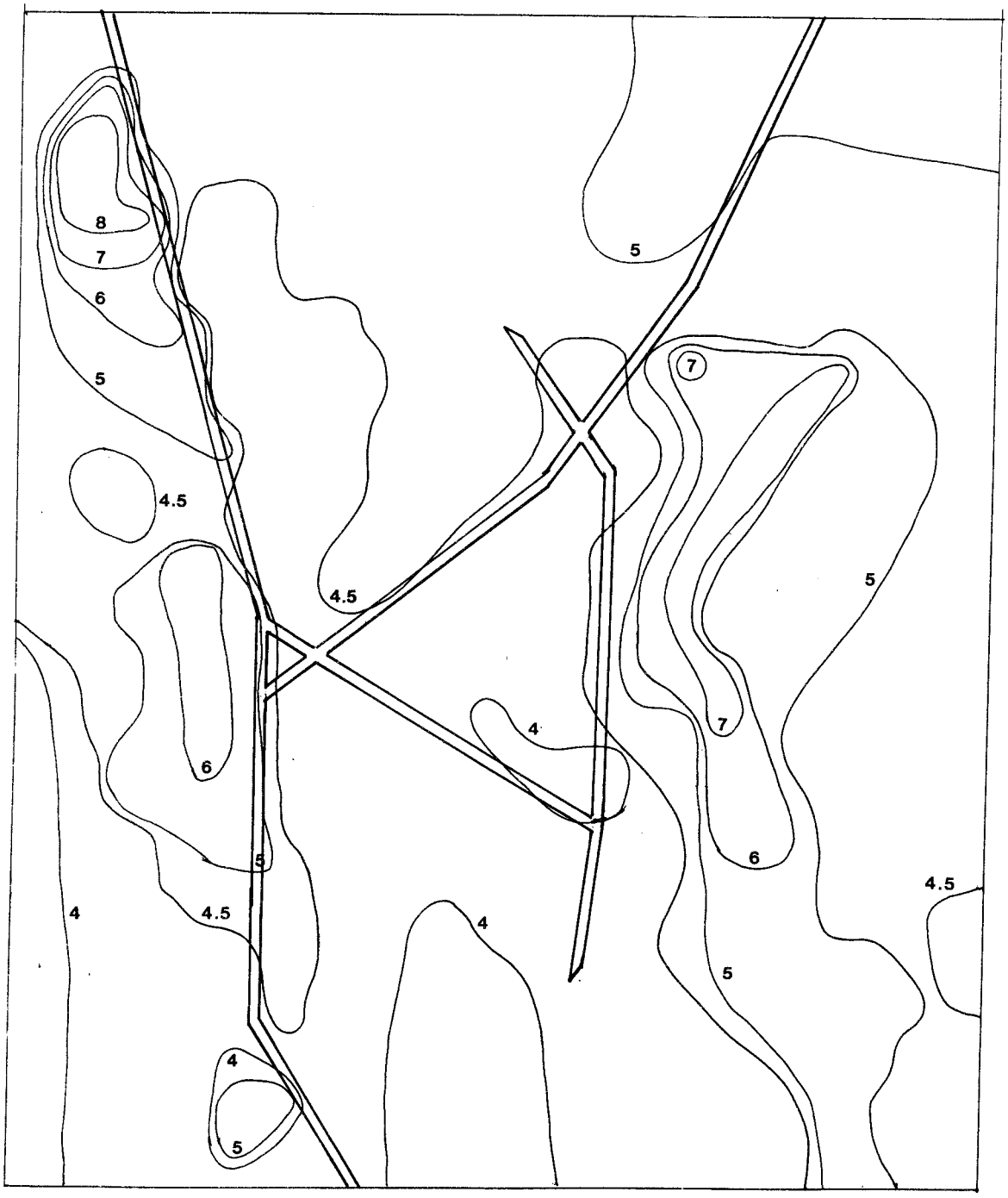

Figure 4b. Calculated age of groundwater at the -500 metre level. Digits in the figure denote years in exponenents of ten.

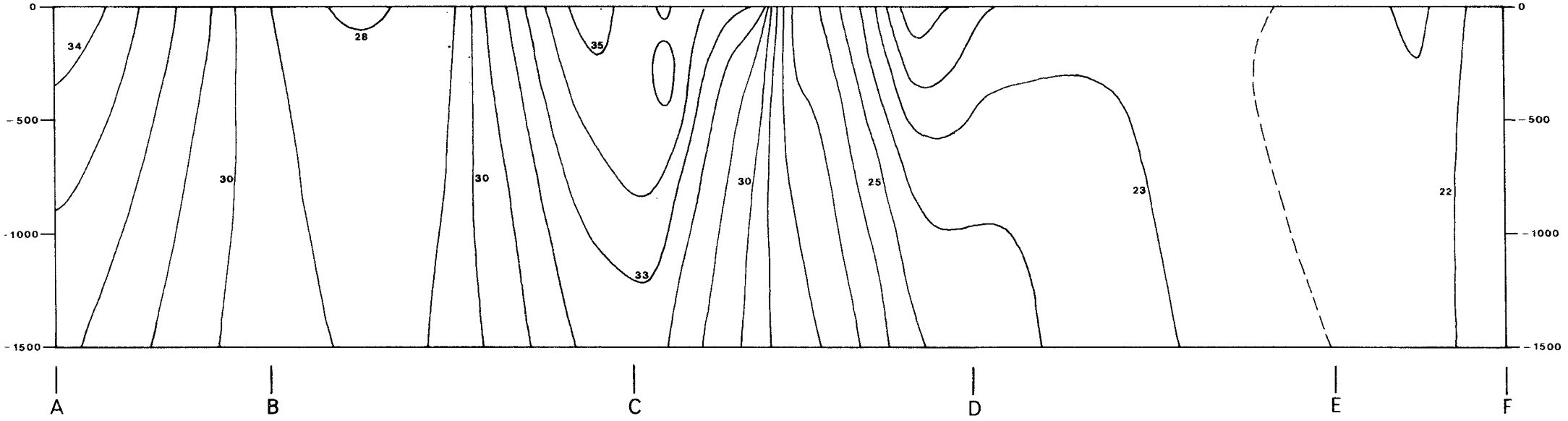

Figure 5. Vertical cross-section through the flow domain showing the piezometric head distribution along the profile A-B-C-D-E-F (see figure 2a).

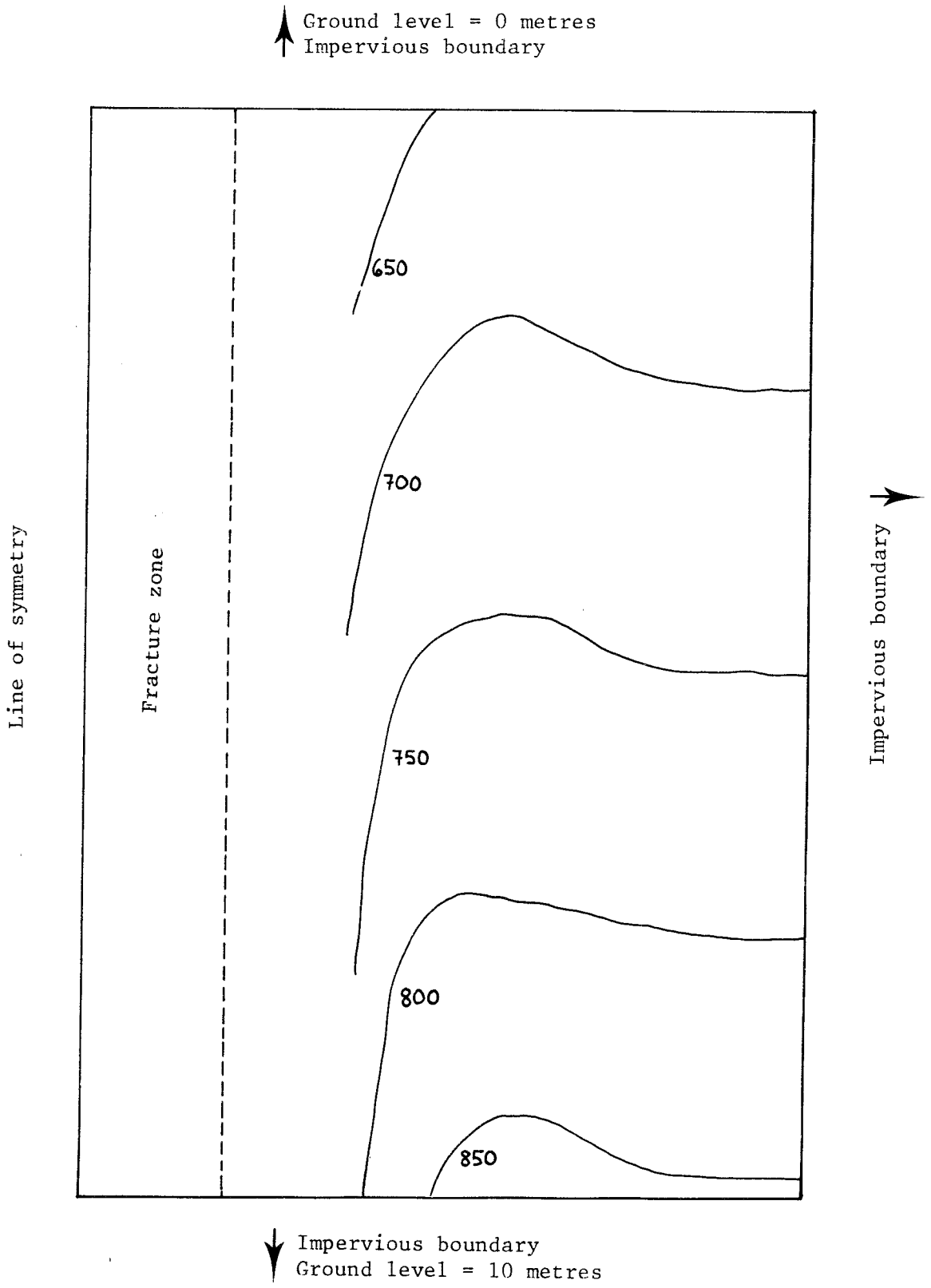

Figure 6. Flowtimes for a synthetic example with a single fracture zone parallel to the topographic gradient.

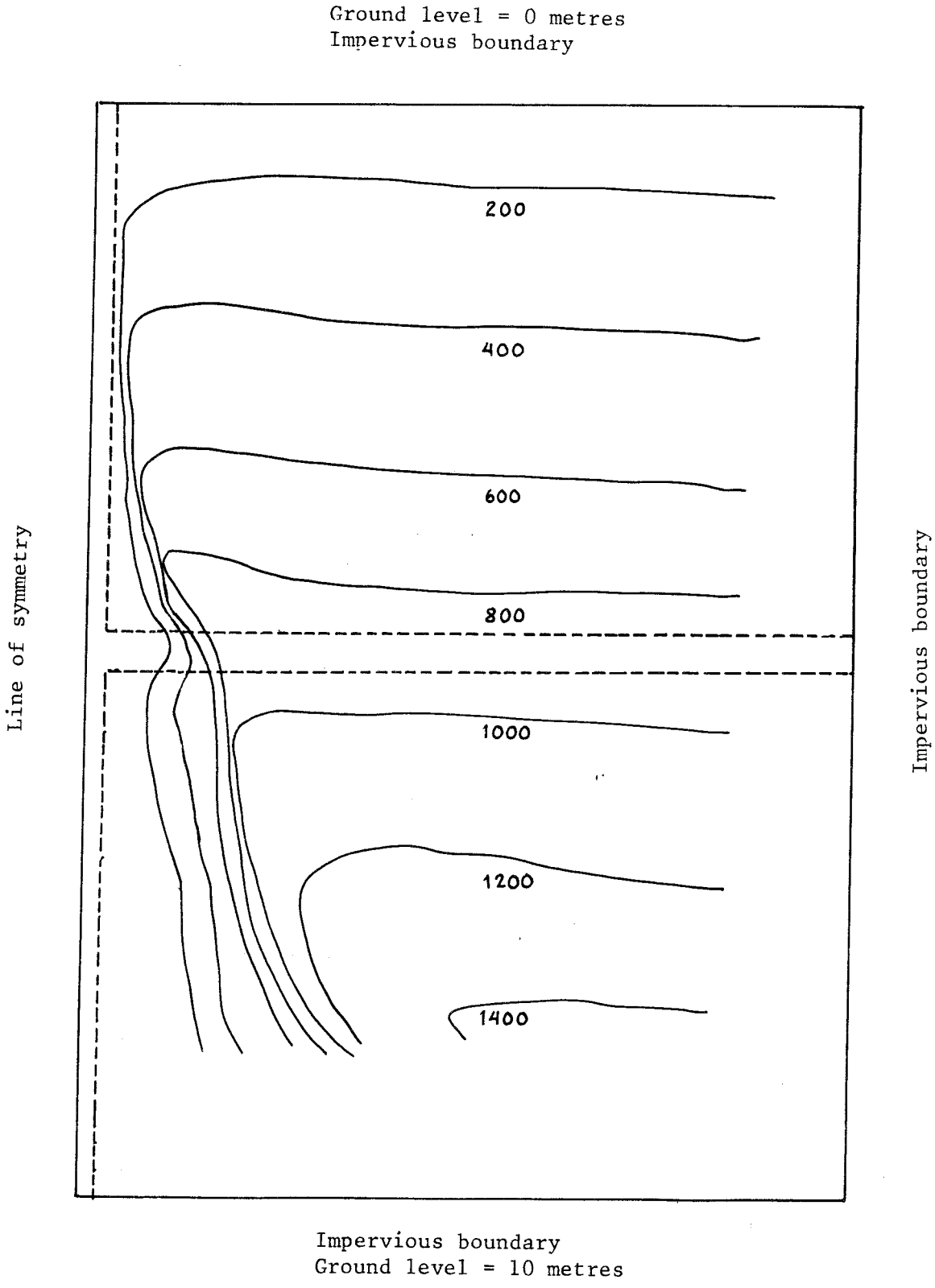

Figure 7. Flowtimes for a synthetic example with two fracture zones intersecting at right angles (Fracture zones are dashed).

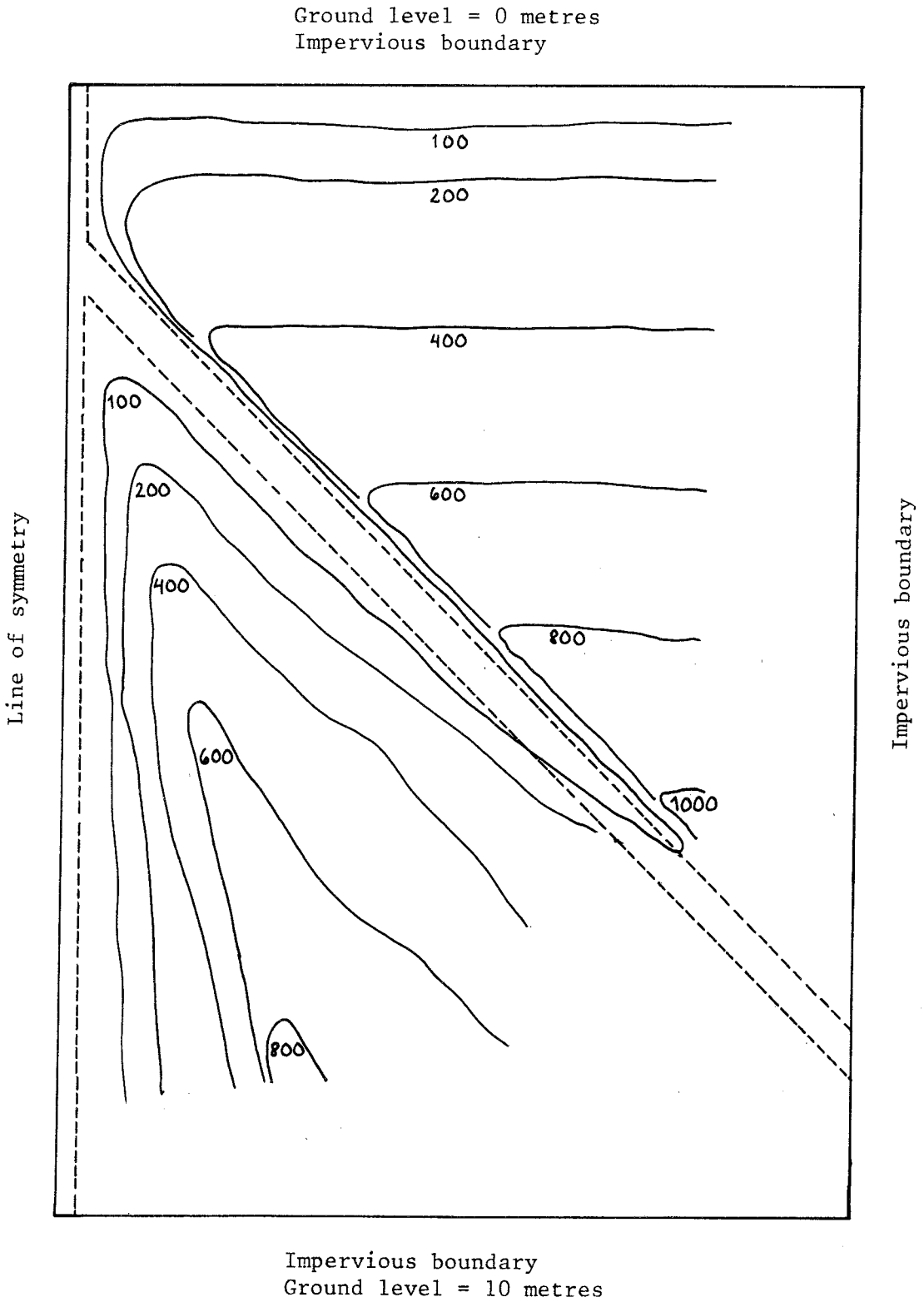

Figure 8. Flowtimes for a synthetic example with fracture zones intersecting at acute angles (Fracture zones are dashed).

LIST OF KBS TECHNICAL REPORTS

01 Källstyrkor i utbränt bränsle och högaktivt avfall från en PWR beräknade med ORIGEN
Nils Kjellbert
AB Atomenergi 77-04-05

02 PM angående värmeledningstal hos jordmaterial
Sven Knutsson
Roland Pusch
Högskolan i Luleå 77-04-15

03 Deponering av högaktivt avfall i borrhål med buffertsubstans
Arvid Jacobsson
Roland Pusch
Högskolan i Luleå 77-05-27

04 Deponering av högaktivt avfall i tunnlar med buffertsubstans
Arvid Jacobsson
Roland Pusch
Högskolan i Luleå 77-06-01

05 Orienterande temperaturberäkningar för slutförvaring i berg av radioaktivt avfall, Rapport 1
Roland Blomquist
AB Atomenergi 77-03-17

06 Groundwater movements around a repository, Phase 1, State of the art and detailed study plan
Ulf Lindblom
Hagconsult AB 77-02-28

07 Resteffektstudier för KBS
Del 1 Litteraturgenomgång
Del 2 Beräkningar
Kim Ekberg
Nils Kjellbert
Göran Olsson
AB Atomenergi 77-04-19

08 Utlakning av franskt, engelskt och kanadensiskt glas med högaktivt avfall
Göran Blomqvist
AB Atomenergi 77-05-02

09 Diffusion of soluble materials in a fluid filling a porous medium
Hans Häggblom
AB Atomenergi 77-03-24

10 Translation and development of the BNWL-Geosphere Model
Bertil Grundfelt
Kemakta Konsult AB 77-02-05

11 Utredning rörande titans lämplighet som korrosionshärdig kapsling för kärnbränsleavfall
Sture Henriksson
Kjell Pettersson
AB Atomenergi 77-08-24

12 Bedömning av egenskaper och funktion hos betong i samband med slutlig förvaring av kärnbränsleavfall i berg
Sven G Bergström
Göran Fagerlund
Lars Rombén
Cement- och Betonginstitutet 77-06-22

13 Urlakning av använt kärnbränsle (bestrålad uranoxid) vid direktdeponering
Ragnar Gelin
AB Atomenergi 77-06-08

14 Influence of cementation on the deformation properties of bentonite/quartz buffer substance
Roland Pusch
Högskolan i Luleå 77-06-20

15 Orienterande temperaturberäkningar för slutförvaring i berg av radioaktivt avfall
Rapport 2
Roland Blomquist
AB Atomenergi 77-05-17

16 Översikt av utländska riskanalyser samt planer och projekt rörande slutförvaring
Åke Hultgren
AB Atomenergi augusti 1977

17 The gravity field in Fennoscandia and postglacial crustal movements
Arne Bjerhammar
Stockholm augusti 1977

18 Rörelser och instabilitet i den svenska berggrunden
Nils-Axel Mörner
Stockholms Universitet augusti 1977

19 Studier av neotektonisk aktivitet i mellersta och norra Sverige, flygbildsgenomgång och geofysisk tolkning av recenta förkastningar
Roberg Lagerbäck
Herbert Henkel
Sveriges Geologiska Undersökning september 1977

20 Tektonisk analys av södra Sverige, Vättern - Norra Skåne
Kennert Röshoff
Erik Lagerlund
Lunds Universitet och Högskolan i Luleå september 1977

21 Earthquakes of Sweden 1891 - 1957, 1963 - 1972
Ota Kulhánek
Rutger Wahlström
Uppsala Universitet september 1977

22 The influence of rock movement on the stress/strain situation in tunnels or bore holes with radioactive canisters embedded in a bentonite/quartz buffer mass
Roland Pusch
Högskolan i Luleå 1977-08-22

23 Water uptake in a bentonite buffer mass
A model study
Roland Pusch
Högskolan i Luleå 1977-08-22

24 Beräkning av utlakning av vissa fissionsprodukter och aktinider från en cylinder av franskt glas
Göran Blomqvist
AB Atomenergi 1977-07-27

25 Blekinge kustgnejs, geologi och hydrogeologi
Ingemar Larsson KTH
Tom Lundgren SGU
Ulf Wiklander SGU
Stockholm augusti 1977

26 Bedömning av risken för fördröjt brott i titan
Kjell Pettersson
AB Atomenergi 1977-08-25

27 A short review of the formation, stability and cementing properties of natural zeolites
Arvid Jacobsson
Högskolan i Luleå 1977-10-03

28 Värmeledningsförsök på buffertsubstans av bentonit/pitesilt
Sven Knutsson
Högskolan i Luleå 1977-09-20

29 Deformationer i sprickigt berg
Ove Stephansson
Högskolan i Luleå 1977-09-28

30 Retardation of escaping nuclides from a final depository
Ivars Neretnieks
Kungliga Tekniska Högskolan Stockholm 1977-09-14

31 Bedömning av korrosionsbeständigheten hos material avsedda för kapsling av kärnbränsleavfall. Lägesrapport 1977-09-27 samt kompletterande yttranden
Korrosionsinstitutet och dess referensgrupp

32 Egenskaper hos bentonitbaserat buffertmaterial
Arvid Jacobsson
Roland Pusch
Högskolan i Luleå 1978-06-10

33 Required physical and mechanical properties of buffer masses
Roland Pusch
Högskolan i Luleå 1977-10-19

34 Tillverkning av bly-titankapsel
Folke Sandelin AB
VBB
ASEA-Kabel
Institutet för metallforskning
Stockholm november 1977

35 Project for the handling and storage of vitrified high-level waste
Saint Gobain Techniques Nouvelles, October 1977

36 Sammansättning av grundvatten på större djup i granitisk berggrund
Jan Rennerfelt
Orrje & Co, Stockholm 1977-11-07

37 Hantering av buffertmaterial av bentonit och kvarts
Hans Fagerström, VBB
Björn Lundahl, Stabilator
Stockholm oktober 1977

38 Utformning av bergrumsanläggningar
Alf Engelbrektson, VBB
Arne Finné, KBS
Stockholm december 1977

39 Konstruktionsstudier, direktdeponering
Bengt Lönnerberg
ASEA-ATOM Västerås september 1978

40 Ekologisk transport och stråldoser från grundvattenburna radioaktiva ämnen
Ronny Bergman
Ulla Bergström
Sverker Evans
AB Atomenergi 1977-12-20

41 Säkerhet och strålskydd inom kärnkraftområdet.
Lagar, normer och bedömningsgrunder
Christina Gyllander
Siegfried F Johnson
Stig Rolandson
AB Atomenergi och ASEA-ATOM 1977-10-13

42 Säkerhet vid hantering, lagring och transport av använt kärnbränsle och förglasat högaktivt avfall
Ann-Margret Ericsson
Kemakta Konsult AB november 1977

43 Transport av radioaktiva ämnen med grundvatten från ett bergförvar
Bertil Grundfelt
Kemakta Konsult AB 1977-12-13

44 Beständighet hos borsilikatglas
Tibor Lakatos
Glasforskningsinstitutet, Växjö december 1977

45 Beräkning av temperaturer i ett envånings slutförvar i berg för förglasat radioaktivt avfall. Rapport 3
Roland Blomquist
AB Atomenergi 1977-10-19

46 Temperaturberäkningar för slutförvar för använt bränsle
Taivo Tarandi
Vattenbyggnadsbyrån Stockholm juni 1978

47 Investigations of groundwater flow in rock around repositories for nuclear waste
John Stokes
Roger Thunvik
Inst för Kulturteknik KTH maj 1978

48 The mechanical properties of the rocks in Stripa, Kråkemåla, Finnsjön and Blekinge
Graham Swan
Högskolan i Luleå 1977-09-14

49 Bergspänningsmätningar i Stripa gruva
Hans Carlsson
Högskolan i Luleå 1977-08-29

50 Lakningsförsök med högaktivt franskt glas i Studsvik
Göran Blomqvist
AB Atomenergi november 1977

51 Seismotechtonic risk modelling for nuclear waste disposal in the Swedish bedrock
F Ringdal
H Gjöystdal
E S Husebye
Royal Norwegian Council for scientific and industrial research oktober 1977

52 Calculations of nuclide migration in rock and porous media, penetrated by water
H Häggblom
AB Atomenergi 1977-09-14

53 Mätning av diffusionshastighet för silver i lera-sand-blandning
Bert Allard
Heino Kipatsi
Chalmers tekniska högskola 1977-10-15